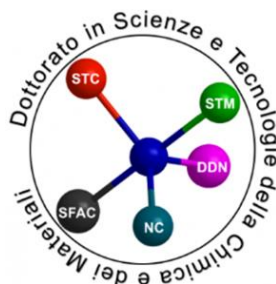


Università degli studi di Genova



Doctorate in Sciences and Technologies of Chemistry and Materials

Curriculum: Pharmaceutical, Food and Cosmetic Science

Cycle: XXXVI

Coordinator: Prof. Renata Riva

PhD candidate: Rizzo Marco

Supervisor: Prof. Michele Tonelli

The development of cycloguanil-based derivatives for the treatment of parasitic diseases

Index

1. Introduction

1.1. Neglected tropical diseases

1.2. Human African Trypanosomiasis

1.2.1 Trypanosoma brucei

1.2.2 Vector

1.2.3 Clinical features

1.2.4 Therapeutic Treatments

1.3 Leishmania

1.3.1 Vector and protozoa life cycle

1.3.2 Clinical features

1.3.3 Therapeutic treatments

1.4 Folate Pathways

1.4.1 DHFR

1.4.2 Pteridine Reductase 1

2. Aim of the work

2.1 Structural analysis of cycloguanil binding mode in complex with *TbPTR1*

2.2 Structural analysis of pyrimethamine binding mode in complex with *TbDHFR*

2.3 Development of novel cycloguanil-based series as antiprotozoal agents

3. Molecular modeling studies

3.1 Methodology

3.2 Molecular docking

3.3 Drug design

4. Conclusions & final remarks

5. Experimental section

6. References

LIST OF ABBREVIATIONS

NTDs	Neglected Tropical diseases
WHO	World Health Organization
HAT	Human African Trypanosomiasis
<i>Tb</i>	<i>Trypanosoma brucei</i>
SRA	serum resistance-associated
VSG	variant surface glycoprotein
DHFR	dihydrofolate reductase
<i>Tb</i> DHFR	<i>Trypanosoma brucei</i> dihydrofolate reductase
hDHFR	human dihydrofolate reductase
PTR1	pteridine reductase 1
DALYs	disability adjusted life years
MCL	mucocutaneous leishmaniasis
CL	cutaneous leishmaniasis
VL	visceral leishmaniasis
EMA	European medicines agency
NECT	nifurtimox-eflornithine combination therapy
MTX	methotrexate
DNA	deoxyribonucleic acid
DHB	7,8-dihydrobiopterin
THB	5,6,7,8-tetrahydrobiopterin
DHF	7,8-dihydrofolate
DHFR-TS	dihydrofolate reductase-thymidylate synthase
FBT	folate-biopterin transporter

NADPH nicotinamide adenine dinucleotide phosphate
PYR pyrimethamine
CYC cycloguanil
XP extra precision
IFD induce fit docking
EtOH abs. absolute ethanol
NaOH sodium hydroxide
THF tetrahydrofuran
EDC 1-ethyl-3-(3-dimethylaminopropyl)carbodiimide
Et₃N triethylamine
HOBT hydroxybenzotriazole
TFA trifluoroacetic acid
MeOH methanol
EC₅₀ half maximal effective concentration
CC₅₀ half maximal cytotoxic concentration
SI EC₅₀/CC₅₀ selectivity index
ACN acetonitrile

Summary

Parasitic diseases still represent a plague that provokes a major impact to public health, and overall social and economic well-being of affected countries, mainly of developing countries. Parasites belonging to Trypanosomatidae family are the etiological agents of human and animal vector-borne diseases, including human African trypanosomiasis (HAT), which is caused by *Trypanosoma brucei*, and Leishmaniasis, which is caused by several *Leishmania* spp. Although treatment options for these infections exist, their use is limited by several factors, including toxicity, suboptimal efficacy, difficult route of administration, and cost. Moreover, the emergence of drug resistance threatens the positive therapy outcome. This scenario claims the need of addressing more adequate therapies. Targeting the enzymes of the folate metabolism has demonstrated to be a successful approach in the treatment of bacterial infections and malaria, and recently it has been proposed also for the development of novel antiparasitic treatments. Trypanosomatids are auxotrophic for folates and pterins that are crucial cofactors for biosynthesis of nucleic acids and proteins. The inhibition of the key enzymes involved in the folate pathways, namely dihydrofolate reductase (DHFR) and pteridine reductase-1 (PTR1) should provide an effective treatment for these trypanosomatidic infections. The antimalarial drug cycloguanil

(CYC), a known DHFR inhibitor, was shown to be also an inhibitor of *TbPTR1*. Considering the structural analysis of CYC binding modes to *TbPTR1* and *TbDHFR*, the efforts of my PhD work have concerned the development of four novel series of antiprotozoan agents exploring the chemical space around the amino 1,6-dihydrotriazine core structure of CYC. Series 1 includes 2-aminotriazino[1,2-a]benzimidazole derivatives and their chemical precursors, the 2-guanidino benzimidazoles, while series 2 is characterised by the azaspiro-2,4-diamino-1,6-dihydrotriazine scaffold, decorated at C(6) of CYC with the benzyl-piperidine spirane moiety.

CYC-like 2,4-diamino-1,6-dihydrotriazines form series 3, whilst series 4 has explored the N-benzyl benzamide chain replacing the 4-Cl atom of CYC.

Each series of compounds has reached a different stage of research, so it is dealt with separately. In general, the compounds have been investigated for their on-target activity, human DHFR inhibition to ascertain their selectivity for the protozoan enzymes, cytotoxicity and antiparasitic effect. In the case of series 2, I have also performed docking studies to better understand the binding mode of these compounds to parasite and human enzymes of the folate pathway.

Overall, the SAR analysis derived from this study has allowed to obtain key insights for the future design of more promising antifolates for the treatment of protozoan diseases.

1. Introduction

1.1. Neglected Tropical Disease

Neglected Tropical Diseases (NTDs) are a group of diseases that take place under tropical and sub-tropical climate conditions. They are extremely linked to poverty⁽¹⁾. Therefore, they prosper in areas where access to adequate sanitation, clean water and healthcare is limited, and people live in proximity to animals and infective vectors.

NTDs affect the poorest and marginalized Countries like Africa, Asia and South and Central America.^(1,2)

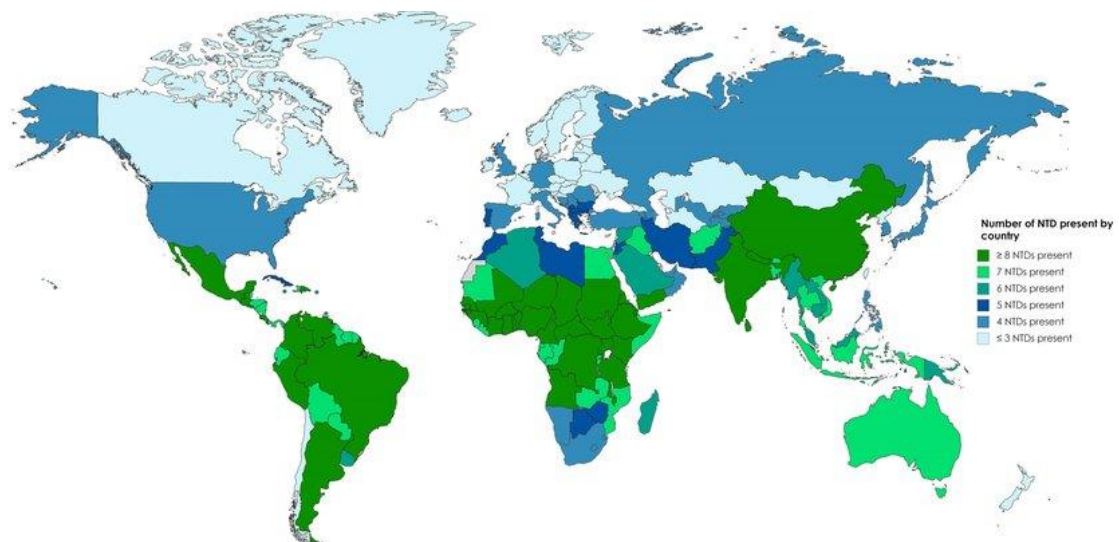


Figure 1: Prevalence of NTDs by country. Data from World Health Organization Control of Tropical Neglected Disease (2020).⁽³⁾

NTDs represent a group of 20 different transmissible diseases widespread in 150 countries that affect about one billion people. They are caused by bacteria, parasites, viruses and helminths⁽⁴⁾.

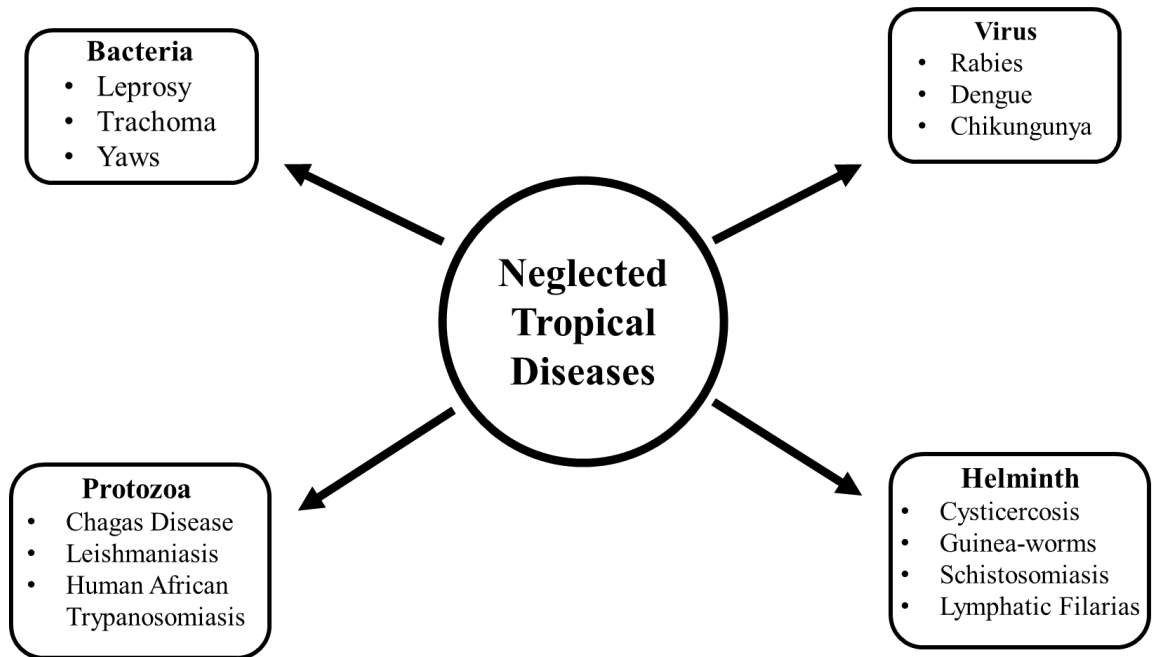


Figure 2: aetiological agents of NTDs.

These diseases produce a significant impact on public health, and heavily impact the overall economic and social life of the affected countries; in fact, they lead to long term disability and poverty^(5,6). As a consequence, from the disfigurement and their transferability, they keep children out of school, adults out of works, trapping the affected communities in endless cycle of poverty.

They also lead to impaired childhood growth and development, adverse outcomes of pregnancy and reduced productive capacity^(7,8,9).

NTDs may be lethal if untreated, and globally cause approximately 200,000 deaths every year and 19 million disability adjusted life years (DALYs) lost annually⁽¹⁰⁾.

Due to the disability and the poverty associated with these diseases, NTDs pose a threat to the health and economic development of low-income countries. In many cases, they still do not receive the proper attention from the funding agencies to implement research and health programs which remain underdeveloped⁽¹¹⁾.

Most of NTDs are vector-borne disease, basing on an intricate array of interactions among pathogens, vectors (ectoparasite) and reservoir hosts⁽¹²⁾. The rapid global expansion of travels, the growing contacts between humans and the animal reservoirs of pathogens and vector species, the environmental problems make the scenario very complex.

Therefore, despite the progress made so far, the efforts to be paid are still a lot.

On the base of a One Health approach, WHO, seizing the mutual dependence among human being, animal, and environment, has set a roadmap to eradicate NTDs by 2030. This achievement is founded on more adequate investments in product development and basic research, new vector control strategies and most advanced technologies, with a view to expressly helping the poor and solve their poverty-related health problems.

Among protozoan parasites, trypanosomatids are the etiologic agents of various threatening NTDs including Human African

Trypanosomiasis (HAT), Chagas disease (African Trypanosomiasis) and Leishmaniasis.

The following chapters deal with HAT and the state of the art of HAT therapy and the new research approaches in the field directed to a more promising management of this protozoan disease.

1.2. Human African Trypanosomiasis

Human African Trypanosomiasis (HAT), also known as Sleeping sickness is caused by an extracellular protozoa, member of the genus *Trypanosoma*, and species *Trypanosoma brucei*.

It is a vector-borne parasitic disease, which means that the transmission is mediated by an insect vector belonging to the genus *Glossina* (tse-tse fly). Other possible ways of transmission are represented by: the congenital way, the sexual way, the blood transfusion, the organ transplantation and laboratory accident^(13,14,15).

Two species are pathogenic to humans, namely *Trypanosoma brucei gambiense* and *Trypanosoma brucei rhodesiense*⁽⁹⁾, that display different clinical manifestations with dissimilar course and severity⁽¹⁶⁾. The characterization of the two pathogens and related forms of illness can be performed through molecular methods.^(17,18)

Another key component in the differential diagnosis of HAT is represented by the geographical distribution: *Tb gambiense* occurs

in West and Central Africa while *Tb rhodesiense* takes place in East Africa⁽¹⁹⁾ (Figure 3).

- *T. b. gambiense* accounts for more than 95% of cases and is responsible for a chronic infection which can evolve into a severe disease, many years after the parasite infection⁽²⁰⁾.
- *T. b. rhodesiense* causes an acute infection, which can rapidly invade the central nervous system, when the parasites penetrate the blood–brain–barrier⁽²¹⁾.
- *T. b. brucei* is a third subspecies which infects animals and, since it recapitulates infectious characteristics similar to the other two species, is largely used in research owing to its non-pathogenic profile towards humans.

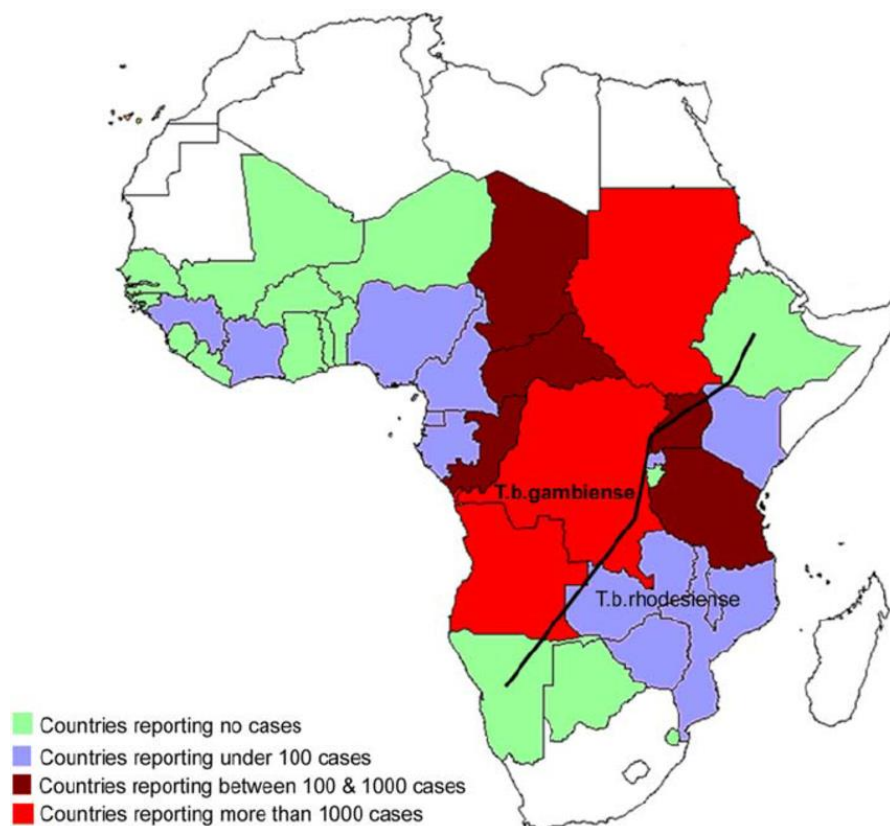


Figure 3: geographical distribution of *Tbgambiense* and *Tbrhodesiense* in Africa⁽²²⁾.

1.2.1 *Trypanosoma brucei*

Trypanosoma brucei is a hemoflagellate protozoa responsible for Human African Trypanosomiasis.

Tb gambiense and *Tb rhodesiense* are unicellular organisms featured by elongated cells of 15-30 μm , whose movements are possible thanks to the presence of a flagellum. Their cellular organization is like any eukaryotic cell, plus a tubular mitochondrion that contains the kinetoplast, an organelle containing a condensation of circular mitochondrial DNA. These organisms are extracellular parasites and they can be observed with a microscope, although they result to be indistinguishable⁽²³⁾.

The only way to distinguish them is to verify the presence of a specific molecular marker known as *serum resistance-associated (SRA)* gene, which is only present in *Tb rhodesiense*⁽²⁴⁾. *Tb gambiense* can be identified by looking at a different and specific molecular marker, the TgsGP gene⁽²⁵⁾.

The protozoa life cycle is characterized by two stages (*figure 4*): the mammalian stage and the vector stage, during which it always remains extracellular and evolves through metabolic and morphological adaptations.

The life cycle is extremely complex and during the two stages there are different biological phases. When infecting the vector, the protozoa are ingested like bloodstream trypomastigotes and migrate to the midgut where they differentiate to procyclic

trypomastigotes and replicate *in situ*; moving across the peritrophic membrane they reach the proventriculus, where they become mesocyclic trypomastigotes, and subsequently epimastigotes. (26,27,28,29)

Then they migrate *via* the oesophagus, reaching the salivary glands, and there they replicate assuming the infective metacyclic form.^(26,27,28) This form is the only one able to infect mammalian hosts, it is harvested by a variant surface glycoprotein (VSG) coat, a sort of shield that protects the parasite from the host's immune response⁽³⁰⁾, such as the complement. Considering that these immunogenic glycoproteins trigger a specific antibody response leading to the destruction of the protozoa, trypanosomes adapt to the host by developing an antigenic variation which replaces the coat with an antigenically different one.

The life cycle of the protozoa in the vector takes 18-35 days to be completed and, once the insect is infected, it remains so for its entire lifespan.

The mammalian host infection starts from the blood meal of the tsetse fly, that injects the metacyclic trypanosomes through the skin.

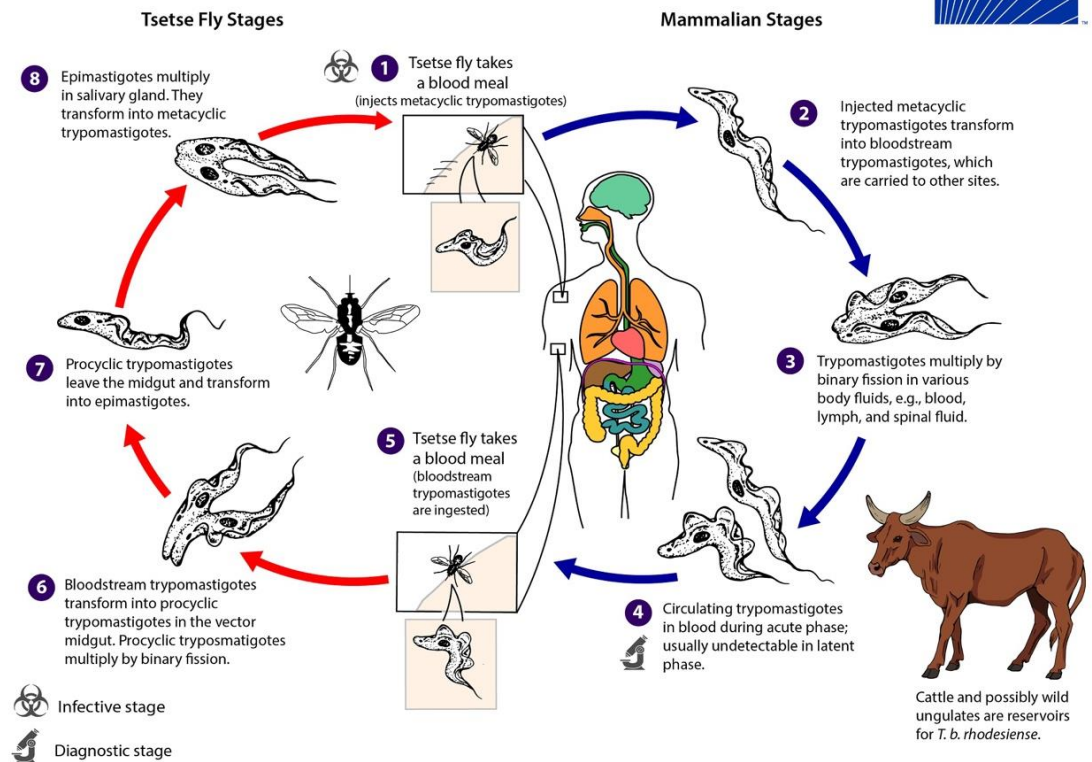


Figure 4. *Trypanosoma brucei* life cycle⁽³¹⁾.

When the protozoa infect a human host, after several days of multiplication in the injection site, they spread throughout the blood, lymph and tissues, assuming a spindle-shaped form,⁽³⁰⁾ a kind of cell that can assume dimension around 20-30 μm or shorter and are characterized by wriggling movements.

In the bloodstream they assume the trypomastigote form, which is the proliferative form, capable of infecting all the body fluids such as the cerebrospinal fluid and also crossing the placenta⁽³²⁾.

1.2.2 The vector

The HAT transmission relies on tsetse flies (genus *Glossina*), both sexes of this species are hematophagous and can spread the disease. The vector is viviparous, and females deposits a developed larva into the ground to become mature and after a month it comes out as an adult fly.

There are thirty-one species and subspecies of tsetse fly that are divided into three groups⁽³³⁾, generally associated to different habitat:

- *Nemorhina* group lives in Western and Central Africa, in vegetation like forests, riverbanks, lakes and swamps. To this group belong *G. palpalis palpalis* and *G. p. gambiense* which are responsible for the transmission of *Tb gambiense*, and *G. fuscipes* that transmits both *Tb gambiense* and *Tb rhodesiense*. *G palpalis* is more common on the Atlantic coast from Senegal to Angola, while *G. fuscipes* is located in areas from Congo to Cameroon.
- *Glossina* or *morsitans* group is linked to the presence of wild fauna, so it is common to find it in savannah environment and Eastern Africa. *G. morsitans*, *G. swynnertoni* and *G. pallides* belong to this group. They can spread *Tb rhodesiense*.
- *Austenina* or *fusca* group is common in forest belts. Indeed, there is no evidence that it can transmit HAT.

Tsetse flies are restricted at latitudes between 14°N and 29°S and need a certain range of temperatures (16°-38° C) and humidity (50%-80%) to grow and survive.

The lifespan is variable according to the season: between 3-5 months in the rainy season, and 1-2 months in dry season⁽³⁴⁾. Generally, females live longer than males. It is worth noting that although the chance of getting infected are higher in the first meal,⁽³⁵⁾ the flies can be infected at any point of their life.

1.2.3 Clinical features

The clinical manifestation of human African trypanosomiasis depends on several factors such as the parasite subspecies, host immune response and disease stage, but both forms can lead to death if untreated.

T. b. gambiense is associated with a chronic form of the disease with a slow clinical course and a delayed manifestation with respect to the time of infection⁽³⁶⁾. *T. b. rhodesiense* is associated with a form of acute pathology with a faster course, and tendentially lethal within 2 weeks of infection^(37,38). In humans, the first manifestation of Human African Trypanosomiasis (HAT) occurs after a minimum of 5 days following inoculation and evolves in two distinct clinical phases: the first phase refers to the parasitic infection at the systemic level (hemolymphatic stage) with symptoms overlapping with those of a common cold with fever,

headache, and joint pain. The transition to the second phase takes several weeks (spp *rhodesiense*) or months (spp *gambiense*) after infection, when the parasite crosses the blood–brain–barrier (meningoencephalitic stage), infecting the central nervous system. In *T. brucei gambiense* the first stage usually presents intermittent fever, headache, lymphadenopathy. Less frequently the host can show hepatosplenomegaly, oedema and endocrine dysfunction like amenorrhoea, infertility and miscarriage in women, while reduced libido and impotence in men.

In the second-stage disease, the host develop neuropsychiatric disorders, like alteration of the sleep cycles, that gave the name sleeping sickness to the disease, hypertonicity or hypotonicity, fasciculation, motor weakness, ataxia, tremor of hands and fingers. Mental changes are common in this phase, including emotional lability, attention deficit, apathy, or aggressive behaviour.

T. brucei rhodesiense diseases have a similar clinical manifestation, except for thyroid dysfunction, adrenal insufficiency and hypogonadism which are more common in *rhodesiense* disease.

Half of the patients infected by the *rhodesiense* subspecies also show gastrointestinal symptoms and less frequent, but anyway, severe complications like renal failure, multiorgan failure, coagulopathy and coma.⁽³⁹⁾

1.2.4 Therapeutic Treatments

In the fight to HAT, the World Health Organization ensures the distribution of some drugs, completely free of charge, considering that is endemic in poor countries.

To date there are only five drugs which are used in therapy based on the disease stage, whereby they can be divided into two groups, the first stage treatments and second stage treatments.

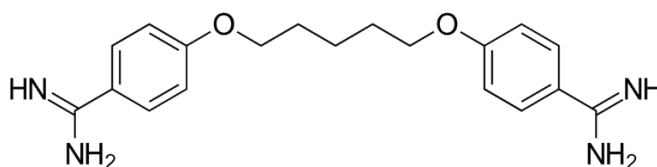


Figure 5: Pentamidine

- **First stage treatments:** one of the first line treatment against *T. brucei gambiense* is represented by Pentamidine isethionate (figure 5); it can also be used for *T. brucei rhodesiense* infections, although data on its efficacy are limited.^(40,41)

The mechanism of action is not clearly understood; it seems to interfere with the DNA, RNA, phospholipid, and protein synthesis of Trypanosoma parasites.

Pentamidine efficacy on *T brucei gambiense* is around 95-98%; it can be administered intramuscularly once daily for 7 days, or by intravenous infusion over 2 h. Before the injection, an ingestion of

sugar is necessary to prevent hypoglycaemia, followed by resting in supine position to avert hypotension. It is generally well-tolerated, but may cause adverse effects such as pain in the injection site, swelling, hypoglycaemia, hypotension, abdominal pain and gastrointestinal problems.⁽⁴²⁾

Another drug is represented by suramin (*figure 6*) that, and despite it is effective against both forms of parasite, it is used only against *T. brucei rhodesiense* because of the risk of heavy adverse events in patients co-infected with onchocerciasis occurring in *T. brucei gambiense* endemic areas.

It is accepted that Suramin has affinity with a lot of parasitic enzymes, such as glycolytic enzymes thus suppressing ATP synthesis⁽⁴³⁾, but also for DHFR and thymidine kinase.

Suramin sodium is available only in a parenteral formulation for slow intravenous infusion. Adverse effects are mostly reversible and include pyrexia, nephrotoxicity, peripheral neuropathy, agranulocytosis, and thrombocytopenia.

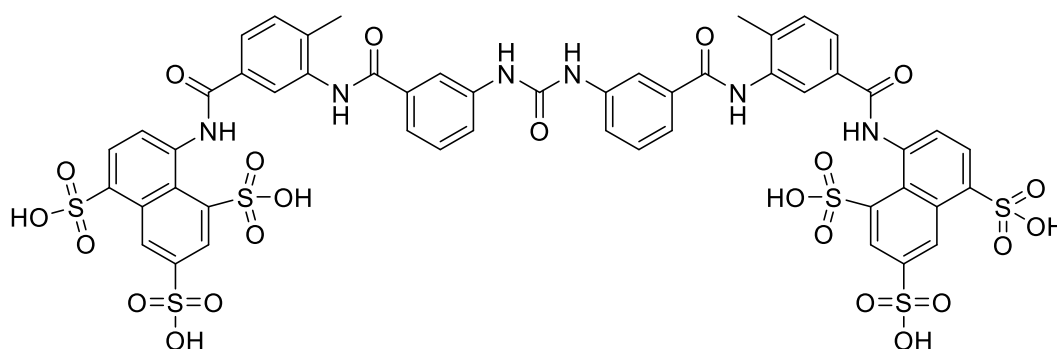


Figure 6: Suramin

- **Second Stage treatments:** the combination of nifurtimox-eflornithine (NECT) (*figure 7*) represents a valid option due to the high efficacy (95-98%), low fatality rate <1% and less severe side effects and the avoidance of drug resistance phenomena in *T. brucei gambiense* infections.^(44,45) Regarding the association NECT eflornithine is delivered intravenously while nifurtimox is delivered orally.

Nifurtimox acts causing oxidative stress to DNA and lipids of the parasitic cellular membrane.

Eflornithine is an inhibitor of ornithine decarboxylase, an enzyme that catalyses the formation of polyamines which play an important role in cell division and differentiation⁽⁴⁶⁾.

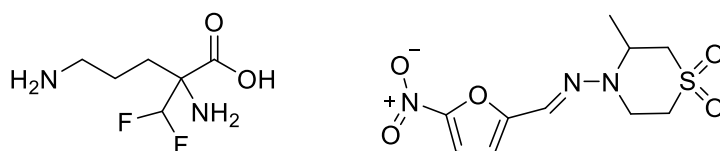


Figure 7: eflornithine, nifurtimox

Another treatment option is melarsoprol, a trivalent arsenical compound mainly used against *T. brucei rhodesiense*; after metabolization to melarsen oxide it interacts nonspecifically with the SH groups of proteins thereby targeting a wide range of enzymes. It also inhibit crucial parasitic pathways involving the

glycolytic enzymes, phosphogluconate dehydrogenase and trypanothione reductase⁽⁴³⁾. It is administered intravenously as once a day for 10 consecutive days.

The most severe adverse reaction caused by melarsoprol (*figure 8*) is represented by the encephalopathic syndrome, that manifests in the 18% of patient with a high fatal incidence rate⁽⁴⁷⁾.

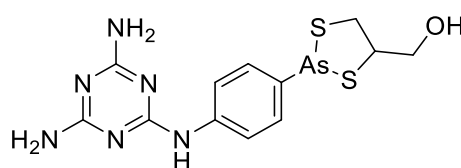


Figure 8: melarsoprol

More recently, fexinidazole (*figure 9*) was approved by the European Medicines Agency (EMA) as a first-line treatment drug, for the treatment of *T. brucei gambiense* infections, as a daily dose (for 10 days) against both disease's stages.

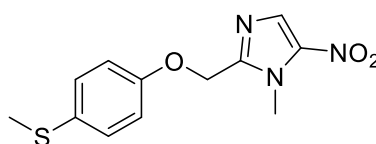


Figure 9: Fexinidazole

1.3 Leishmania

Another neglected disease is represented by Leishmaniasis, caused by different species of Leishmania, belonging to the *Trypanosomatidae* family.

Leishmaniasis is endemic in many tropical and sub-tropical Countries throughout Asia, Africa, Middle east, South and Central America leading to approximately 1.3 million new cases of the disease with a mortality rate of 30 000 deaths per year⁽⁴⁸⁾. After schistosomiasis and malaria leishmaniasis is considered as the third-most-common vector-borne disease based on the morbidity and disability-adjusted life years (DALYs)⁽⁴⁹⁾.

The Leishmania parasites count more than 20 diverse species, which are responsible for the three forms of Leishmaniasis: Cutaneous Leishmaniasis (CL) the most common, and the Mucocutaneous Leishmaniosis (MCL) the most disabling form of illness and Visceral Leishmaniasis (VL) the most severe, which is fatal if untreated⁽⁵⁰⁾.

Nowadays is the most widespread disease after malaria with a range of 0,7 to 1,2 million of new cases every year for CL⁽⁵¹⁾, and 0,4 million of new cases for VL.

All the 20 different species of Leishmania are transmitted by 70 different types of *Phlebotomine* sandflies.

Considering the number of species, Leishmaniasis can be geographically divided into Old world, including Asia, Middle

East, Africa and Southern Europe, and New world referring to Americas⁽⁵²⁾.

1.3.1 Vector and protozoan life cycle

Leishmaniasis is transmitted by the bite of Phlebotomine sandflies, belonging to the family *Diptera*, *Psychodidae* species, which can be classified in two subspecies: *Phlebotomus* in the Old World and *Lutzomyia* in the New World⁽⁵³⁾.

The sandflies life cycle depends on their geographical location, in tropical areas they can complete it in one month while in subtropical areas they can only complete it during warmer months⁽⁵⁴⁾.

Leishmania parasites can exist in two forms during life cycle (figure 10): promastigote and amastigote^(54,55).

The promastigote form presents a flagellum that allows mobility in the insect vector body. When the sandfly makes a bloodmeal from a mammalian host, it injects the promastigotes directly into the skin that are phagocytosed by mononuclear cells, thus differentiating into the non-motile amastigote forms^(54,55). In this form, they can multiply in the reticuloendothelial system and can cause asymptomatic or symptomatic disease.⁽⁵⁵⁾ Amastigotes exploit the bloodstream or the lymphatic system to spread all over the host body.

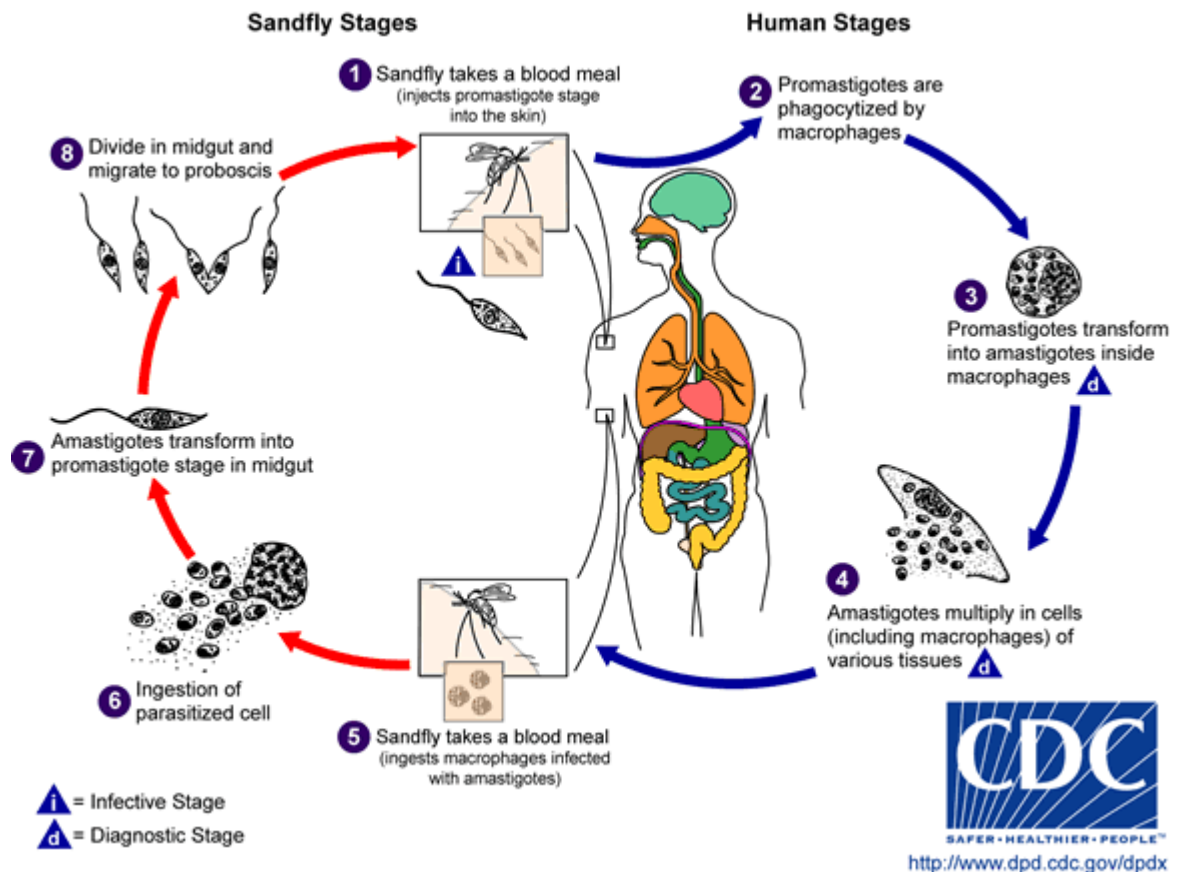


Figure 10: Leishmania life cycle⁽⁵⁵⁾

1.3.2 Clinical features

The clinical manifestations of Leishmania can be different, depending on the phenotypic category.

Cutaneous Leishmaniasis, caused by *L. major*, *L. tropica*, *L. aethiops*, *L. venezuelensis*, *L. amazonensis*, *L. mexicana* typically produces lesions on the injection site as solitary non-supportive papule. From weeks to months the papules can evolve to painless ulcers with gathered borders. Several atypical cutaneous manifestations can occur, like nodular, sporotrichosis,

disseminated, psoriasiform, verrucous, eczematous or erysiploid.⁽⁵⁶⁾

Mucocutaneous Leishmaniasis, typically leads to facial deformities years after the initial cutaneous phase are healed. This form is caused by *L. Viannia* subgenus and the parasite reaches the nasopharyngeal mucosa thorough the bloodstream and lymphatic system⁽⁵⁷⁾. The patients with ML very often shows nasal symptoms as epistaxis, secretions, ulcerations, bleedings and perforations of the nasal septum.⁽⁵⁸⁾

The most lethal form, Visceral Leishmania also known as kala-azar the Hindi word for black fever, cause systemic infections affecting several organs as spleen, liver, hematogenous and lymphatic system. This infection is caused mainly by the species *L. donovani*, *L. infantum* and *L. chagasi*⁽⁵⁷⁾. The infected host with VL typically presents symptoms like hepatosplenomegaly, cachexia, pancytopenia and hypergammaglobulinemia⁽⁵⁹⁾; other reported symptoms are fatigue, abdominal pain and unintentional weight loss. It is also possible that people with kala-azar syndrome can develop CL after the resolution of the first one with its classical manifestations.

1.3.3 Therapeutic Treatments

Treatments against Leishmaniasis are limited and they not always match the satisfactory standards, and most of the drugs used against leishmaniasis are repurposed from other diseases⁽⁴⁹⁾. Therapy is based on pentavalent antimonials, pentamidine, amphotericin B and miltefosine.

One of the first-line treatment is represented by pentavalent antimonials, used against both VL and CL. Among them, Sodium Stibogluconate and Meglumine Antimoniate were used for decades, and, despite this, their mechanism of action is not well elucidated yet.

What is clear is their limitation for long term use and toxicity, in fact antimonials cause cardiotoxicity and hepatotoxicity⁽⁶⁰⁾.

As aforementioned, several drugs were repurposed for the treatment of Leishmaniasis, the first one is represented by the antifungal agent amphotericin B⁽⁶⁰⁾. (*Figure 11*)

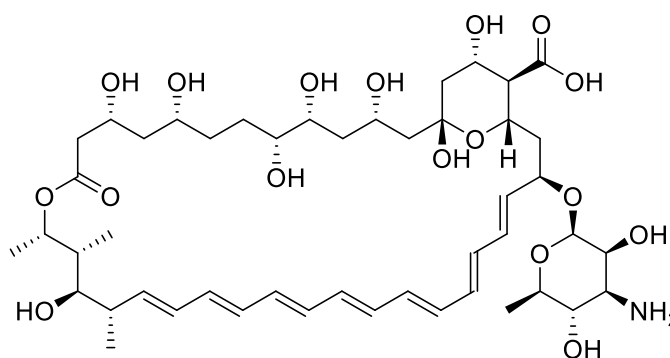


Figure 11: Amphotericin B

Amphotericin B targets sterols like ergosterols present in parasite wall cell leading to cell lysis⁽⁶¹⁾. Even if amphotericin B is very effective against VL⁽⁶²⁾ and Indian Post Kala-azar dermal leishmaniasis (PKDL)⁽⁶³⁾ several adverse effects are reported like renal complications and hypokalaemia⁽⁶⁴⁾.

Miltefosine (hexadecyl phosphocholine) (*figure 12*) is the first antileishmanial drug following oral administration, and exhibiting an effectiveness around 94%⁽⁶⁵⁾.

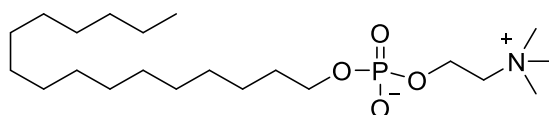


Figure 12: miltefosine

Miltefosine was shown to impair the biosynthesis of the cell surface components of the parasite, leading the cell to death^(66,67).

As the other frontline drugs, its use is limited due to the high toxicity, as gastrotoxicity, hepatotoxicity and nephrotoxicity furthermore the long half-life of the drug increases the probability of drug resistance.

1.4 Folate Pathway: general overview

Folate is an essential nutrient supplemented from the diet, as mammals (including humans) do not possess the capacity of synthesizing it *de novo*.

Protozoa belonging to the genus *Trypanosoma* and *Leishmania* are auxotrophic for folates and other pterines, so they need to supply them from the infected hosts, like vectors and mammals.^(68,69,70)

Trypanosomatids rely on several transporters for guaranteeing an adequate folate and pterins intake⁽⁷¹⁾. *Leishmania* may exploit 14 members of the folate-biopterin transporter (FBT) family⁽⁷²⁾, whilst *Trypanosoma brucei* just 8 members of FBT family⁽⁷³⁾. Following the intake, folate is reduced through two-steps reaction up to the active tetrahydro derivative THF, by the action of a reduced nicotinamide adenine dinucleotide (NADPH)-dependent enzyme, the dihydrofolate reductase-thymidylate synthase (DHFR-TS).

THF is a crucial cofactor involved in the purine and thymidylate synthesis, in the methionine cycle and redox defence^(74,75).

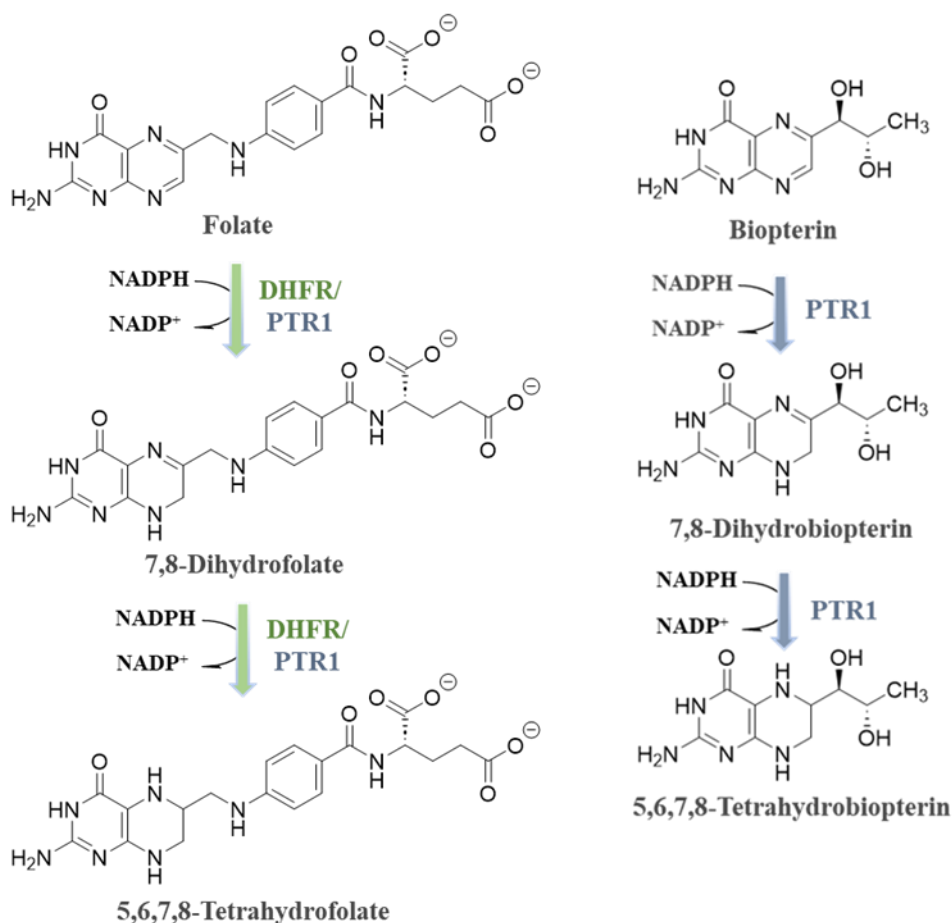


Figure 13: two stage reduction of folate to 7,8-dihydrofolate (DHF) and 5,6,7,8-tetrahydrofolate (THF) catalized by DHFR and PTR1. Two stage reduction of Biopterin to 7,8-Dihydrobiopterin (DHB) and 5,6,7,8-tetrahydrobiopterin (THB) catalized by PTR1. The reactions require the presence of NADPH as cofactor. DHFR is the main responsible for the folate reduction, however PTR1 as well can be involved in the folate reduction when DHFR is inhibited.

When DHFR is inhibited during the treatment with conventional antifolates, such as MTX, the parasites can exploit another enzyme PTR1, mainly responsible for biopterin metabolism, to also reduce folate, thus enabling the parasites to survive.

Folate antagonists targeting DHFR are currently applied in diverse pharmacological settings, such as antimalarial (cycloguanil, the

active metabolite of proguanil), antibacterial (trimethoprim) and antineoplastic (methotrexate/pralatrexate) therapy.

To date bulk of evidence shows that the inhibition of only one of these folate-dependent enzymes is not sufficient for an effective antiparasitic activity to treat HAT and Leishmaniasis, supporting the concept that dual inhibition could offer the prospect of a better disease management.

Indeed, further investigations are in due course to incorporate a more in-depth knowledge about the fine interplay between the two enzymes and the respective pathways connection.

1.4.1 Dihydrofolate reductase

DHFR structure from different protozoan parasites belonging to *Trypanosoma* and *Leishmania* genus was characterized by crystallography, showing that ~50% of their primary sequences is conserved. More interestingly, only 26% sequence identity to the homologue human isoform was demonstrated, thus pointing out a low risk for off-target effects⁽⁷⁶⁾.

Table 1: Identity level among some DHFRs.

	<i>T. brucei</i>	<i>T. cruzi</i>	<i>L. major</i>
<i>Umano</i>	26	27	26
<i>L. major</i>	46	50	
<i>T. cruzi</i>	58		

Relevant differences between *Tb*DHFR and *h*DHFR can be observed in the folate binding site, as follows:

- There is a small tunnel under the pteridine ring in *Tb*DHFR.
- Gly20 and Asp21 in the human isoform are overall negatively charged and are replaced by neutral residues Gly45-Thr46 in *T. brucei*.
- Phe31 in *h*DHFR is occupied by Met55 in the protozoan active site which results in a larger binding pocket.
- Gln35 and Asn69 in *h*DHFR are replaced by Arg39 and Phe94 in *Tb*DHFR.

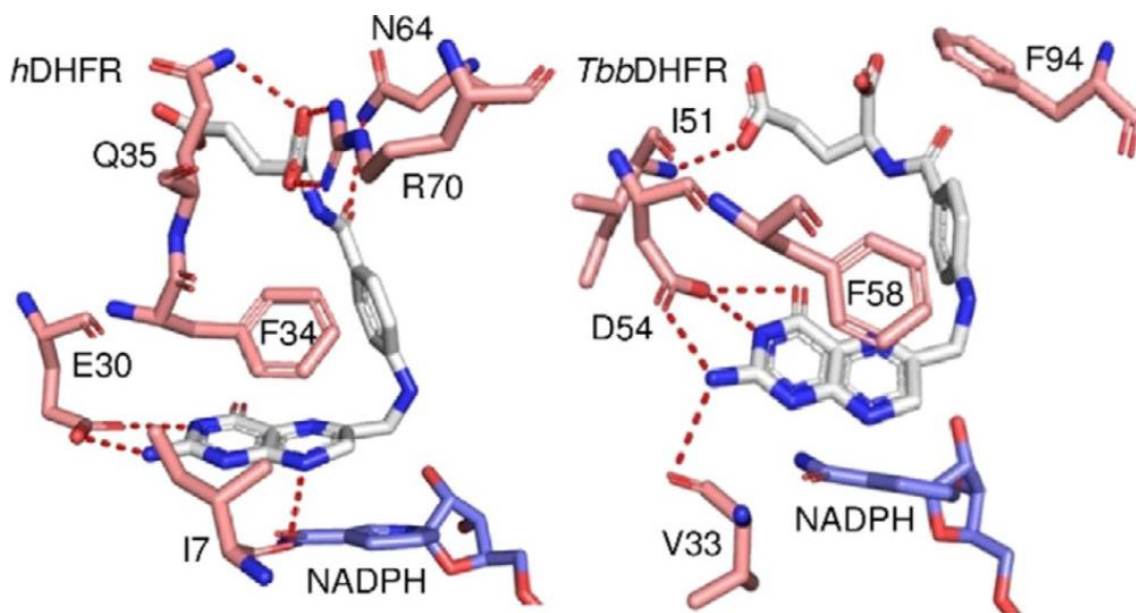


Figure 14: Binding modes of DHF (white) within the hDHFR and TbbDHFR (rose). NADPH is represented in light blue⁽⁷⁷⁾.

The secondary structure of this enzyme is organized in C- and N-terminal domains separated by a fissure where the Nicotinamide Adenine Dinucleotide Phosphate (NADPH) binding site is located⁽⁷⁸⁾. The cofactor binds in an extended conformation, stabilized by a network of conserved interactions with the surrounding residues.

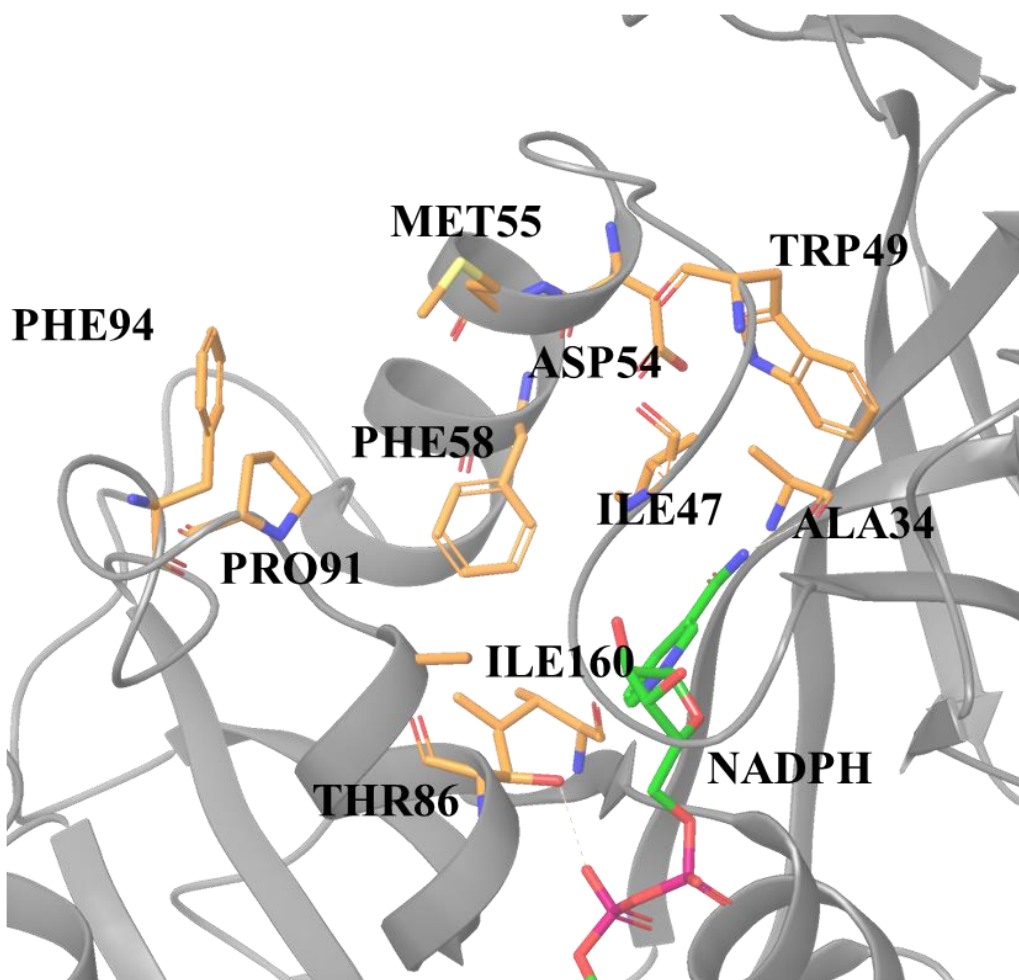


Figure 15: TbDHFR active site in complex with NADPH (green) (PDB ID: 3QFX)⁷⁸

1.4.2 Pteridine Reductase 1

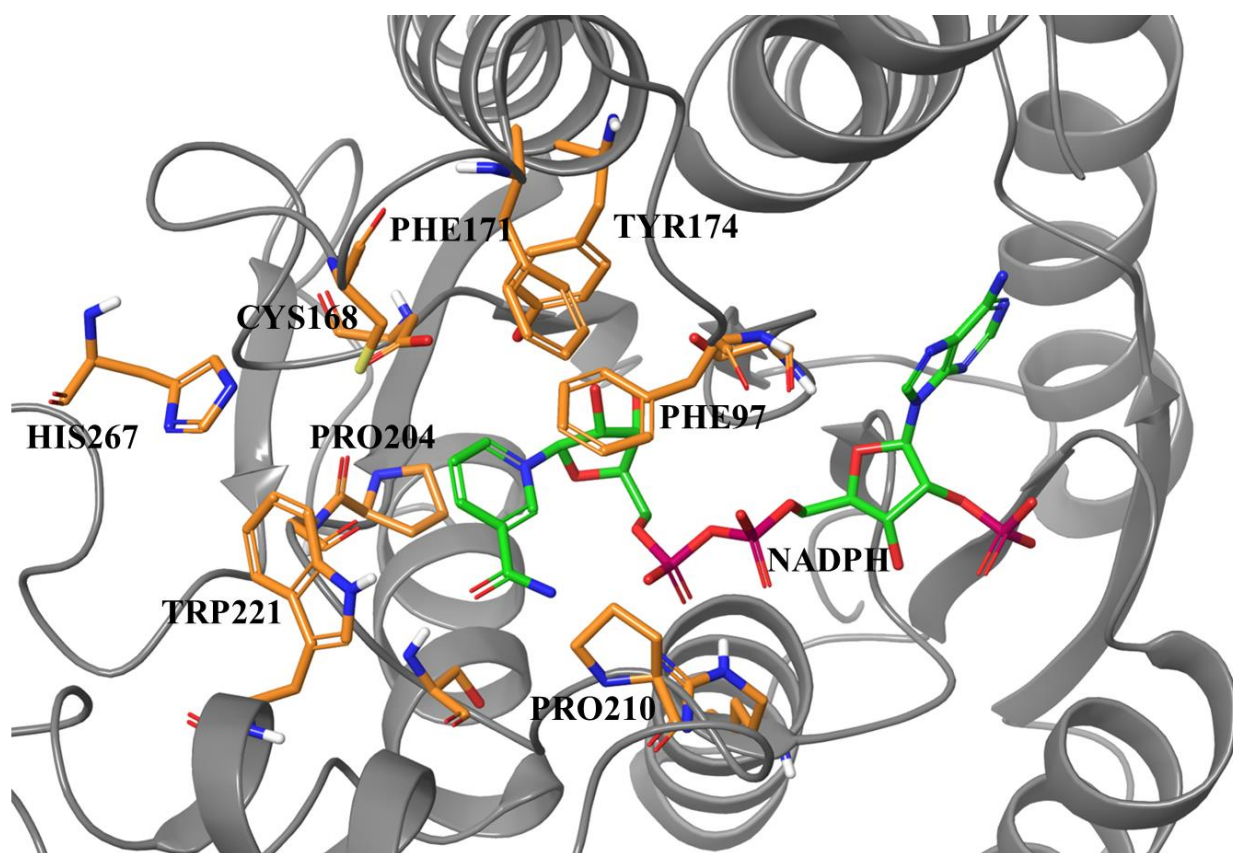


Figure 16: PTR1 active site, chemical composition, chemical composition in orange, cofactor NADPH in green. (PDB ID:2X9G)⁷⁹

Pteridine reductase 1 (PTR1) is an enzyme that can be found in trypanosomatids belonging to the short chain dehydrogenase/reductase (SDR) family; it is a tetramer composed of 288 residues and there is no actual evidence of cooperation between them.

PTR1 catalyses the reduction of biopterin to dihydrobiopterin (DHB) and subsequently to 5,6,7,8-tetrahydrobiopterin

(THB)^(80,81), contributing to the regulation of parasite growth and defence against oxidative stressful conditions⁽⁸²⁾.

Indeed, growing knowledge about PTR1 pathway is opening the way to new pharmacological strategies of intervention, especially for diverse diseases associated with mitochondrial dysfunction.

PTR1 can be also part of folate metabolism, acting as metabolic bypass of DHFR, when the last is inhibited, thus refurnishing the pool of THF necessary for parasite survival^(83,84,85,86). The essential role of PTR1 for parasite proliferation was demonstrated in vitro and in vivo through genetic studies. ^(75,81)

On the wave of these findings both protozoal DHFR and PTR1 enzymes can be considered validate targets for the development of innovative treatments against Trypanosoma and Leishmania infections.

2. Aim of the work

In the field of infectious diseases, targeting folate metabolism has already been proven to be a successful approach to tackle bacteria and malaria infections,^(87,88) as demonstrated by the drugs trimethoprim and cycloguanil (through its prodrug, proguanil) respectively. Hence, it's reasonable to think these two folate-dependent enzymes as promising targets also for treatment of other parasitic diseases.

To date, *Tb*PTR1 and *Tb*DHFR inhibitors have been designed mimicking the substrate pterin moiety: monocyclic and bicyclic aromatic systems such as pyrimidines, pteridines, quinolines, pyrrolo-pyrimidines, benzimidazoles and benzothiazoles^(89,90,91,92), may be regarded as the most frequently investigated scaffolds to this aim.

Also, a 2,4-diamino pyrimido[4,5-b]indole derivative was reported as the first tricyclic compound capable of targeting *Tb*PTR1 (K_i of 83 μ M) through an interaction network similar to Pyr and Cyc, but it formed additional contacts within the hydrophobic pockets close to the catalytic site of *Tb*PTR1⁽⁹⁰⁾. A such behavior suggested that the enzyme catalytic cavity could also accommodate more expanded molecular cores, opening the way for the exploration of other chemotypes.

Despite showing nanomolar activity against at least one of these enzymes, only a moderate in vitro and in vivo efficacy was observed, supporting the concept that their inhibition should occur simultaneously and, also by a similar degree of potency^(74,93,89).

Also the antimalarial drug cycloguanil (CYC), featured by a dihydrotriazine core, was discovered targeting *Tb*PTR1 to a lesser extent (IC_{50} 31.6 μ M)⁽⁹⁴⁾ than *Plasmodium falciparum* (K_i = 1.5 nM)⁽⁹⁵⁾ and *Trypanosoma brucei* (K_i = 256 nM)⁽⁷⁸⁾ DHFR-TS⁽⁹⁴⁾ enzymes.

CYC was originally identified in the 1970s as a human DHFR inhibitor eliciting anticancer activity in rat models of leukaemia⁽⁹⁶⁾.

More recent studies have confirmed that CYC and its analogues are human DHFR-directed anticancer agents, impacting cellular nucleotide metabolism, and decreasing STAT3 transcriptional activity⁽⁹⁷⁾.

2.1 Structural analysis of cycloguanil binding mode in complex with *Tb*PTR1

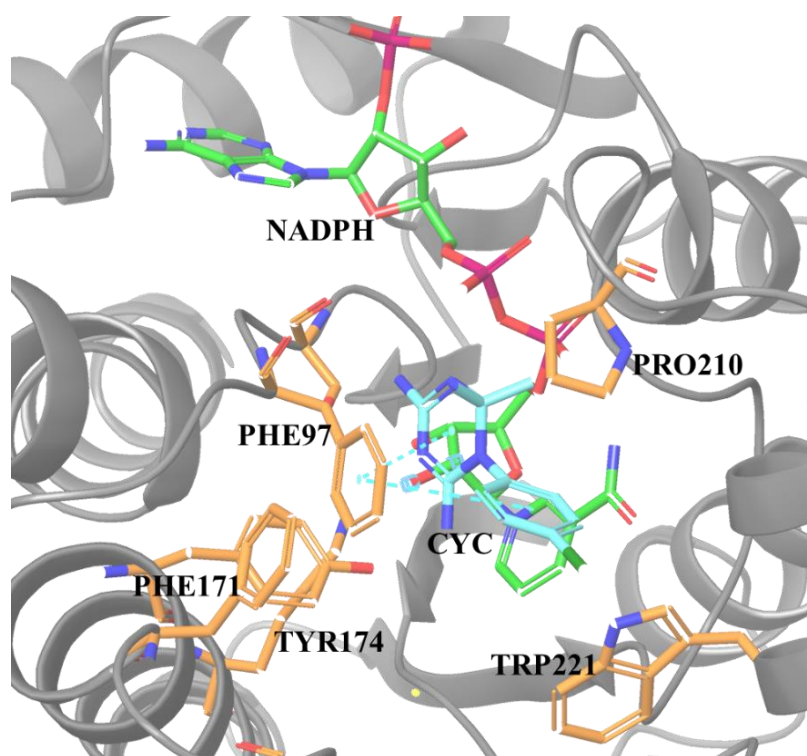


Figure 17: CYC (cyan) in complex with PTR1 (PDB ID: 6HNC)⁽⁹⁴⁾ and NADPH (green), in orange the chemical composition of the active site.

The functional PTR1 enzyme is a tetramer in which the cofactor NADPH plays a key role in composing both the catalytic site and the substrate-binding pocket through an extended network of H-

bonds^(81,76). Natural pterin substrates bind to this pocket forming a particular π -sandwich interaction lined by the aromatic side chain of Phe97 and the cofactor nicotinamide ring^(81,76).

The 2,4-diamino-1,6-dihydrotriazine ring of CYC is engaged in the π -sandwich interaction and forms an array of H-bonds through its multiple nitrogen atoms with the NADPH and several residues implicated in catalytic process like Ser95 and Tyr174.

One of the two methyl groups in position C(6) establishes Van der Waals contacts with Phe97 and Pro210. The p-chlorophenyl ring is rotated with respect to the plane of the dihydrotriazine ring, and is halogen bonded to the with the indole ring of the Trp221.^(80,82)

2.2 Structural analysis of pyrimethamine binding mode in complex with *Tb*DHFR

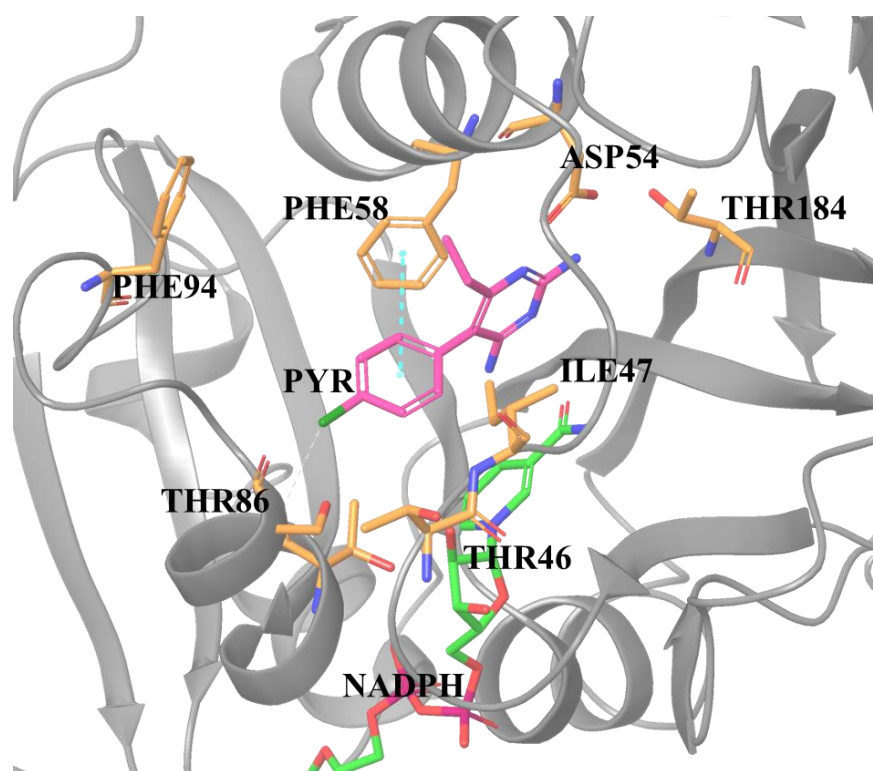


Figure 18: PYR (magenta) in complex with TbDHFR and NADPH (green), in orange the chemical composition of the active site. Complex visualized with Maestro Schrodinger.(PDB ID 3QFX)⁽⁷⁸⁾

While for *Tb*PTR1 the co-crystal structure with CYC has been released, that for *Tb*DHFR is not available yet. For this reason, the complex of the antimalarial drug pyrimethamine (PYR) within *Tb*DHFR was selected as a model for that of CYC. The two drugs defer for the chemical structure of their core, namely a planar pyrimidine for PYR and a non-aromatic 1,6-dihydrotriazine ring for CYC. Additional support was derived from the observation that they display superimposable bonding interactions in the complex

with *TbPTR1* active site, establishing the same array of polar and hydrophobic contacts⁽⁹⁸⁾.

In *TbDHFR*, Pyr is H-bonded to Val32 and Ile160, on one side, and to Asp54, on the other. Moreover, it is stabilized by van der Waals contacts with Ile47, Phe58, and Ile160, and through its *p*-chlorophenyl ring it a halogen bond with Thr86⁽⁹⁸⁾.

2.3 Development of novel cycloguanil-based series as antiprotozoal agents

On the wave of these findings, during my PhD, I worked on the synthesis of novel series of antiprotozoan agents in the attempt to explore the chemical space around the amino 1,6-dihydrotriazine core structure of CYC and deepen the SAR insights.

SERIES 1: 2-aminotriazino[1,2-*a*]benzimidazole derivatives and their chemical precursors, the 2-guanidino benzimidazoles

SERIES 2: azaspiro-2,4-diamino-1,6-dihydrotriazine derivatives, bearing in position 1 an aromatic ring, variously substituted, and the benzyl-piperidine spirane moiety at C(6) of CYC.

SERIES 3: CYC-like 2,4-diamino-1,6-dihydrotriazines, in which the aromatic ring in position 1 was functionalized with various

groups, and in some cases the two methyl groups at C(6) of CYC were replaced by bulky spirocyclic moieties.

SERIES 4: N-benzyl benzamide analogues of CYC, where longer and bulkier chains substitute the 4-Cl atom of CYC.

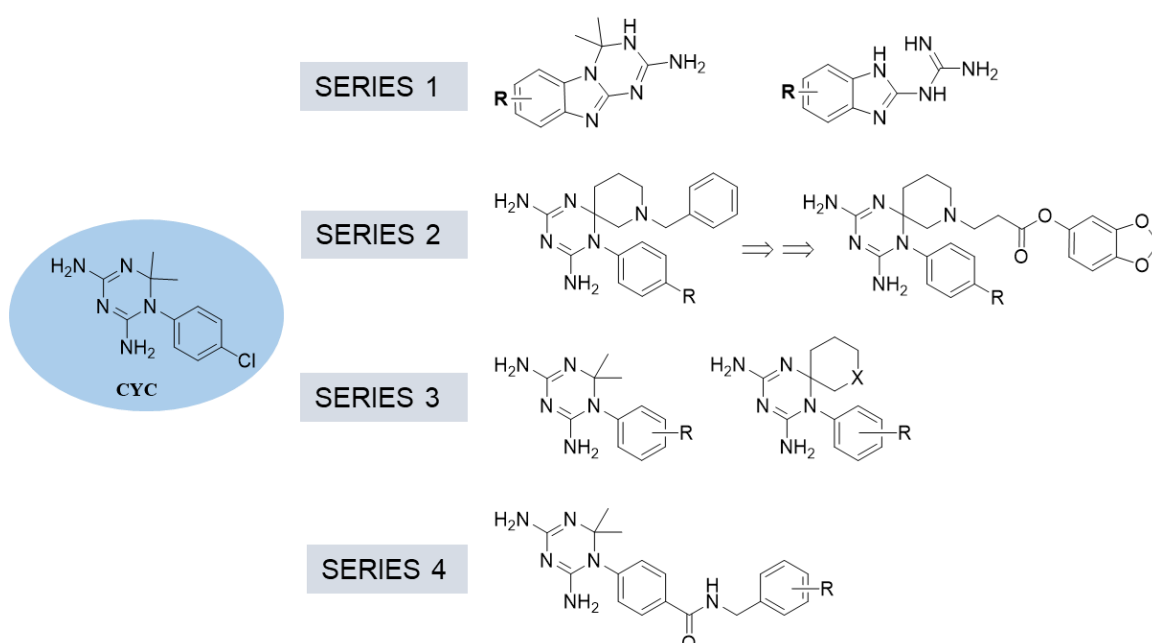


Figure 19: Chemical structures of the investigated series of compounds as antiprotozoal agents.

The compounds series underwent evaluation of their on-target activity against trypanosomatidic PTR1 and DHFR, human DHFR inhibition to ascertain their selectivity for the protozoan enzymes, cytotoxicity, and antiparasitic effect.

The enzymatic screening (IC_{50} and K_i) was performed by the Drug Discovery and Biotechnology Lab of Prof. Maria Paola Costi, University of Modena and Reggio Emilia, while cellular tests (cytotoxicity, CC_{50} and antiparasitic activity, EC_{50}) were performed

by the Parasite Disease group of Prof. Anabela Cordeiro da Silva, University of Porto.

The CC_{50} (concentration of compound able to produce the half of the maximal concentration showing non-toxic effects) was taken as a parameter of reference for the toxicity of the compounds against human cells and used to calculate the Selectivity Index (SI), as the ratio between CC_{50} and the EC_{50} (compound concentration causing the inhibition of the 50% of the cell growth). The antiparasitic activity was tested in two media: complete HMI-9 medium, corresponding to a final folate concentration of 9 μM ; deficiency HMI-9 medium, corresponding to a final folate concentration of 20 nM, assuming a competitive inhibition mechanism for the investigated compounds.

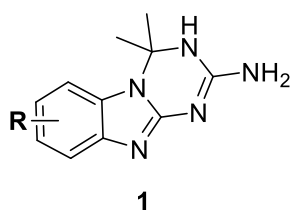
Each series of compounds has reached a different stage of research, so it is discussed separately for the chemical and biological profiling and different studies dealt with.

The SAR analysis derived from this study will allow to obtain key insights for the future design of more promising antiprotozoal agents.

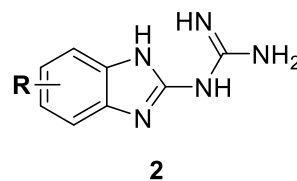
These studies are part of the COST Action CA2111 - One Health drugs against parasitic vector borne diseases in Europe and beyond-supported by COST (European Cooperation in Science and Technology).

SERIES 1

The first set includes the tricyclic compounds 2-aminotriazino[1,2-a]benzimidazoles (**1**) where the amino triazino motif of CYC is merged with the benzimidazole ring, that recurs in several examples of antiprotozoal agents as main unit or important substructure⁽⁹⁹⁾. Also, their open ring analogues, the 2-guanidinobenzimidazoles (**2**), have been taken into consideration as pseudo-ring structures that, being endowed with a greater flexibility, may arrange in a similar conformation to 2-aminotriazino benzimidazoles.



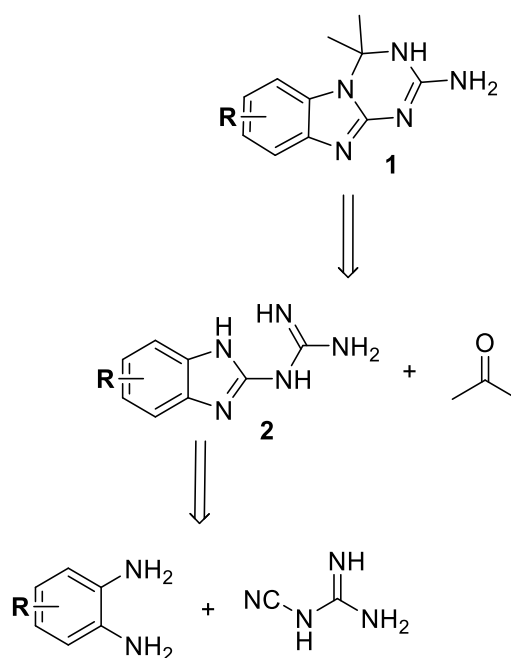
R= H (**1a**), 7(8)-Cl (**1b**), 7,8-diCl (**1c**)
7,9-diCl (**1d**), 7(8)-CF₃ (**1e**),
7(8)-OCH₃ (**1f**), 7,8-diCH₃ (**1g**)



R= H (**2a**), 5(6)-Cl (**2b**), 5,6-diCl (**2c**)
4,6-diCl (**2d**), 5(6)-CF₃ (**2e**)
5(6)-OCH₃ (**2f**), 5,6-diCH₃ (**2g**)

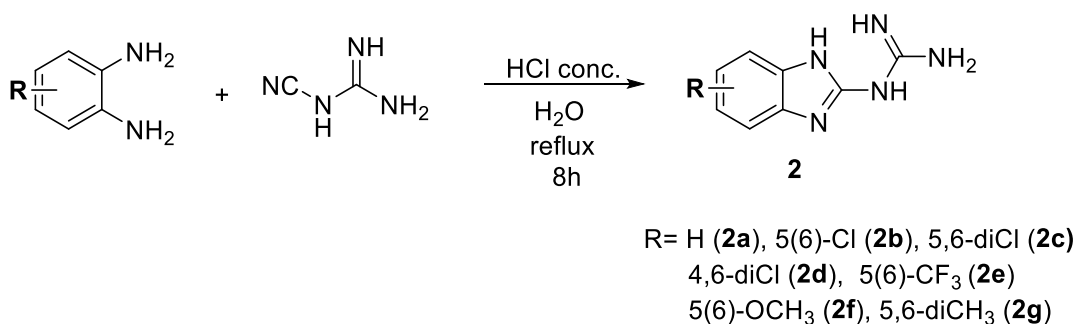
Chemistry

The triazino benzimidazole **1a**⁽¹⁰⁰⁾ and 2-guanidino benzimidazoles **2a-c**, **2e** and **2f**⁽¹⁰¹⁾ were obtained according to the cited references. For the first set of compounds (**1**) and (**2**), we planned the following synthetic route. (Scheme 1)



Scheme 1. Retrosynthesis of compounds **1** and **2**.

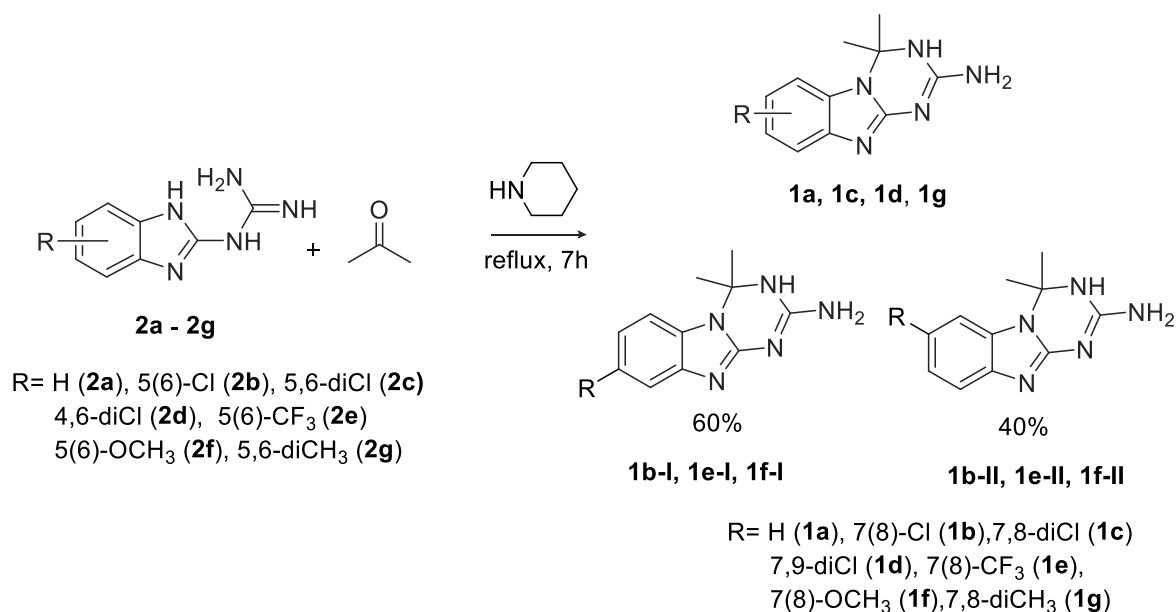
First, we synthesize compounds **2**, by reacting the proper 1,2-phenylenediamine with dicyandiamide in acid catalyzed conditions (Scheme 2).



Scheme 2

Subsequently, 2-amino-3,4-dihydrotriazino[1,2-a]benzimidazoles **1** were obtained through the cyclization of 2-guanidino

benzimidazoles **2** with acetone under piperidine catalysis (Scheme 3).



Scheme 3

By the analysis of NMR spectra, cycloaddition of acetone to compounds **2** (**2b**, **2e** and **2f**) did not show regioselectivity and gave the tricyclic compounds **1** as a mixture of isomers **I** (60%) and **II** (40%), respectively, namely **1b-I** and **1b-II**, **1e-I** and **1e-II** and **1f-I** and **1f-II** (Scheme 3).

The assignment of each specific isomeric peak and the definition of the proportions between the two isomers in the ¹H NMR spectra, COSY and NOESY experiments agreed with a previous analogue, the 7(8)-methyl triazino[1,2-a]benzimidazole.⁽¹⁰⁰⁾ The electronic nature of R group in series **2** did not seem to significantly influence the annellation reaction involving N-1 and N-3 of the guanidino moiety; the isomer **I**, substituted at C(8) of the tricyclic system always formed in higher percentage with respect to isomer **II**,

bearing the substituent at C(7). The ratio between the two isomers may be the consequence of the steric hindrance of the dimethyl moiety of acetone during the ring closure.

In the case of the asymmetric disubstituted compound **1d** only 7,9-diCl isomer is yielded, as confirmed by NOESY-2D and 1D experiments, where a strong cross-peak for the doublet at 7.41 at C(6) and the singlet at 1.74 (*gem*-diCH₃) was observed.

The attempt to separate the two isomers of **1f**, such as representative sample of series **1**, by HPLC (eluent A: H₂O/HCOOH 0.1% v/v, eluent B: ACN/HCOOH 0.05% v/v) gave a negative result, so the 7(8)-monosubstituted triazino benzimidazoles **1b**, **1e** and **1f** were assayed in mixture.

In vitro biological profiling

These derivatives have been evaluated for their inhibitory activities against *TbPTR1* and *TbDHFR*.(Table 2)

In the search for broad spectrum antiprotozoan agents, several of them were also screened versus *T. cruzi* and *L. major* DHFR enzymes. Along with *T. brucei* and *Leishmania spp*, *Trypanosomatidae* family include *T. cruzi* which is the etiologic agent of Chagas disease which also poses a great concern in many parts of the world.

To estimate the species-specificity preferences of the compounds towards the parasitic enzymes, the human DHFR (*hDHFR*)

inhibition was then assessed. Finally, the antiparasitic effect (EC_{50}) of the series was evaluated against *T. brucei brucei* and *L. infantum* promastigotes and toxicity (CC_{50}) against THP-1 human macrophages.

Table 2: Inhibition constant (K_i) of compounds (**1**) and (**2**) against TbPTR1, and DHFR enzymes; SD < 5%. Activity is compared with that of CYC, PYR and MTX, as reference.

Cmp	Enzymatic evaluation				
	TbPTR1 Ki (μ M)	TbDHFR-TS Ki (μ M)	hDHFR Ki (μ M)	LmDHFR Ki (μ M)	TcDHFR Ki (μ M)
1a H	15.19	0.054	3.34	0.74	9.7
1b 7(8)-Cl	22.09	0.315	1.64	0.59	1.12
1c 7,8-diCl	53.95	0.258	0.69	1.4	1.17
1d 7,9-diCl	37.14	0.24	1.56	0.24	2.36
1e 7(8)-CF ₃	36.29	0.479	9.96	24.34	14.62
1f 7(8)- OCH ₃	4.35	0.061	10.85	11.93	8.44
1g	11.49	0.655	1.68	3.61	1.98

7,8- diCH ₃					
2a H	16.19	0.034	2.26	//	//
2b 5(6)-Cl	34.5	0.095	2.54	0.8	3.41
2c 5,6-diCl	2.98	0.530	1.26	1.11	//
2d 4,6-diCl	5.41	0.117	3.03	//	//
2e 5(6)-CF ₃	15.67	0.039	3.16	//	//
2f 5(6)- OCH ₃	9.83	0.145	12.74	//	//
2g 5,6- diCH ₃	58.93	0.009	4.42	1.02	0.63
CYC	3.48	0.256	0.27	ND	ND
PYR	0.016	0.032	0.57	ND	ND
MTX	0.144	0.0055	0.0031	ND	ND

ND: not determined

This study points out the ability of the compounds to mainly target *Tb*DHFR with sub-micromolar potencies and *Tb*PTR1 at lower extent. In general, the 2-guanidino benzimidazoles result to be more potent than tricyclic derivatives. In particular, compound **2g** is found to be the best performing inhibitor of *Tb*DHFR ($K_i = 9$ nM), endowed with 6500-fold higher selectivity than *Tb*PTR1 ($K_i =$

58.93 μM). In perspective, this highly selective and potent *Tb*DHFR inhibitor is worthy of further investigations in drug combination tests with a potent and selective *Tb*PTR1 inhibitor, conceivably with a view to getting a better management of HAT. Regarding the other DHFRs from *L. major* and *T. cruzi*, the first enzyme seems to be more sensitive, against which approximately 60% of the compounds tested show sub-micromolar K_i values. The 7,9-diCl triazino benzimidazole (**1d**) and the unsubstituted analogue (**1a**) are the most effective inhibitors with K_i equal to 0.24 and 0.74 μM versus the *Lm*DHFR. The same compound exhibit 5- and 11-fold preferential selectivity for *Lm*DHFR, compared to the human and *T. cruzi* enzymes.

These encouraging data let envisage the validity of these chemotypes towards the development of broad-spectrum antiprotozoal agents.

The compounds initially underwent the evaluation of toxicity profile towards the monocytic THP-1 cell line of human leukemia. (Table 3)

Apart from the 7,8-dichloro-2-aminotriazino compound (**1c**) which exhibits some degree of cytotoxicity ($\text{CC}_{50} > 50 \mu\text{M}$), the other compounds show a high margin of safety ($\text{CC}_{50} > 100 \mu\text{M}$). Interestingly, the highest affinity valued for the hDHFR ($K_i = 0.69 \mu\text{M}$) experienced by **1c** well matches up with the observed toxicity in cell-based assays.

Table 3: Antiparasitic activity (EC50), against *Tbrucei* in folate deficiency conditions (w/o), cytotoxicity (CC50) and selectivity index (SI); data are from two independent experiments, SD < 10%.

Cmp	Cellular activity					<i>L.infantum</i> EC50
	<i>Tbrucei</i> EC50 μM	<i>Tbrucei</i> EC50 μM w/o	CC50 μM	SI CC50/EC50	SI CC50/EC50 w/o	
1a H	>20	>20	>100	//	//	>20
1b 7(8)-Cl	>20	>20	>100	//	//	>20
1c 7,8- diCl	>20	>20	>50	//	//	>20
1d 7,9- diCl	>20	>20	>100	//	//	>20
1e 7(8)- CF ₃	>20	>20	>100	//	//	>20
1f 7(8)- OCH ₃	>20	>20	>100	//	//	>20
1g 7,8- diCH ₃	6.63	18.18	>100	15.08	5.5	>20
2a	>20	>20	>100	//	//	>20

H						
2b 5(6)-Cl	15.21	15.16	>100	6.58	6.60	>20
2c 5,6- diCl	7.82	6.52	95.3	12.19	//	22.50
2d 4,6- diCl	2.91	5.97	>100	34.38	16.76	6.62
2e 5(6)- CF ₃	18.18	>20	>100	5.5	//	>20
2f 5(6)- OCH ₃	>20	>20	>100	//	//	>20
2g 5,6- diCH ₃	14.47	13.81	>100	6.91	7.2	>20
CYC	>80	27.19	221	//	8.12	>80
PYR	17.3	2.08	105	6.07	50.4	99.22
MTX	23.3	0.0054	ND	//	//	//

ND: Not determined.

On the base of the enzymatic results, the title derivatives were evaluated for their in vitro antiparasitic activities against cultured bloodstream form of *T. brucei brucei* and promastigote stage of *L. Infantum*. From the data obtained it can be observed that the most sensitive parasite to the action of the compounds is *T. brucei* with the 2-guanidino benzimidazole compound (**2d**) showing the lowest

EC₅₀ value, equal to 2.91 μM. This compound also demonstrates to be active against *L. infantum* (EC₅₀= 6.62 μM) together with **2c** (EC₅₀= 22.5 μM), comparing favourably with the reference drug Miltefosine, EC₅₀= 8.90 μM.

Regarding the 2-guanidino benzimidazoles, they exhibit an EC₅₀ value trend in the low micromolar range, between 2.9 (**2d**) and 15.2 μM (**2b**). The four compounds endowed with activity are mono-substituted at position 5 (**2b**, **2e**), di-substituted at positions 5 and 6 (**2g**), or 4 and 6 (**2d**) of the benzimidazole ring with lipophilic groups, both electron-withdrawing (Cl, CF₃) and electron-donating (CH₃). Substitution with polar groups such as 5-OCH₃ (**2f**) rather than the absence of substituents in the aforementioned positions (**2a**) are associated with the loss of activity (EC₅₀ > 20 μM). In the set of triazino benzimidazoles, only the 7,8-dimethyl substitution (**1g**) is tolerated, while the other lipophilic and electron-withdrawing groups Cl and CF₃ exert a negative effect, respectively abolishing the activity (**1b**) or causing cytotoxicity (**1c**, CC₅₀> 50 μM).

The screening against *T. brucei* carried out in folate deficiency (w/o folate), aimed at verifying the possible competitive inhibition behaviour of the investigated molecules against the natural substrate of TbDHFR, did not explicitly confirm this hypothesis, as the effective concentrations are similar to those obtained in standard culture conditions. On the contrary, in the case of CYC, and more evidently for MTX, the activity notably increases in

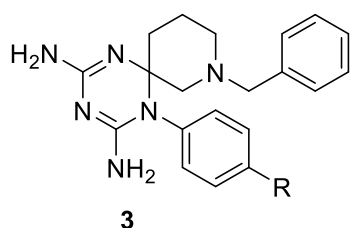
folate deficiency medium. MTX shows a 23.3 μM activity in standard conditions and nanomolar activity ($\text{EC}_{50} = 5.4 \text{ nM}$) in folate deficiency medium, with a ratio of 4300.

This behaviour of series 1 intimates that other mechanisms of action may contribute to the observed antiparasitic effect, warranting further investigations.

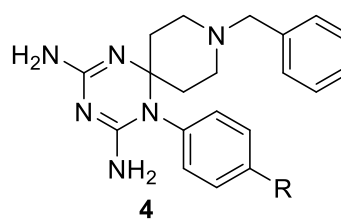
SERIES 2

The present series was developed on the base of the dual inhibition of *Tb*DHFR and *Tb*PTR1 showed by CYC and the 30-fold increase of the inhibitory performance against *Tb*PTR1 displayed by a closely-related dihydrotriazine analogue, characterized by a bulky spiro-cyclohexyl moiety in place of the two methyl groups at C(6) of CYC. The tolerance for cumbersome groups of *Tb*PTR1 hydrophobic pockets close to the enzyme catalytic one was observed also for other chemotypes⁽¹⁰²⁾.

Thus, the dihydrotriazine scaffold of the novel compounds was substituted in position 1 with an aromatic ring, variously functionalized, and the benzyl-piperidine spirane moiety out of the C(6) of CYC to increase the compound lipophilicity with respect to CYC and probe the impact of a higher steric hindrance.



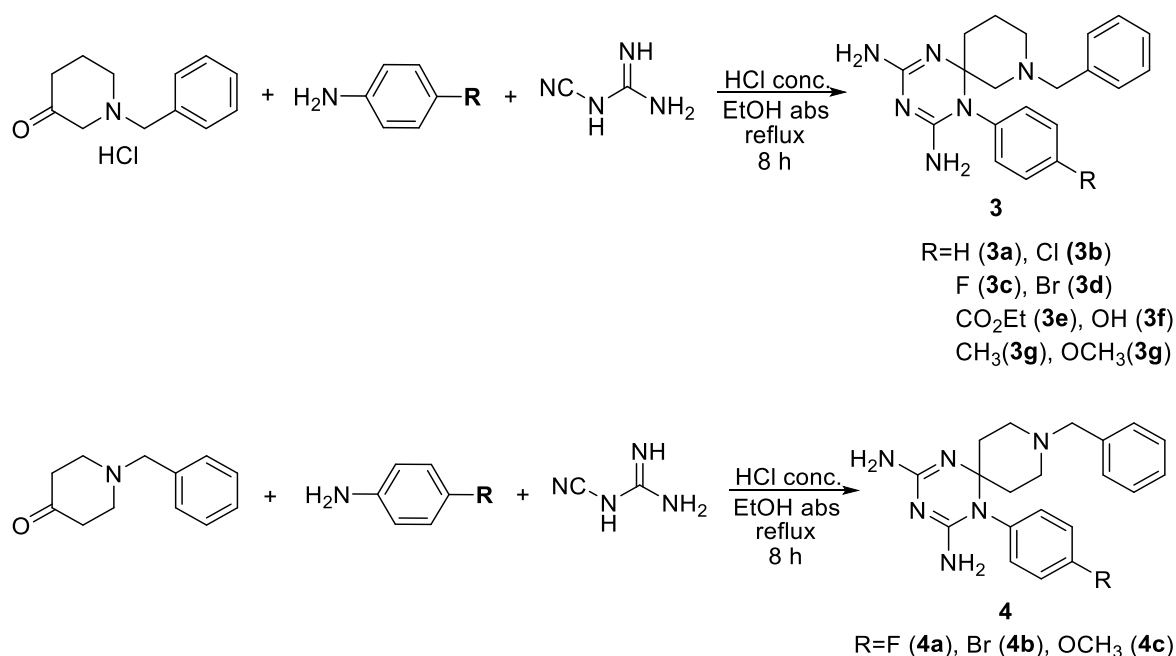
R=H (**3a**), Cl (**3b**)
F (**3c**), Br (**3d**)
CO₂Et (**3e**), OH (**3f**)
CH₃(**3g**), OCH₃(**3g**)



R=F (**4a**), Br (**4b**), OCH₃ (**4c**)

Chemistry

Compounds **3** and **4** were synthesized by a one pot acid-catalyzed cyclocondensation, where a solution of the proper aniline, N-benzyl-3-piperidone hydrochloride, or N-benyl-4-piperidone and dicyandiamide were refluxed in absolute ethanol for 8 hours in the presence of triethyl orthoacetate, as a water scavenger (Scheme 4).



Scheme 4.

The progress of the reaction was monitored, observing the negative result of coloured copper complex which forms characteristically between the biguanide intermediate product with a freshly cuprammonium sulphate solution.

The structure of the novel compound was confirmed using ¹H and ¹³C NMR and elemental analysis.

In vitro biological profiling

The compounds underwent enzymatic screening and biological evaluation against *T. brucei* and *L. infantum*. In Table 4 are summarized the results till now available.

Table 4: Inhibition constants (K_i) on TbPTR1, TbDHFR-TS, and hDHFR and cytotoxicity (CC₅₀) and antiparasitic activity (EC₅₀) against *T. brucei* of compounds **3** and **4** and reference drugs. Data are from two independent experiments and are expressed as means, SD<10%.

Cpd	Enzymatic screening			Cellular screening		
	TbPTR1 K _i μM	TbDHFR-TS K _i μM	hDHFR K _i μM	<i>Tbrucei</i> EC ₅₀ μM	<i>Tbrucei</i> EC ₅₀ μM w/o	CC ₅₀ μM
3a H	0,452	12,01	2,023	>20	ND	ND
3b 4-Cl	0,166	3,32	0,451	2,11	ND	ND
3c 4-F	0,361	7,7	0,501	4,88	5,00	60,15
3d 4-Br	1,032	9,03	0,472	1,90	1,0	34,41
3e 4- CO ₂ Et	ND	ND	ND	6,7	5,83	61,58
3f 4-OH	ND	ND	ND	>40	>40	323,2
3g 4-CH ₃	ND	ND	ND	16,17	12,34	239

3h 4- OCH ₃	ND	ND	ND	17,67	>40	127,5
4a 4-F	0,614	9,21	0,357	>40	>40	109
4b 4-Br	ND	ND	ND	21,3	6,42	127,2
4c 4- OCH ₃	ND	ND	ND	>40	>40	216,7
CYC	3,48	0,256	0,27	>80	27,19	221
PYR	0.016	0,032	0,57	17,03	2,08	105
MTX	0,144	0,0055	0,0031	23,3	0,0054	ND

ND: Not determined.

By the results the compounds showed to target both folate enzymes of *T. brucei*, with a PTR1 preferential inhibition of about one order of magnitude with respect to DHFR. The unsubstituted derivative **3b** and the 4-F-phenyl analogue (**3c**) resulted to be as the most active against *Tb*PTR1 and *Tb*DHFR-TS, while the introduction of halogen atoms endowed with an increasing atomic radius as for **3d** (4-Cl) and **3e** (4-Br) is responsible for a slight and stepwise reduction of the Ki value versus both enzymes. However, the compounds also were proven to target the hDHFR, showing the same range of potency experienced against protozoan enzymes (mainly PTR1), thus suggesting the risk of a manifest toxicity. In fact, these data are in agreement with those derived from cellular tests, in which the THP-1 cell line replication was found to be affected by the compounds toxicity. Anyhow the azaspiro compounds were active in the low micromolar range against *T.*

brucei and showed a favorable selectivity index (CC_{50}/EC_{50}) that fell in the range 6 (**4b**) – 18 (**3d**), surpassing the activity profile of reference drugs. None of the compounds caused the inhibition of *L. infantum* cell growth (data not shown). As before discussed for series 1, also series 2 display a comparable anti-*T. brucei* activity both in normal folate and deficiency folate media, therefore implying that other targets/paths could be involved.

The lack of selectivity showed by the enzymatic tests, and the inhibition of hDHFR on an equal basis along with the protozoan folate enzymes, highlighted the need of further investigations. To this aim docking studies were performed, modelling known drugs and compounds **3** and **4** to analyze their interaction with parasite and human enzymes of the folate pathway. The models built were then used as a basis to design new derivatives to inhibit the parasite enzymes more selectively, thus preventing the *hDHFR*-mediated off-target effects.

3. Molecular modeling studies

From the biological evaluations of these compounds we gain important information: one of them is their lack of selectivity. In order to design new more selective compounds, the first step was molecular docking, to understand on a molecular level the behaviour of the azaspiro-2,4-diamino-1,6-dihydrotriazine in our targets.

In this chapter, methods and results from molecular docking will be discussed, moreover will be discussed the idea behind the new drug design.

3.1 Methodology

Compounds Preparation

All the compounds considered in this study were drawn in 2D, using the Maestro 2D sketcher. The force field applied was OPLS_2005 from Schrödinger LigPrep⁽¹⁰³⁾. Generation of stereoisomers up to 8 per compound, possible tautomers and ligand ionization states between pH 7.0 ± 1.0 were determined with Ionizer.

Protein Preparation

TbPTR1

PDB-ID: 2X9G⁽⁷⁹⁾, split the protein in chains and pick chain A, PTR1 has an arginine or histidine from a neighbouring subunit pointing into the active site of another chain that should be included for docking. Select chain D and import the last amino acid sequence VHA (for TbPTR1: Val266-His267-Ala268). Merge it with chain A.

Import methotrexate structure from PDB-ID: 2C7V.

Solvent molecules were eliminated, for TbPTR1, and replaced with 17 water molecules identified by Watch clustering^(104,105).

Protein hydrogens and bond orders were added using the Protein Preparation Wizard of Schrodinger Maestro^(106,107).

The protonation states of the NADPH/NADP⁺ cofactor and the amino acid residues for pH 7.0 were determined with Epik⁽¹⁰⁸⁾ and PROPKA, respectively.

The hydrogen-bonding network was optimized and all hydrogen positions were minimized in a restrained energy minimization with the OPLS 2005 force field.

TbDHFR and hDHFR

For *TbDHFR* PDB-ID:3RG9⁽⁷⁸⁾. There is no need to use conserved water molecules, import methotrexate from PDB-ID: 3CL9⁽¹⁰⁹⁾. Split the protein by chain and use chain A.

For *hDHFR* PDB-ID: 1U72⁽¹¹⁰⁾. Split the protein by chain and use subunit A. There's no need to use conserved solvent molecules or to import Methotrexate structure.

For protein preparation use the above mentioned protocol.

Grid Generation

Identify the ligand as “Molecule” by clicking on MTX.

Grid centers:

- TbPTR1: Phe97
- TbDHFR: Phe58
- hDHFR: Phe34

Rotatable groups:

- for TbPTR1: OH/SH in Ser95, Cys168, Tyr174 and NADP⁺ ribose, the one bound to nicotinamide.
- For TbDHFR: OH in Thr46, Thr62, Thr86, Ser89, Ser98, Tyr166, Thr184 and NADP⁺ ribose.
- For hDHFR: OH in Thr38, Thr39, Ser59, Tyr121 and NADP⁺ ribose.

Rigid Docking

For the docking, we used Schrödinger Glide⁽¹¹¹⁾ protocol XP (eXtra Precision).

Ligand sampling is flexible, select: sample nitrogen inversions and ring conformations.

Bias sampling for torsion for amides only: penalizing nonplanar conformations. Add Epik⁽¹⁰⁸⁾, enhance planarity of conjugated pi groups and reward intramolecular hydrogen bonds.

Problems&problem solving for rigid docking

Using the protocol mentioned above we faced a big problem. The compounds did not fit in the active site (figure 20)

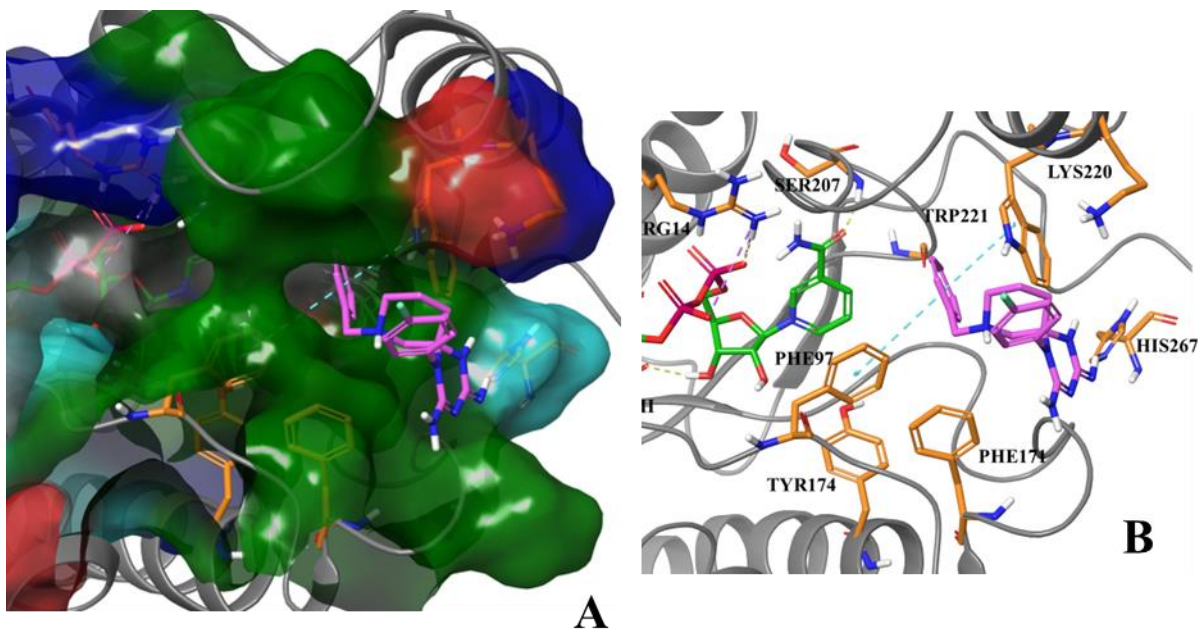


Figure 20: first rigid docking, compound 3c (magenta), orange chemical. Composition of PTR1 active site. Compound 3c outside the active site.

To overcome this problem, we docked pyrimethamine (PYR) (IC_{50} 0.090 μ M) with the same protocol. (Figure 21)

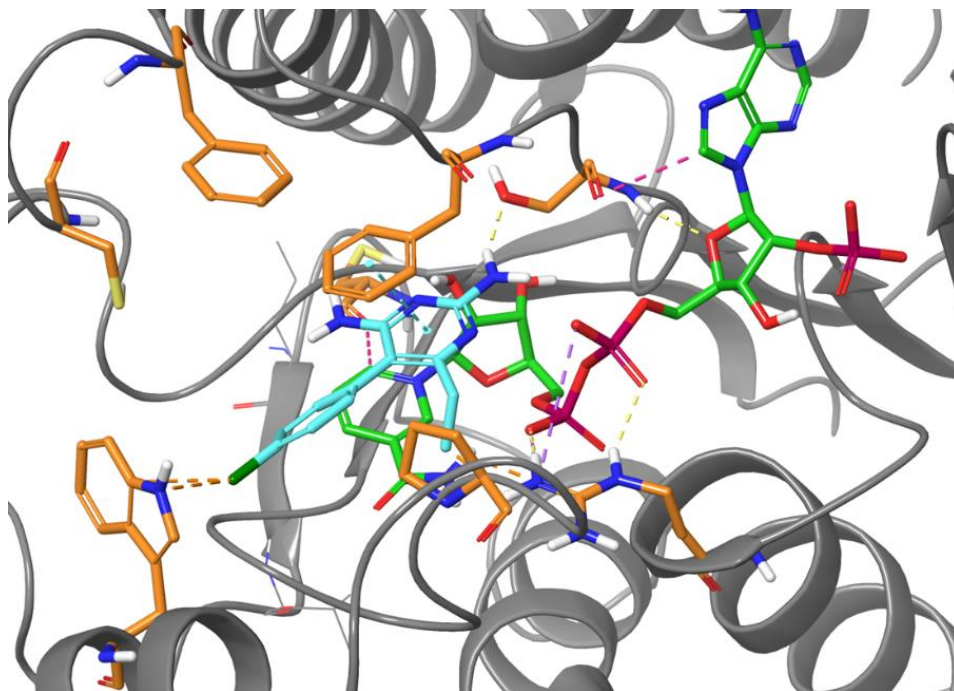


Figure 21: Pyrimethamine in PTR1 active site

Subsequently, using Maestro 3D sketcher, the benzyl-piperidonic moiety was added, and Desmond Minimization⁽¹¹²⁾ was used to reduce the clashes.(Figure 22)

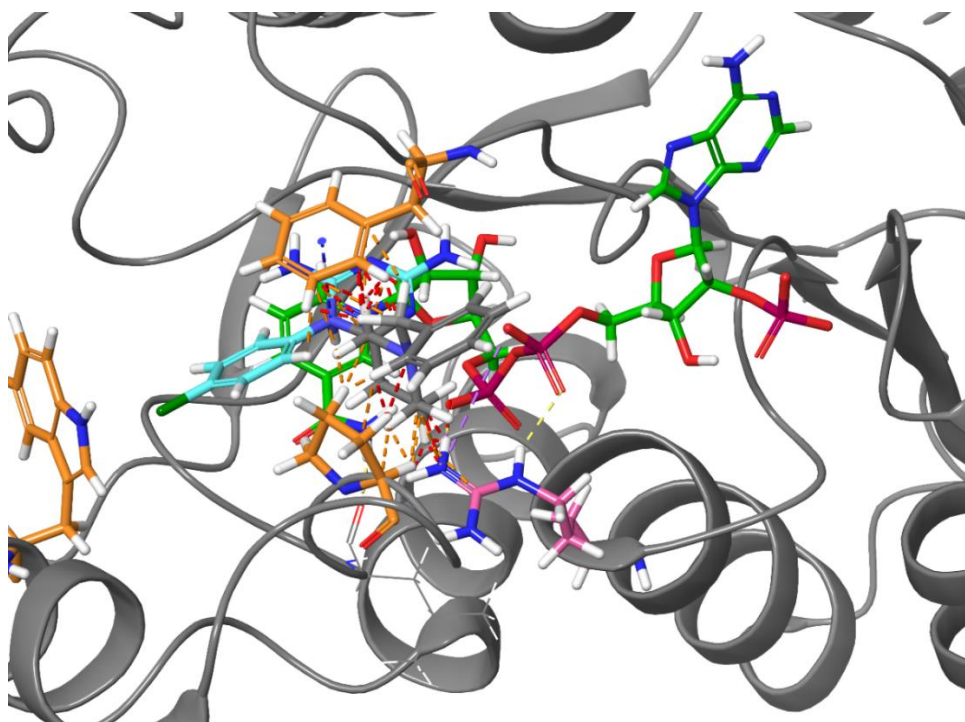


Figure 22: azaspiro-like compound manually designed in 3D, we added the benzyl-piperidone moiety (grey licorice), red and orange dashes represent bad clashes, visualization before Desmond minimization.

Desmond Minimization⁽¹¹²⁾ panel executes a quick low-temperature Brownian motion Molecular Dynamics simulation to remove steric clashes and move the system away from an unfavorable high-energy conformation. (*Figure 23*)

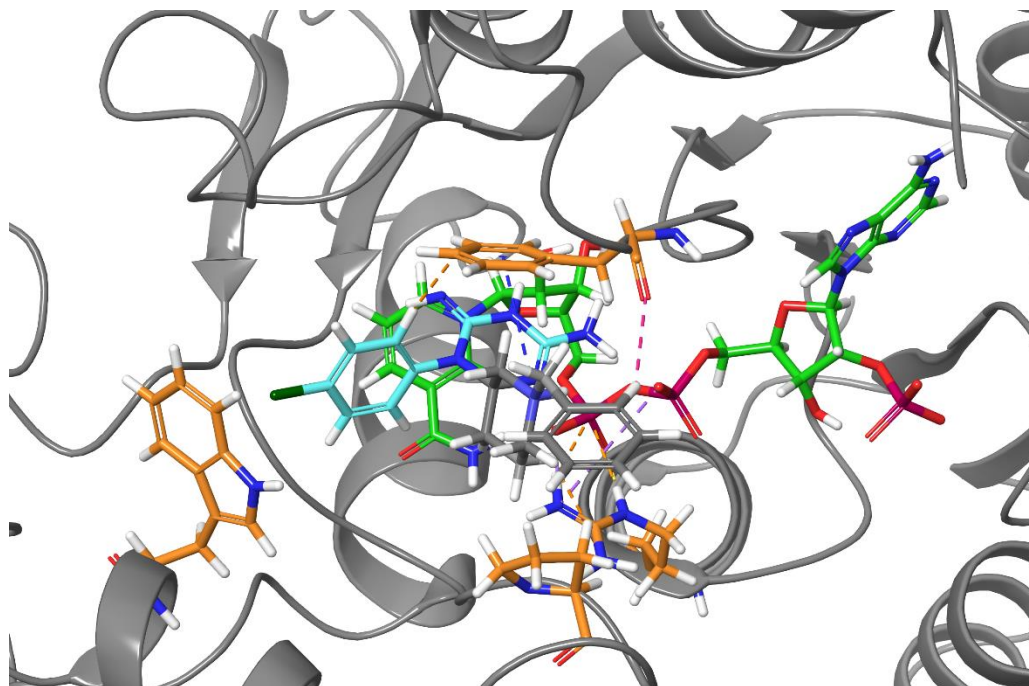


Figure 23: active site with azaspiro dihydrotriazine compound manually drawn after Desmond minimization, clashes resolved.

The protein conformation obtained from Desmond minimization was used for docking the compounds discussed in this thesis work. The new model was validated by docking the Cycloguanil structure from PDB-ID 6HNC⁽⁹⁴⁾ in our model. The pose was maintained, we calculated the RMSD of the ligands. (figure 24)

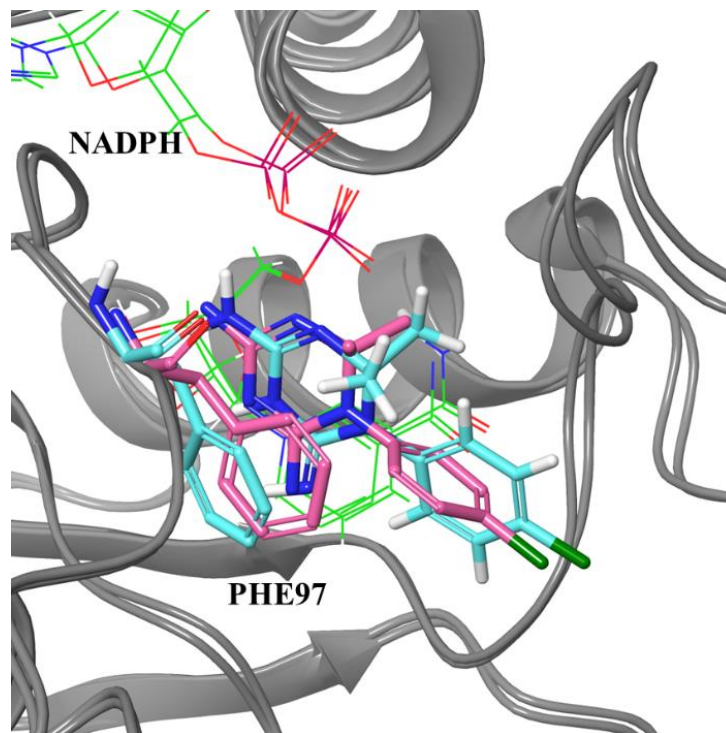


Figure 24: validation on PTR1. Superimposition: Magenta CYC and Phe97 from crystal structure PDB-ID 6HNC, cyan CYC and Phe97 docked in our model. RMSD of ligands atoms = 0.3 Å.

The same process was repeated on TbDHFR with PYR from PDB-ID: 3QFX⁽⁷⁸⁾ and hDHFR with compound 9DR from PDB-ID: 4KD7⁽¹¹³⁾ (figure 25).

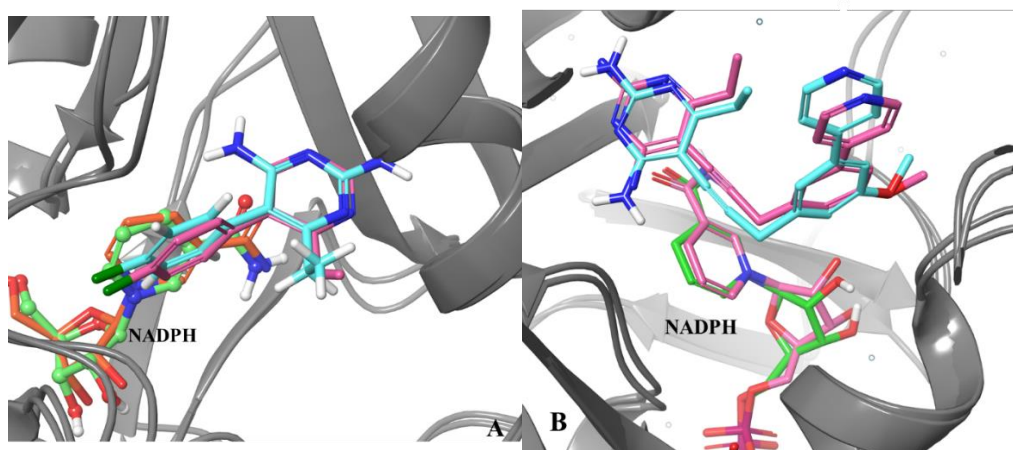


Figure 25: A) validation on TbDHFR superimposition (magenta PYR in PDB-ID: 3QFX, cyan PYR in our model. RMSD = 0.2 Å) B) validation on hDHFR (magenta 9DR compound in PDB-ID 4KD7, cyan 9DR in our model RMSD = 0.25 Å).

Subsequently, we docked all the compounds with the rigid docking using the protocol above mentioned.

Induced Fit Docking

For Induced Fit Docking⁽¹¹⁴⁾ (IFD), we used the Standard protocol. The centroid in TbPTR1 receptor is Phe97. We also select the sample ring conformations with Energy window 2.5 Kcal/mol, penalizing nonplanar conformation for Amide bonds and enhancing planarity of conjugated pi groups.

Then, with Glide we set: the receptor van der Waals scaling: 0.5, ligand van der Waals scaling 0.5 and the maximum number of poses (20 poses).

In Prime refinement: we select to refine residues within 5 Å.

In Glide redocking we select to redock into structures within 30.0 kcal/mol of the best structure, and within the top 20 structures overall, setting the precision as XP (eXtra Precision).

3.1 Molecular Docking

We analyzed all the azaspiro-2,4-diamino-1,6-dihydrotriazines from a computational point of view against *Trypanosoma brucei* enzymes PTR1, TbDHFR and also hDHFR.

For the docking, Schrodinger Glide was used, employing XP protocol for the rigid docking, with the settings mentioned in the previous chapter.

Crystal structures used: PTR1 (PDB 2x9g resolution 1.10 Å), TbDHFR (PDB 3RG9 resolution 2.0 Å), hDHFR (PDB 1u72 resolution 1.90 Å), PDB were chosen according to resolution.

The molecular docking generates up to 80 poses, and we chose the best one.

It can be seen that the docking results agree with the biological results of this series of compounds, more specifically the absence of selectivity and the lack of inhibition of the two parasitic enzymes in equal measure. It is not possible to correlate them directly but they can be taken as a basis for the design of future molecules.

(Table 5)

Table 5: XP rigid docking scores, the more negative is the score, the better the affinity towards the enzyme. In brackets the -R group on the aromatic ring of every compound.

Compound	Docking scores		
	PTR1	TbDHFR	hDHFR
3b (Cl)	-8.2	-8.3	-9.6
3c (F)	-8.5	-7.1	-9.5
3d (Br)	-7.7	-8.2	-9.6
3e (CO ₂ Et)	-7.5	-7.1	-9.5
3f (OH)	-8.8	-6.6	-9.5
3g (CH ₃)	-8.3	-8.3	-9.5
3h (OCH ₃)	-7.5	-7.1	-9.3
4a (F)	-8.5	-8.0	-7.9
4b (Br)	-8.8	-8.2	-6.0

4c (OCH ₃)	-8.2	-7.9	-4.9
----------------------------------	------	------	------

Later we compare the poses ranked by Glide, with the preliminary crystal structures and we notice that they match with the results of the Induce Fit Docking. (Figure 26)

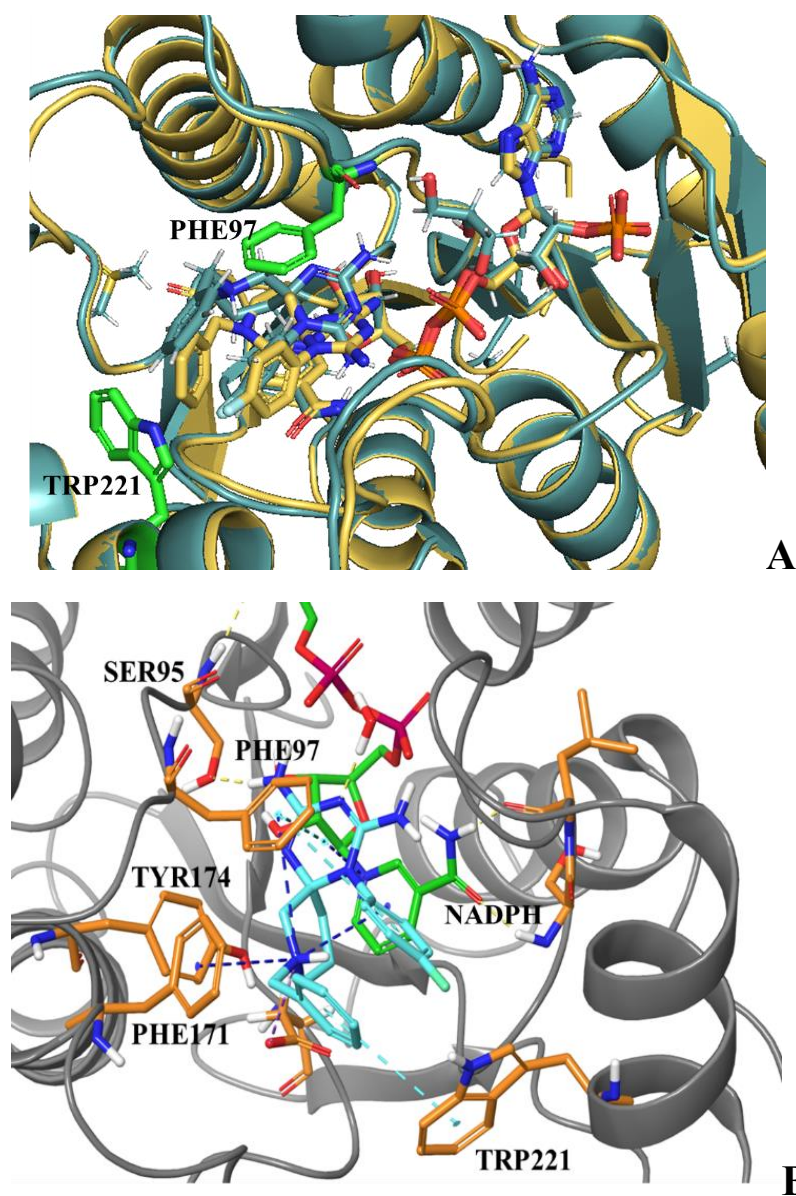


Figure 26: A) Superimposition between the crystal structure of compound **3c** in PTR1 active site (yellow, unpublished data from C. Pozzi, University of Siena) and the result from the Induced Fit Docking (IFD) (blue, cartoon representation for the protein, licorice representation for the ligands). Picture visualized with Pymol⁽¹¹⁵⁾. In green residues Phe97 and Trp221. RMSD: 3.4 Å.

B) IFD of compound **3c** (cyan), interaction between the compounds and PTR1 active site (yellow H-bond, Cyan π - π , and dark blue π -cation).

The preliminary crystal structure allow us to have a better idea of the real pose assumed by our compounds in PTR1 active site.

Unfortunately, is not possible to ascertain the poses for the other enzymes, as the crystal structures are not yet available, consequently it is not possible to establish which are the main ligand-protein interactions.

What came out from all these experiments is that the triazine ring, in both docking method used, keep the interactions mentioned for the CYC. The π -sandwich interactions between the triazine ring, the nicotinamide ring and Phe97 is maintained.

Halogens such as chlorine and bromine can provide a halogen bond with Trp221 because they have a bigger atomic ray, rather than fluorine.

The N-benzyl portion can provide an extra interaction with the residue Phe171.

We investigated also the ADME properties of this set of compounds using Qikprop⁽¹¹⁶⁾. (Table 6)

Table 6: Descriptors for compounds serie 3&4 calculated with Qikprop⁽¹¹⁹⁾. QPlogKp: skin permeability; QPlogPo/w: octanol/water partition coefficient; QPlogKhsa: binding to human serum albumin. CIQPlogS: Conformation-independent aqueous solubility log S, with S in mol dm³ (concentration of solute in a saturated solution in equilibrium with the crystalline solid). CNS: Predicted central nervous system activity. %Human Oral Absorption: Predicted human oral absorption on 0 to 100% scale. The prediction is based on a quantitative multiple linear regression model. This property usually correlates well with HumanOralAbsorption, as both measure the same property.

	Predicted value						
	CNS	QPlogKp	QPlogKhsa	QPlogPo/w	CIQPlogS	%H.Oral Abs.	QPlog Herg
Recc. Range	-2—+2	-8.0 -1.0	-1.5 - 1.5	-2.0 - 6.5	-6.5 - 0.5	>80% <20%	concern below -5
Cmp							
3b	0	-4.763	0.280	2.601	-4.540	80.746%	-5.104
3c	0	-4.850	0.189	2.149	-4.223	77.489%	-4.493
3d	0	-4.731	0.332	2.829	-5.411	81.479%	-5.886
3e	-2	-6.495	-0.128	-0.308	-3.953	36.864%	-3.217
3f	-2	-5.604	0.060	1.583	-3.831	64.526%	-6.028
3g	0	-4.624	0.321	2.526	-4.146	81.224%	-5.534
3h	0	-4.503	0.147	2.157	-4.204	78.310%	-5.471
4a	0	-4.728	0.154	2.140	-4.223	78.100%	-4.817
4b	0	-4.854	0.215	2.364	-5.411	78.702%	-4.894
4c	0	-4.716	0.182	2.186	-4.203	76.714%	-5.654

Drug design

In order to improve the affinity versus the parasitic enzymes, we analyzed the space around the ligands, using Maestro Ligand Designer, and noticed that was possible to increase the length of the N-benzyl chain. (Figure 27)

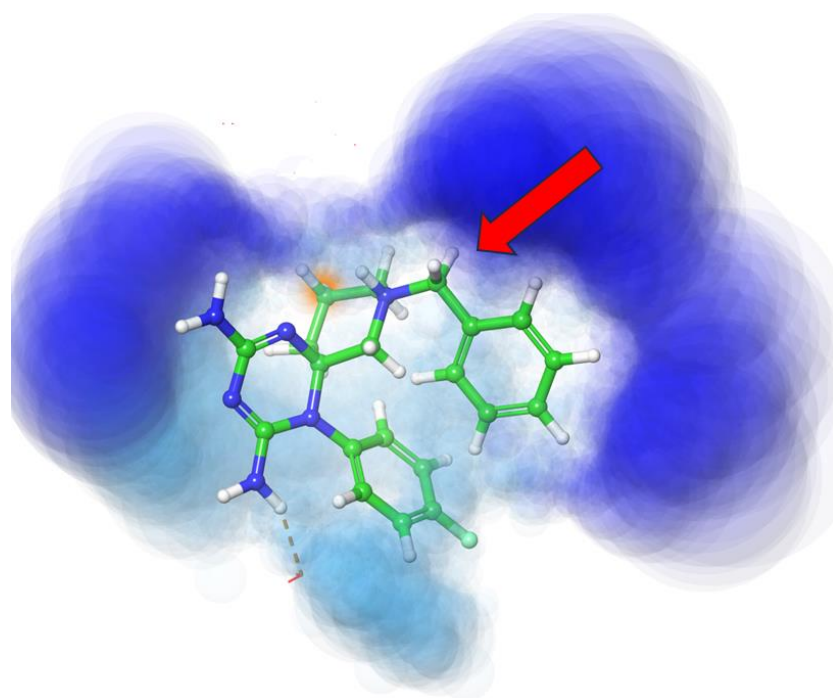


Figure 27: graphic representations of compound 3c, visualized with Maestro ligand designer tool. The blue cloud represent the available growth surface. The arrow indicates the moiety that we planned to modify.

For the library generation, we selected as parameters to increase the length of the side chain with -R groups and replacing the aromatic ring with isosters. The goal behind these choices was to explore how modifications of the benzyl moiety could impact

affinity and binding mode towards the enzymes object by this study.

The library generated by Maestro, consisting of more than two hundred compounds, was screened by docking each compound in our targets, the best one, UNK_04, was chosen as lead compound for the new drug design. (Figure 28)

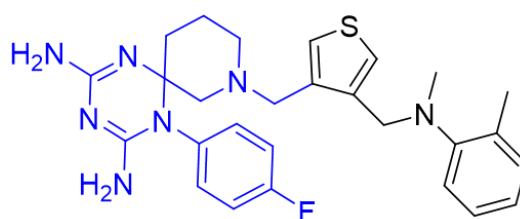


Figure 28: UNK_04 with docking scores

PTR1 XP Glide rigid docking score: -8.7 kcal/mol
TbDHFR XP Glide rigid docking score: -8.5 kcal/mol
hDHFR XP Glide rigid docking score: -5.5 kcal/mol

Despite the good scores, we tried to improve the affinity for the parasitic enzymes by changing the part of the chain that was not involved in any kind of relevant interactions.

The idea was to increase the number of hydrogen interactions within the parasitic enzymes, thereby increasing affinity and stability.

The first modification is represent by compounds UNK_4_mod. (figure 29)

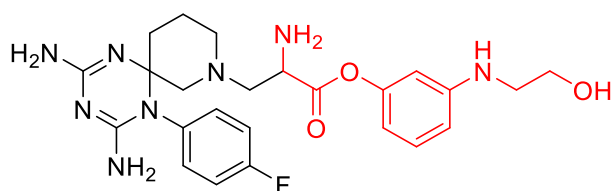


Figure 29: UNK_4_mod

We actually increase the number of hydrogen bonds, but the aminoethanol chain is still exposed to the solvent. (figure 30)

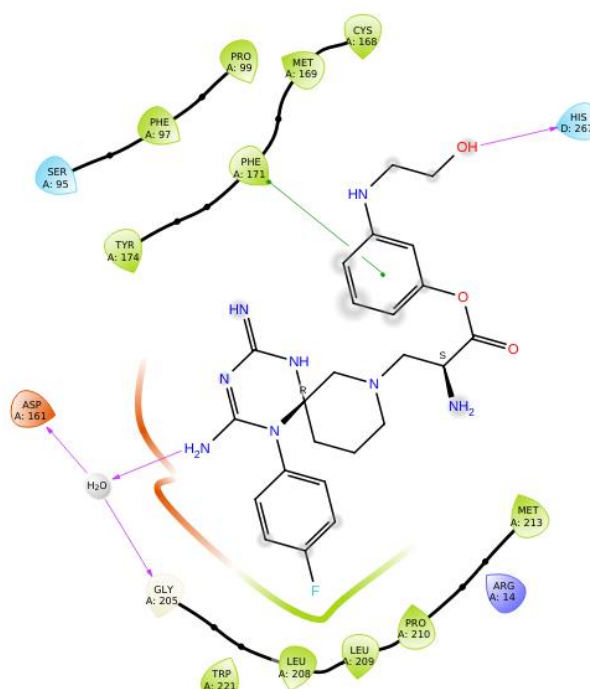


Figure 30: Compound UNK_4_mod in PTR1 active site, Ligand 2D diagram, grey dots represent the solvent exposition. The introduction of the aminoethanol chain provides an extra H-bond with His267, while by distancing the benzyl portion from the azaspiro ring we gain an extra π - π stacking interaction with Phe171.

To avoid this level of exposition, we modified the aminoethanol chain with a hydroxymethyl chain, which is shorter than the previous one, and the oxygen from the hydroxyl group could provide an extra hydrogen bond.

The position of the aromatic ring is unchanged. (Figure 31)

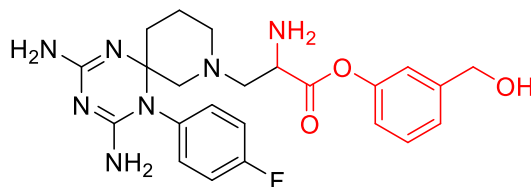


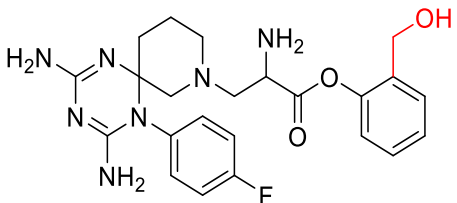
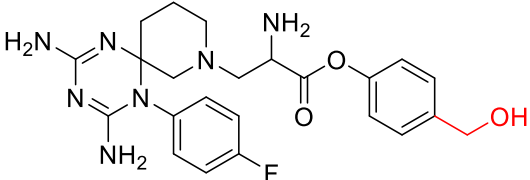
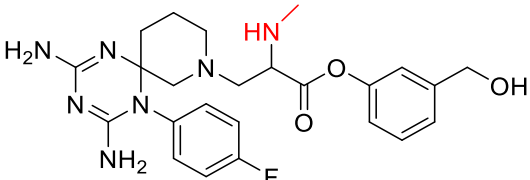
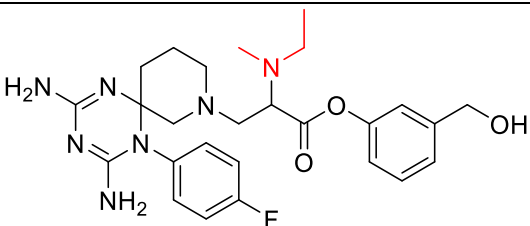
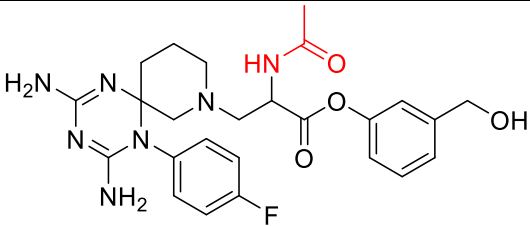
Figure31:UNK_4_1

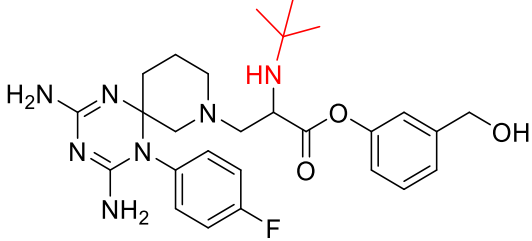
Table 7: XP rigid docking scores of compound UNK_4_1.

Docking Scores Kcal/mol		
PTR1 PDB:2x9g	TbDHFR PDB:3rg9	hDHFR PDB:1u72
-9.1	-9.2	-7.74

From the scores given by the docking of compound UNK_4_1, it is possible to see that the affinity towards the parasitic enzymes is improved, while the affinity versus the human isoform is decreasing (XP glide rigid docking score: -7.74 kcal/mol).

Table 8: N.T. not tested because the scores on PTR1 were no better than the reference compound Porto35. In this table are reported in red all the modifications attempted on this first set of new compounds.

Compound	Docking scores Kcal/mol		
	PTR1	TbDHFR	hDHFR
 UNK_4_1_1	-8.55	N.T.	N.T.
 UNK_4_1_2	-8.9	N.T.	N.T.
 UNK_4_1_3	-7.79	N.T.	N.T.
 UNK_4_1_4	-9.76	N.T.	-9.06
 UNK_4_1_5	-8.31	-5.4	N.T.

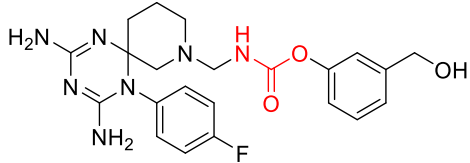
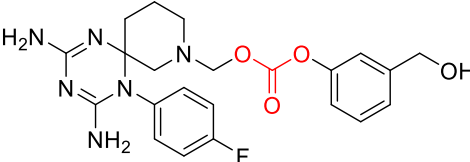
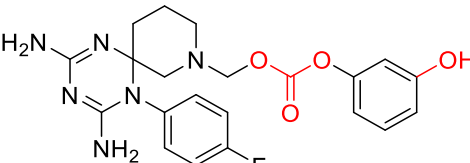
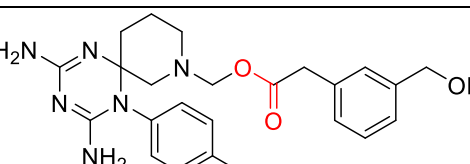
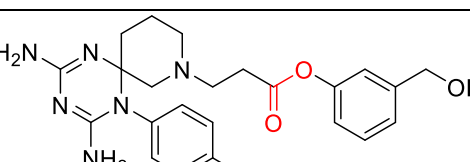
 <p>UNK_4_1_6</p>	-9.23	-8.95	-5.5
--	-------	-------	------

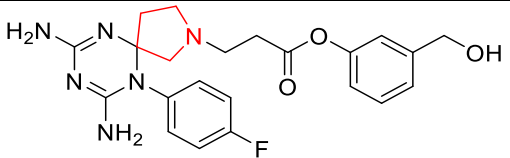
In order to further improve selectivity, we explore how different modification on the $-NH_2$ group, reported in table 8, may affect the binding mode.

We also change the hydroxymethyl chain position, to see if this could have a role in improving the docking scores.

We only tested compounds with a score below -9 on PTR1, taking Porto-35 score as reference, in order to discard the bad ones. From this first row of compounds only compounds UNK_4_1_6 seems to show good qualities in terms of scores, unfortunately that extra amine group could provide an extra positive charge and complicate, due to the basicity of the compounds, purifications and stability. We decided to remove it and change again the structure. (Table 9)

Table 9: docking scores of the serie UNK_4_2.

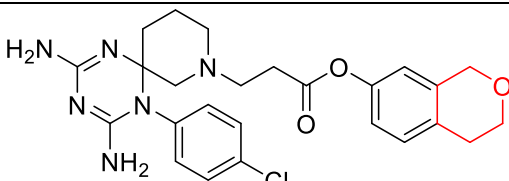
Compound	Docking scores Kcal/mol		
	PTR1 PDB:2x9g	TbDHFR PDB:3rg9	hDHFR PDB:1u72
 UNK_4_2_1	-8.56	-8.37	-6.05
 UNK_4_2_2	-9.2	-8.69	-5.7
 UNK_4_2_3	-8.25	N.T.	N.T.
 UNK_4_2_4	-7.9	-9.20	-6.53
 UNK_4_2_5	-9.09	-9.05	-6.0 PDB:4KD7 -10.5

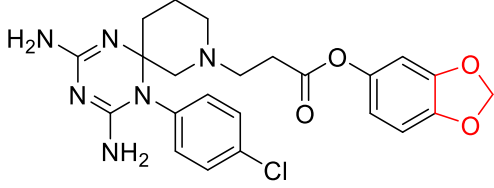
 <p style="text-align: center;">UNK_4_2_6</p>	-8.78	N.T.	N.T.
--	-------	------	------

Only 3 compounds from this set of compounds shows good results, UNK_4_2_1 and UNK_4_2_2, unfortunately they are plagued by instability, and their synthesis would be very difficult. Compound UNK_4_2_5 actually seems to be very promising also from a chemical point of view, but we docked it in another crystal structure of the human enzyme (PDB-ID: 4KD7) that presents a more opened active site and the score improved to -10.5 Kcal/mol.

The last modification we attempted is the replacement of the hydroxymethyl chain with a heterocycle moiety. (Table 11)

Table 10: docking scores of the new modifications applied to compound UNK_4, the replace of the hydroxymethyl chain with a dioxol moiety seems to be promising.

Compound	Docking score Kcal/mol		
	PTR1 PDB:2x9g	TbDHFR PDB:3rg9	hDHFR PDB:1u72
 <p style="text-align: center;">UNK_4_3_1</p>	-8.9	-9.94	-6.51

 <p style="text-align: center;">UNK_4_3_2 (HD_1)</p>	-9.4	-9.4	-5.6 4KD7 -7.6
---	------	------	----------------------

Compound UNK_4_3_2 (HD_1) shows good results, in terms of scores towards the parasitic enzymes (-9.4 kcal/mol on PTR1 and TbDHFR compared to our reference compound Porto35 -8.5 kcal/mol on PTR1 and -7.7 on TbDHFR).

Compound HD_1 also shows an improvement in selectivity (-5.6 Kcal/mol on hDHFR versus -9.5 Kcal/mol of compound against Porto35), this difference is maintained also in the second human crystal structure (PDB-ID 4KD7), that presents a more open structure (XP rigid docking score: -7.5 kcal/mol), ensuring a gap of two orders of magnitude.

The chlorine atom on the aromatic ring in position 7 can be substituted with fluorine and bromine or different electron-donor or electron-withdrawing groups.

All these considerations allow us to think that compound UNK_4_3_2 (HD_1), might represent the ideal candidate for a new generation of azaspiro-dihydrotriazines.

Lately, compound HD_1 has been docked in PTR1 active site using the Induced Fit Docking technique and the outcome has been superimposed with the preliminary crystal structure of compound **3c**. (Figure 32)

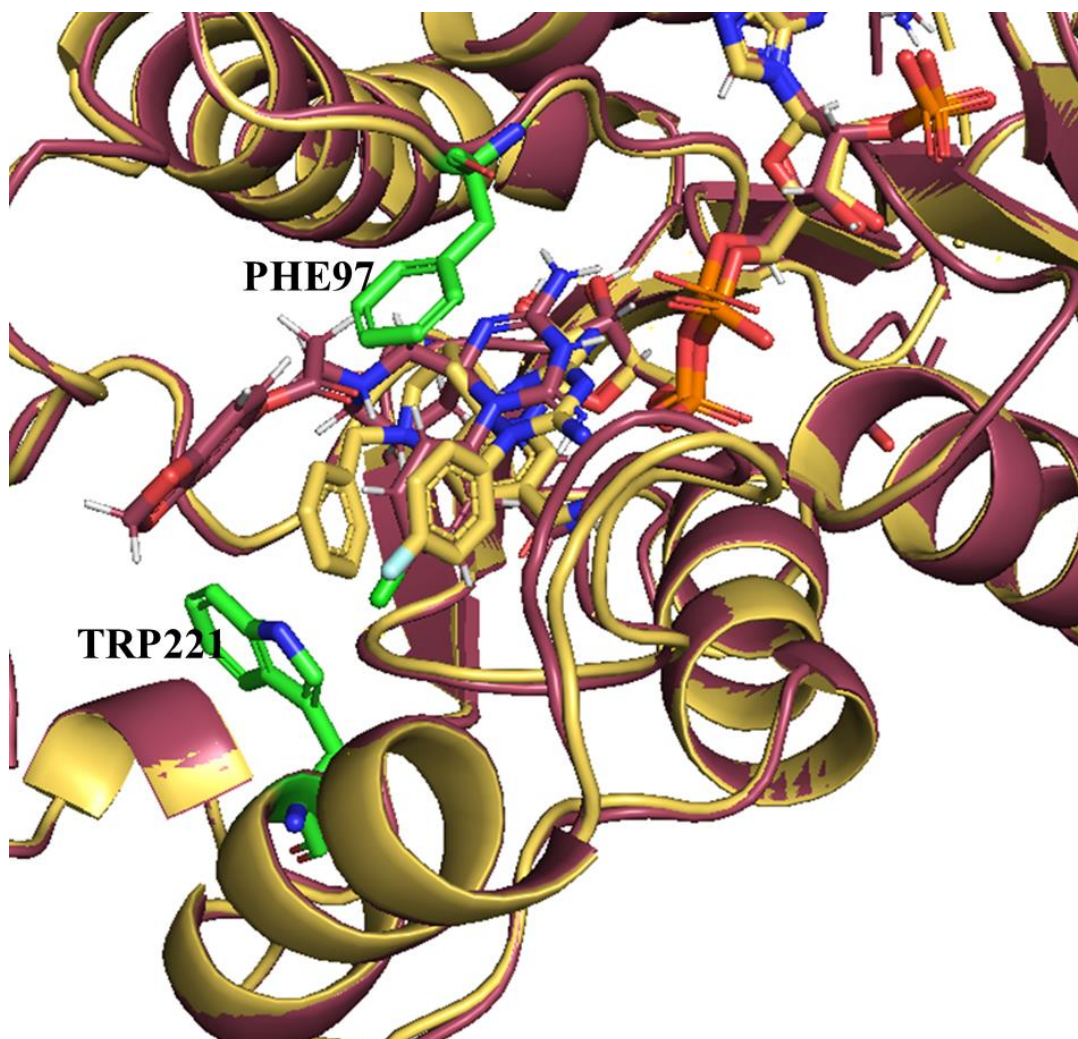


Figure 32: superimposition between the crystal structure of compound **3c** (yellow gold) and compound HD_1 (dark pink) in PTR1 active site. RMSD 3.8 Å.

Further investigations are needed to ascertain the stability of this compound within the three enzymes under investigation in this study, but this might represent the first step forward in achieving an equally powerful, and selective cycloguanil-like inhibition towards parasitic enzymes.

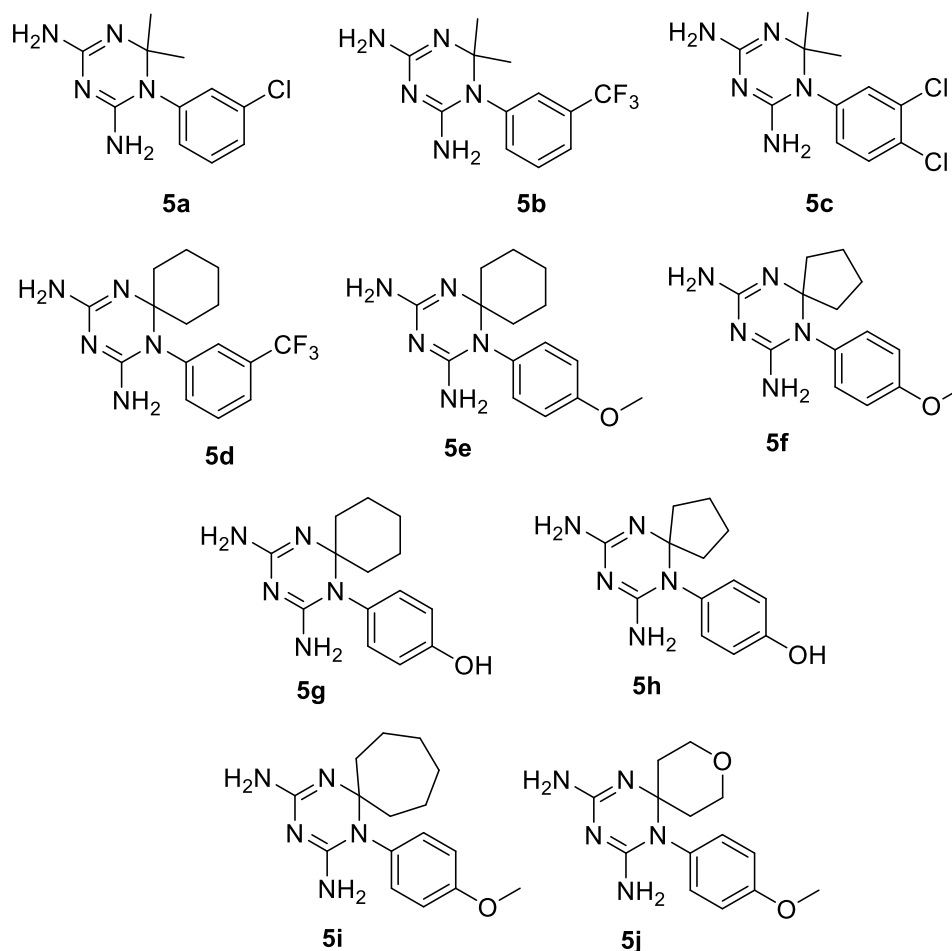
ADME-T properties were also evaluated for compound HD_1.
(Table 11)

Table 11: Descriptors for compound HD_1 calculated with Qikprop. QPlogKp: skin permeability; QPlogPo/w: octanol/water partition coefficient; QPlogKhsa: binding to human serum albumin. CIQPlogS: Conformation-independent aqueous solubility log S, with S in mol dm³ (concentration of solute in a saturated solution in equilibrium with the crystalline solid). CNS: Predicted central nervous system activity. %Human Oral Absorption: Predicted human oral absorption on 0 to 100% scale. The prediction is based on a quantitative multiple linear regression model. This property usually correlates well with HumanOralAbsorption, as both measure the same property.

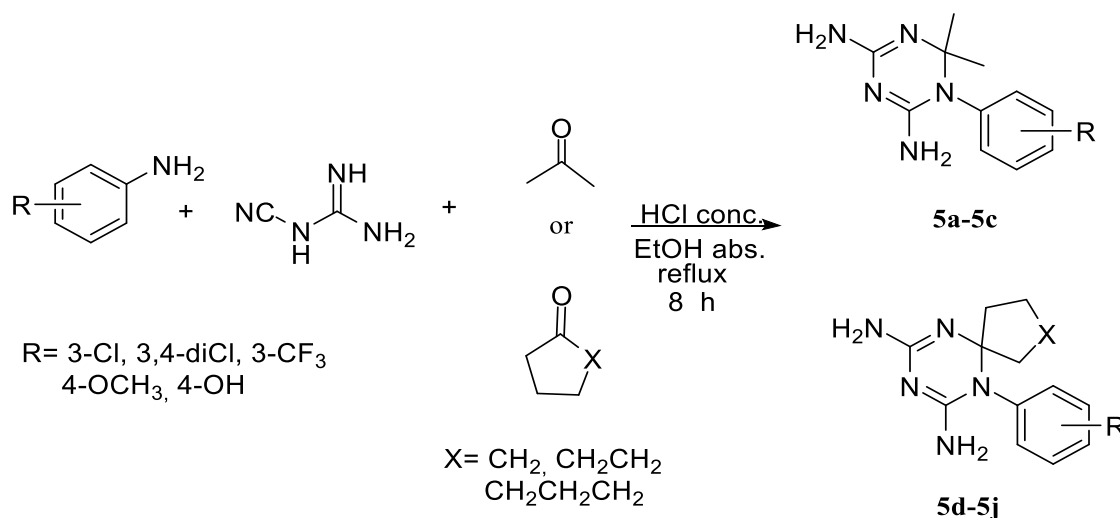
Predicted Descriptor	Recommended Range	Predicted value
CNS	-2 — +2	0
QPlog	Concern	-5.70
HERG	Below -5	
QPlogKp	-8.0 — -1.0	-5.108
QPlogKhsa	-1.5 — 1.5	0.051
QPlogPo/w	-2.0 — 6.5	2.049
CIQPlogS	-6.5 — 0.5	-3.318
%HumanOral Absorption	>80% is high <25% is poor	73.258%

SERIES 3

This set represents the prosecution of a previous study in which some closely related CYC analogues demonstrated an improved inhibitory activity performance against *Tb*PTR1, mainly due to the introduction of two structural variations on CYC scaffold, such as the presence of a bulky spiro-cyclic substituent in position 6 and a polar and electron-donating group (like OCH₃) in position 4 on the phenyl ring⁽⁹⁸⁾. The following dihydrotriazines were prepared to deepen the SAR around CYC scaffold and understand how their substitution pattern influences the inhibition of *Tb*PTR1.



Compounds **5** were achieved using the three-component synthesis described by Modest⁽¹¹⁷⁾, reacting an aromatic amine, dicyandiamide and a carbonyl compound in acid-catalyzed conditions (Scheme 5)



Scheme 5

Since the compounds **5a-5d** were already known^(117,118), their chemical structure was only confirmed by elemental analysis. The characterization of compounds **5e-5j** by NMR spectra is reported in the experimental section.

In vitro biological profiling

Actually, only data against *TbPTR1* are available for most of the compounds, as listed in Table 12.

Table 12: Data on inhibition (IC_{50}) of *TbPTR1*. Data are representative of three independent experiments and are expressed as means (errors on IC_{50} are within 10 %).

Compound	<i>TbPTR1</i>
	IC_{50} (μ M)
5a	4.14
5b	23.1
5c	9.4
5d	4.3
5e	10.8
5f	23.7
5g	ND
5h	ND
5i	ND
5j	ND
CYC	27.2
MTX	0.801

ND: not determined.

From the data obtained so far, the compounds have confirmed the ability to inhibit *TbPTR1*. In particular, compounds **5a**, **5c** and **5d** showed to be more potent inhibitors than CYC prototype, with IC_{50} values between 4.14 and 9.4 μ M. All three compounds bear in the

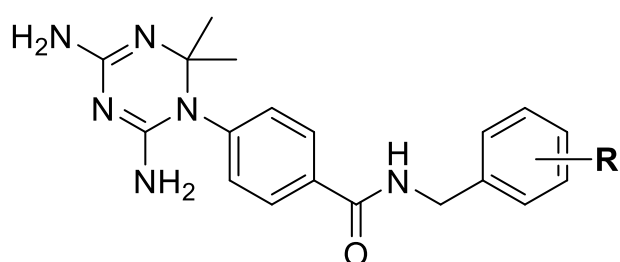
meta position of the aromatic ring a lipophilic and electron-withdrawing substituent.

In the case of compound **5d**, the replacement of the *gem*-dimethyl substituent of compound **5b** with a spiro-cyclohexane moiety, while unvarying the *m*-CF₃ group on the phenyl ring in position 1, led to a 5-fold increase of the inhibitory potency (**5d**, IC₅₀= 4.3 μM). Based on the crystal structure of CYC in complex with *Tb*PTR1, this improvement of activity could be conceivably ascribed to the establishment of additional van der Waals contacts with the hydrophobic pocket of *Tb*PTR1 lined by Phe97, Val206, Leu209 and Pro210 residues by the cycloalkyl moiety.

Subsequent molecular modeling studies will allow to understand the role of these substitutions in promoting the stability of the enzyme-inhibitor complex. The evaluation of the inhibition of *Tb*DHFR and *h*DHFR are currently underway to outline the species-selectivity profile of these molecules.

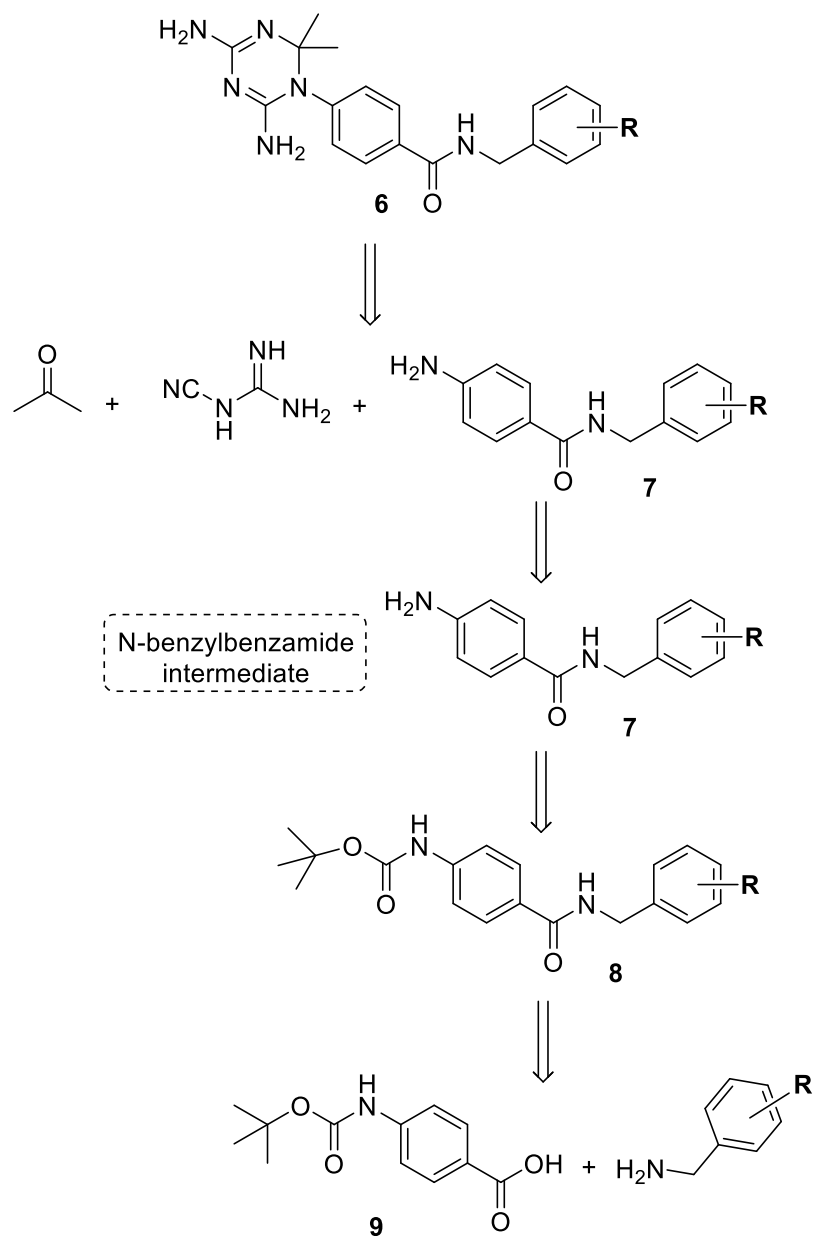
SERIES 4

The last series of compounds was only recently developed with the aim to explore the influence on the inhibition activity caused by a longer and bulkier aromatic side chain replacing the 4-Cl atom of CYC: the N-benzyl benzamide portion was introduced, somehow resembling the topology of the benzoyl moiety of folate.



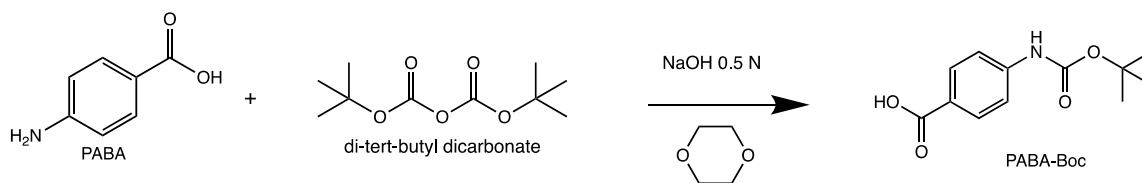
R= H (**6a**), 3-Cl (**6b**), 4-Cl (**6c**), 3,4-diCl (**6d**)
3-OCH₃(**6e**), 4-OCH₃(**6f**), 3,4-diOCH₃(**6g**)

For compounds **6**, we planned this synthetic route (Scheme 6).



Scheme 6. Retrosynthesis of compounds **6**.

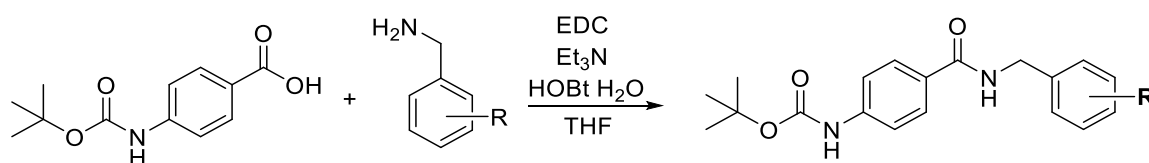
The synthesis of the N-benzylbenzamide intermediate started with the protection of the amino group of *p*-aminobenzoic acid (PABA) with the anhydride Boc₂O in basic medium (Scheme 7).



Scheme 7

9a-g

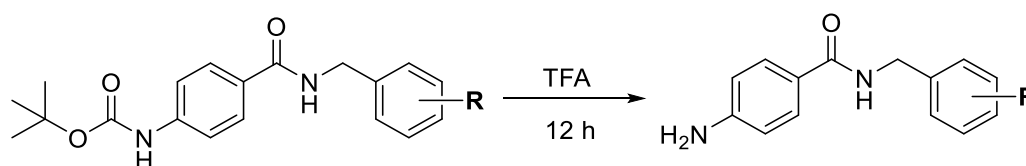
Amide coupling reaction of Boc-4-aminobenzoic acid (PABA-Boc) and the proper benzylamine was carried out in the presence of 1-ethyl-3-(3-dimethylaminopropyl)carbodiimide (EDC) and 1-hydroxybenzotriazole monohydrate (HOBT) *plus* triethylamine in THF. The reaction was stirred at r.t. overnight (Scheme 8).



Scheme 8

8a-g

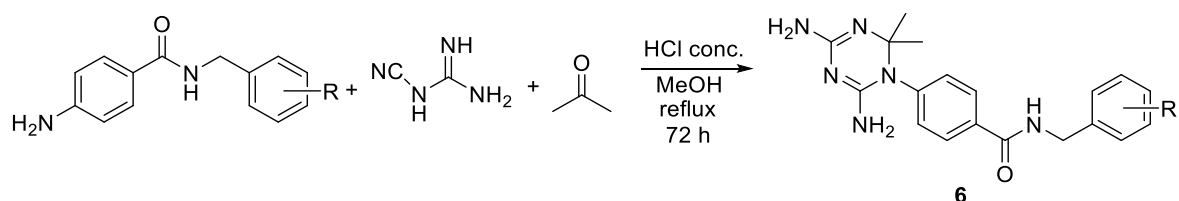
Then the protective group was removed with trifluoroacetic acid (TFA), stirring the solution at r.t. for 12 hours (Scheme 9).



Scheme 9

7a-g

The last step is represented by the one pot reaction among an aromatic amine, dicyandiamide and acetone in acid-catalysis, using methanol as solvent. The solution was refluxed for 72 hours (Scheme 10).



Scheme 10

The intermediates were used as such in the subsequent reaction steps and were not experimentally characterized. The structures of the final compounds **6a-6g** were confirmed by ^1H and ^{13}C NMR.

In vitro biological profiling

Due to the preliminary stage of the study, some of the compounds were evaluated only against TbPTR1 (Table 13).

Table 13: Inhibition constants (K_i) of compounds **6** against *TbPTR1*. Data are representative of three independent experiments and are expressed as means, $SD < 10\%$.

Compound	<i>TbPTR1</i> K_i (μM)
CYC	5,44
6a	43,7
6b	ND
6c	49,4
6d	37,7
6e	31,2
6f	68,74
6g	ND

ND: not determined.

The compounds demonstrated only a modest *TbPTR1* inhibition, with K_i values ranging between 31.2 (**6e**) and 68.74 μM (**6f**).

The most active compounds bear the 3-OMe group (**6e**) or the 3,4-diCl benzyl ring (**6d**) and are approximately 6-fold less potent than CYC. As expected, the longer side chain of series **6** could prevent, owing to a superior steric effect, the formation of the halogen interaction characteristic of the 4-Cl atom of CYC with Trp221 of *TbPTR1*. To understand the on-target structure-activity relationships molecular modelling studies will be performed.

As the inhibitory effect against the target folate enzymes often does not translate to adequate anti-parasitic activity⁽¹¹⁹⁾, some research strategies are directed to target both PTR1 and DHFR to prevent the cross talk among the respective pathways and examine the

outcome of drug combination tests⁽¹²⁰⁾. In this context, the proposed chemotype **6** was developed to identify more selective *Tb*DHFR inhibitors to be associated with selective *Tb*PTR1 inhibitors, thus far discovered, with a view to exploiting their synergistic effects.

4. Conclusions & final remarks

During these three years of my doctorate, the research group led by Prof. Tonelli has developed four series of compounds that explored the modification of the 2,4-diamine-1,3,5-dihydrotriazine ring of the antimalarial drug CYC, seeking for novel antiparasitic agents targeting folate enzymes. The result of the biological studies has demonstrated the validity of CYC scaffold as core structure which has allowed the yield of promising template molecules worthy of further investigations and subsequent optimization.

The co-crystal structures of *Tb*PTR1 and *Tb*DHFR in complex with selected inhibitors of series 2 were compared with those of prototype Pyr and Cyc allowing the understanding in more details of their on-target structure-activity relationships.

Additionally, molecular docking studies were performed on series 2 to investigate the binding interactions at the base of the enzyme inhibitory potency of most active compounds and to elucidate how the inhibitors complement the active site of protozoan and human folate enzymes. The derived information provided valuable suggestions on the species-selectivity profile of series 2, guiding the rational design of more promising dual *Tb*PTR1 and *Tb*DHFR inhibitors, conceivably much less active towards the *h*DHFR.

The new compound (HD_1) is the molecule identified during my stay at the Heidelberg Institute for Theoretical Studies which

embodies the characteristics described above. It will be synthesised and tested in enzymatic and cell-based assays, to validate the in-silico study.

The information from series 3 and 4, actually incomplete and at a preliminary stage, will help understanding what structural modifications can improve the affinity of 2,4-diamino dihydrotriazine-based derivatives towards the relevant targets to be fruitfully used in further studies.

The management of protozoan diseases still represents a challenging task in WHO programmes, which also call the need of implementing the arsenal of medications with new compounds active against *Leishmania* and *Trypanosoma* parasites. Collectively, the insights gathered through this three-year study may give some interesting inputs towards the development of innovative antiprotozoan agents targeting folate pathway.

5. Experimental section

Starting materials were purchased from Sigma-aldrich(Milan, Italy), Merck(Darmstadt, Germany) and fluorochem (Hadfield, United Kingdom).Melting points were determined with a Büchi 530 apparatus. Column chromatography was performed either on silica gel 60 Å (35-70 mesh), ¹H NMR and ¹³C NMR spectra were recorded in DMSO-*d*₆ using a spectrophotometer Jeol 400, δ in ppm, J in Hz. Elemental analyses were performed on Flash 2000 CHNS (Thermo Scientific) instrument in the Microanalysis

Laboratory of the Department of Pharmacy of Genoa University or in a Flash 1112 series Thermofinnigan elemental microanalyzer (A5). HPLC was performed using an Agilent 1100 HPLC-MSD Ion Trap XCT system, equipped with an electrospray ion source (HPLC-ESI-MS/MS) (Agilent Technologies, Santa Clara, CA, USA). Chromatographic analyses were performed using Waters Symmetry 300TM C₁₈ column (particle size 3,5 μ m – 150x1mm) at room temperature and gradient elution with a binary solution.

SERIE 1

General synthesis of compounds 2 a-g

The properly substituted 1,2-phenyldiamine (1,4 mmol) and dicyandiamide (1,4 mmol) were dissolved in 5 mL of H₂O and 0,23 mL (1,4 mmol) of HCl conc. were slowly added to the obtained solution. The mixture was heated to reflux for 6h under magnetic stirring. After cooling to r.t., the solution was alkalized with 6M NaOH inducing the precipitation of an amorphous solid, which was either recrystallized from Et₂O or purified by chromatographic column (SiO₂/Et₂O+10% MeOH), to afford the final product. Compound 2b,2c and 2e, have been converted to their respective hydrochloride salts by adding HCl 1N (ethanolic solution), to perform elemental analysis.

2-Guanidinobenzimidazole (2a)

Yield: 59%. M.p. 237-240 °C (M.p. 243-244 °C)¹²². ¹H NMR (400 MHz, DMSO-*d*₆): δ 10.95 (br s, 1H, benzimidazole exchangeable NH), 7.33-6.46 (br s, 4H, 2NH and NH₂ signals superimposed to H arom.), 7.18-7.12 (m, 2H, H arom.), 6.93 - 6.88 (m, 2H, H arom.), 3.35 (br s, 1H, NH signal partially superimposed to H₂O peak). ¹³C NMR (101 MHz, DMSO-*d*₆) δ 158.96, 158.72, 133.60 (2C), 119.36 (2C), 111.91 (2C).

5(6)-Chloro-2-guanidinobenzimidazole (2b)

Yield: 40%. M.p. 208-211 °C (M.p. 207 °C)¹²⁵. ¹H NMR (400 MHz DMSO-*d*₆). Δ 11.12 (br s, 1H, benzimidazole exchangeable NH), 7.20-6.50 (br s, 3H, NH and NH₂ signals superimposed to H arom.), 7.15 (s, 1H, H arom.), 7.11 (d, *J* = 8.3 Hz, 1H, H arom.), 6.90 (dd, *J* = 8.3, 2.1 Hz, 1H, H arom.), 3.38 (br s, 1H, NH signal partially superimposed to H₂O peak). ¹³C NMR (101 MHz, DMSO-*d*₆) δ 160.16, 158.99, 142.76, 133.63, 123.54, 119.06. Anal. Calcd. For C₈H₈ClN₅·2HCl: C 34.01, H 3.57, N 24.79; found: C 34.06, H 3.45, N 24.88.

5,6-Dichloro-2-guanidinobenzimidazole (2c)

Yield: 70%. M.p. 236-240 °C (M.p. 244 °C)¹²⁵. ¹H NMR (400 MHz, DMSO-*d*6) δ 11.21 (s, 1H, benzimidazole exchangeable NH), 7.29 (s, 2H, H arom.), 6.97 (br s, 3H, NH + NH₂), 3.34 (br s, 1H, NH) ¹³C NMR (101 MHz, DMSO- *d*6): δ 161.01, 159.20, 121.09 (2C), 114.13 (2C), 110.33 (2C). Anal. calcd. for C₈H₇Cl₅N₅·HCl: C 34.25, H 2.87, N 24.96; found C 34.31, H 3.10, N 24.54.

4,6-Dichloro-2-guanidinobenzimidazole (2d)

Yield: 40%. M.p. 244-245.5 °C. ¹H NMR (400 MHz, DMSO-*d*6): δ 11.60 (s, 1H, benzimidazole exchangeable NH), 7.17 (br s, 3H, NH + NH₂), 7.12 (d, *J* = 1.9 Hz, 1H, H arom.), 7.05 (d, *J* = 1.9 Hz, 1H, H arom.). 3.34 (br s, 1H, NH). ¹³C NMR (101 MHz, DMSO- *d*6): δ 159.29, 158.88, 135.72, 131.13, 123.42, 119.11. Anal. Calcd. For C₈H₇Cl₂N₅: C 39.37, H 2.89, N 28.69; found: C 39.44, H 3.02, N 28.38.

5(6)-Trifluoromethyl-2-guanidinobenzimidazole (2e)

Yield: 38%. M.p. 200-203 °C. ¹H NMR(400 MHz, DMSO- *d*6): δ 8.38 (br s, 4H, 2NH + NH₂), 7.72 (s, 1H, H arom.), 7.59 (d, *J* = 8.3 Hz, 1H, H arom.), 7.49 (dd, *J* = 8.5, 1.8 Hz, 1H, H arom.) ¹³C NMR (101 MHz, DMSO-*d*6): δ 156.46, 149.15, 137.33, 134.68, 124.88 (q, ¹*J*CF = 271.5 Hz), 122.61 (q, ²*J*CF = 31.5 Hz), 118.96 (d, ³*J*CF

= 3.9 Hz), 113.70, 110.54. Anal. calcd. For $C_9H_8F_3N_5 \cdot HCl$: C 38.65, H 3.24, N 25.04; found: C 38.41, H 3.21, N 25.01.

5(6)-Methoxy-2-guanidinobenzimidazole (2f)

Yield: 36%. M.p. 201.7 - 202.7 °C. 1H NMR (400 MHz, DMSO-*d*₆): δ 10.88 (br s, 1H, benzimidazole exchangeable NH), 7.20 – 6.26 (br s, 3H, NH and NH₂ signals superimposed to H arom.), 7.03 (d, J = 8.4 Hz, 1H, H arom.), 6.74 (d, J = 2.4 Hz, 1H, H arom.), 6.53 (dd, J = 8.5, 2.5 Hz, 1H, H arom.) 3.71 (s, 3H, C(5)-OCH₃), 3.34 (br s, 1H, NH signal partially superimposed to H₂O peak). ^{13}C NMR (101 MHz, DMSO-*d*₆): δ 158.84, 158.44, 154.02, 133.97, 111.54, 107.05, 96.72, 55.35. Anal. calcd. For $C_9H_{11}N_5O$: C 52.67, H 5.40, N 34.13; found: C 52.63, H 5.45, N 34.43.

5,6-Dimethyl-2-guanidinobenzimidazole (2g)

Yield: 65%. M.p. 167.2-170 °C (M.p. 191°C)¹²². 1H NMR (400 MHz, DMSO-*d*₆): δ 10.84 (s, 1H, benzimidazole exchangeable NH), 6.94 (s, 2H, H arom.), 6.84 (br s, 3H, NH+NH₂ signals partially superimposed to H arom.), 3.35 (br s, 1H, NH), 2.22 (s, 6H, C(5)-CH₃ and C(6)-CH₃). ^{13}C NMR (101 MHz, DMSO-*d*₆): δ 158.98, 158.57, 135.81 (2C), 127.57 (2C), 112.97 (2C), 20.39 (2C). Anal. calcd. for $C_{10}H_{13}N_5$: C 59.10, H 6.45, N 34.46; found C 59.16, H 6.74, N 34.73.

General synthesis of compounds 1 a-g

A mixture of the proper 2-guanidinobenzimidazole (5.7 mmol) and piperidine (2.9 mmol) dissolved in 5 mL of acetone was heated at 70 °C for 7 h. The reaction mixture was then concentrated *under vacuum* and kept cooling to r.t overnight. The expected product precipitated as white solid, which was filtered and recrystallized from acetone/ET₂O an.

2-Amino-4,4-dimethyl-3,4-dihydrotriazine[1,2-a]benzimidazole (1a)

Yield: 59% M.p. 284.8-285.6 °C (M.p. 295-296 °C)¹²³. ¹H NMR (400 MHz, DMSO-*d*₆): δ 7.71(s, 1H, NH), 7.35 (d, *J* = 7.7 Hz, 1H, C(6) – H arom.), 7.24 (d, *J* = 7.7 Hz, 1H, C(9)-H arom.), 6.98 (td, *J* = 7.6, 1.2 Hz, 1H, C(7)-H arom.), 6.91 (td, *J* = 7.6, 1.3 Hz, 1H, C(8)-H arom.), 6.36 (s, 2H, NH₂), 1.77 (s, 6H, C(4)-diCH₃). ¹³C NMR (101 MHz, DMSO-*d*₆) δ 155.21, 153.6, 143.74, 130.67, 120.55, 118.90, 116.08, 109.60, 69.31, 28.50 (2C). Anal. calcd. For C₁₁H₁₃N₅: C 61.38, H 6.09, N 32.54; found: C 61.31, H 6.12, N 32.30.

2-Amino-7(8)-cloro-4,4-dimethyl-3,4-diidrotriazino[1,2-a]benzimidazole (1b)

Yield:41%. M.p. 161.2-163 °C . Ratio **1b-I/1b-II**: 60% **1b-I** and 40% **1b-II**. ¹H NMR (400 MHz, DMSO-*d*₆): **1b-I** δ 7.68 (s, 1H,

NH), 7.35(d, $J = 8.5$ Hz, 1H, C(6)-H arom.), 7.23 (d, $J = 2.1$ Hz, 1H, C(9)-H arom.), 6.89 (dd, $J = 8.5, 2.1$ Hz, 1H, C(7)-H arom.) 6.36 (s, 2H, NH₂), 1.74 (s, 6H, C(4)-diCH₃).

1b-II δ 7.65 (s, 1H, NH), 7.40 (d, $J = 2.0$ Hz, 1H, C(6)-H arom.), 7.20 (d, $J = 8.4$ Hz, 1H, C(9)-H arom.), 6.99 (dd, $J = 8.3, 2.1$ Hz, 1H, C(8)-H arom.), 6.33 (s, 2H, NH₂), 1.75 (s, 6H, C(4).diCH₃).

¹³C NMR (101 MHz, DMSO-*d*₆) **1b-I** δ 155.48, 155.08, 145.27, 129.59, 124.97, 118.32, 115.37, 110.43, 69.79, 28.34 (2C); **1b-II** δ 155.36, 154.56, 142.76, 131.43, 122.94, 120.57, 116.86, 109.30, 69.44, 28.30 (2C). Anal. calcd. For C₁₁H₁₂N₅Cl: C 59.91, H 4.84, N 28.05; found: C 52.89, H 5.16, N 28.09.

2-Amino-7,8-dichloro-4,4-dimethyl-3,4-dihydrotriazino[1,2-a]benzimidazole (1c)

Yield: 56%. M.p. 285.1-285.9 °C. ¹H NMR (400 MHz, DMSO-*d*₆): δ 7.73 (s, 1H, NH), 7.59 (s, 1H, C(6)-H arom.), 7.40 (s, 1H, C(9)-H arom.), 6.43 (s, 6H, C(4)-diCH₃). ¹³C NMR (101 MHz, DMSO-*d*₆) δ 155.75, 155.62 144.11, 130.42, 122.90, 120.39, 116.52, 110.52, 69.58, 28.17 (2C). Anal. calcd. For C₁₁H₁₁N₅Cl₂: C 46.50, H 3.90, N 24.65; found: C 46.43, H 4.00, N 24.30.

2-Amino-7,9-dichloro-4,4-dimethyl-3,4-dihydrotriazino[1,2-a]benzimidazole (1d)

Yield: 89%. M.p. 283.2-283.4 °C. ¹H NMR (400 MHz, DMSO-*d*₆): δ 7.86 (s, 1H, NH), 7.41 (d, $J = 1.8$ Hz, 1H, C(6)-H arom.), 7.11 (d, $J = 1.8$ Hz, 1H, C(8)-H arom.) 6.46 (s, 2H, NH₂), 1.74 (s,

6H, C(4)-diCH₃). ¹³C NMR (101 MHz, DMSO-*d*6): δ 155.64, 155.10, 139.97, 132.97, 132.07, 122.73, 120.11, 119.97, 108.39, 69.74, 28.21 (2C). Anal. calcd. for C₁₁H₁₁N₅Cl₂: C 46.50, H 3.90, N 24.65; found: C 46.68, H 3.71, N 24.71.

2-Amino-7(8)-trifluoromethyl-4,4-dimethyl-3,4-dihydrotriazino[1,2-a]benzimidazole (1e)

Yield: 20%. M.p. 259-261 °C. Ratio **1e-I**/**1e-II**: 60% **1e-I** and 40% **1e-II**. ¹H NMR (400 MHz, DMSO-*d*6): **1e-I** δ 7.78 (s, 1H, NH), 7.53 (d, *J* = 8.3 Hz, 1H, C(6)-H arom.), 7.50 (s, 1H, C(9)-H arom.), 7.20 (dd, *J* = 8.5, 2.1 Hz, 1H, C(7)-H arom.), 6.43 (s, 2H, NH₂), 1.79 (s, 6H, C(4)-diCH₃); **1e-II** δ 7.80 (s, 1H, NH), 7.57 (s, 1H, C(6)-H arom.), 7.36 (d, *J* = 8.2 Hz, 1H, C(9)-H arom.), 7.30 (dd, *J* = 8.4, 2.0 Hz, 1H, C(8)-H arom.), 6.47 (s, 2H, NH₂), 1.79 (s, 6H, C(4)-diCH₃). ¹³C NMR (101 MHz, DMSO-*d*6): **1e-I** δ 155.77, 155.58, 143.82, 133.28, 125.31 (d, ¹*J*_{CF} = 272.7 Hz), 121.42 (q, ²*J*_{CF} = 31.2 Hz), 115.47 (d, ³*J*_{CF} = 3.8 Hz), 112.41 (d, ³*J*_{CF} = 3.7 Hz), 109.71, 69.59, 28.38 (2C); **1e-II** δ 156.18, 155.50, 147.03, 130.36, 125.44 (d, ³*J*_{CF} = 272.7 Hz, CF₃), 118.92 (q, ²*J*_{CF} = 31.5 Hz), 117.77 (d, ³*J*_{CF} = 3.6 Hz), 115.91, 106.10 (d, ³*J*_{CF} = 3.7 Hz), 69.64, 28.32 (2C). Anal. calcd. For C₁₂H₁₂F₃N₅: C 50.88, H 4.74, N 24.72; found C 50.82, H 4.53, N 24.75.

2-Amino-7(8)-methoxy-4,4-dimethyl-3,4-dihydrotriazino[1,2-a]benzimidazole (1f)

Yield: 21%. M.p. 264-266 °C. Ratio **1f-I/1f-II**: 64% **1f-I** and 36% **1f-II**. ¹H NMR (400 MHz, DMSO-*d*₆): **1f-I** δ 7.63 (s, 1H, NH), 7.21 (d, *J* = 8.6 Hz, 1H, C(6)-H arom.), 6.82 (d, *J* = 2.5 Hz, 1H, C(9)-H arom.), 6.52 (dd, *J* = 8.7, 2.5 Hz, 1H, C(7)-H arom.), 6.27 (s, 2H, NH₂), 3.72 (s, 3H, C(8)-OCH₃), 1.72 (s, 6H, C(4)-diCH₃), **1f-II** δ 7.59 (s, 1H, NH), 7.13 (d, *J* = 8.6, 2.4 Hz, 1H, C(8)-H arom.), 6.88 (d, *J* = 2.4 Hz, 1H, C(6)-H arom.), 6.63 (dd, *J* = 8.6, 2.4 Hz, 1H, C(8)-H arom.), 6.22 (s, 2H, NH₂), 3.75 (s, 3H, C(7)-OCH₃), 1.75 (s, 6H, C(4)-diCH₃). ¹³C NMR (101 MHz, DMSO-*d*₆): **1f-I** δ 155.14, 154.70, 153.48, 125.16, 109.58, 106.42, 100.77, 69.21, 55.32, 28.43 (2C); **1f-II** δ 154.81, 154.38, 153.07, 137.97, 131.09, 116.15, 107.56, 95.90, 69.24, 55.72, 28.43 (2C). Anal. calcd. for C₁₂H₁₅N₅O: C 58.76, H 6.16, N 28.55; found: C 59.03, H 6.22, N 28.93.

2-Amino-4,4,7,8-tetramethyl-3,4-dihydrotriazino[1,2-a]benzimidazole (1g)

Yield: 40%. M.p. 266.5-268.5 °C. ¹H NMR (400 MHz, DMSO-*d*₆): δ 7.54 (s, 1H, NH), 7.12 (s, 1H, C(6)-H arom.), 6.16 (s, 1H, NH₂), 2.25 (s, 3H, C(8)-CH₃), 2.21 (s, 3H, C(7)-CH₃). ¹³C NMR (101 MHz, DMSO-*d*₆) δ 154.91, 153.07, 142.09, 129.06, 128.09, 126.73, 116.89, 110.33, 69.14, 28.49 (2C), 19.90, 19.75. Anal.

calcd. for C₁₃H₁₇N₅: C 64.17, H 7.04, N28.78; found: C 64.22, H 7.32, N 28.50.

SERIE 2

General synthesis for azaspiro dihydrotriazines (3-4)

The proper N-benzyl piperidone (1.5 eq.) reacts with the appropriate aniline (1 eq) and cyanoguanidine (1.05 eq) in 5 ml of abs. ethanol plus 1 eq. of conc. HCl. The reaction is then refluxed with stirring for 8 h. Compounds 3a-3c directly crystallised from the reaction mixture as pure hydrochloride salts, while compounds 3e-3f were purified by chromatography (Alumine/Chloroform/MeOH 4:1).

8-Benzyl-2,4-diamino-1-phenyl-1,3,5,8-tetraazaspiro[5.5] undeca-2,4-diene (3a)

Yield: 53%. Mp 240-241 °C (acetone/Et₂O an.). ¹H NMR (200 MHz, DMSO-d₆): 9.69 (s, 1H, NH⁺); 7.74e7.20 (m, 12H, 10 H arom. and 2H, NH₂, superimposed signals); 6.99 (s, 2H, NH₂); 4.06 (s, 2H, CH₂-arom); 2.84 (s, 2H, CH₂-pip); 2.52 (pseudo s, 2H, CH₂-piperidine superimposed to DMSO-d₆ signal); 2.38 (t, J ¼ 7.0 Hz, CH₂-pip); 2.04-1.72 (m, 2H, CH₂-pip). Anal. Calcd for C₂₀H₂₄N₆·HCl: C 62.41; H 6.55; N 21.83. Found: C 62.41; H 6.64; N 21.83

8-Benzyl-1-(4-chlorophenyl)-2,4-diamino-1,3,5,8-tetraazaspiro[5.5]undeca-2,4-diene. (3b)

Yield: 46%. Mp 239.8e240 °C (acetone/Et2O an.). ¹H NMR (200 MHz, DMSO-d₆): 9.67 (s, 1H, NH⁺); 7.86-7.16 (m, 11H, 9 H arom. and 2H, NH₂, superimposed signals); 6.98 (s, 2H, NH₂); 4.07 (s, 2H, CH₂-Ar); 2.85 (s, 2H, CH₂-pip); 2.52 (pseudo s, 2H, CH₂-pip superimposed to DMSO-d₆ signal); 2.40 (t, J ¼ 6.8 Hz, CH₂-pip); 2.00-1.76 (m, 2H, CH₂-pip.). Anal. Calcd for C₂₀H₂₃ClN₆ · HCl: C 57.28; H 5.77; N 20.04. Found: C 56.99; H 5.93; N 19.84

8-benzyl-5-(4-fluorophenyl)-1,3,5,8-tetraazaspiro[5.5]undeca-1,3-diene-2,4-diamine hydrochloride (3c)

Yield:55%. M.p. 250-256 °C. ¹H NMR (400 MHz, DMSO-*d*₆): δ 9.28 (br s, 1H, NH⁺), 7.53-7.40 (m, 2H, NH₂; 4H, arom.), 7.40-7.30 (m, 5H arom.; 1H, NH), 6.92 (s, 1H, NH), 4.05 (s, 2H, CH₂), 2.90-2.72 (m, 2H, CH₂ pip), 2.35 (t, *J* = 7.3 Hz, 2H, CH₂ pip), 1.79 (p, *J* = 7.5 Hz, 2H, CH₂ pip); 2.52-2.50 (m, 2H, CH₂ pip superimposed to DMSO signal). ¹³C NMR (101 MHz, DMSO-*d*₆) δ ,162.52 (d, ¹*J*_{CF} = 247.1 Hz), 158.35, 157.63, 132.15, 131.70, 130.75 (d, ³*J*_{CF} = 9.2 Hz, 2C), 130.33 (2C), 130.02, 129.28, 128.99 (2C), 117.02 (d, ²*J*_{CF} = 22.2 Hz, 2C), 50.19 (2C), 45.88, 23.20, 21.35.

8-benzyl-5-(4-bromophenyl)-1,3,5,8-tetraazaspiro[5.5]undeca-1,3-diene-2,4-diamine hydrochloride (3d)

Yield: 19%. M.p. 225-230 °C. ¹H NMR (400 MHz, DMSO-*d*₆): δ 9.26 (s, 1H, NH⁺), 7.76 (d, *J* = 8.3 Hz, 2H; H arom.), 7.54-7.49 (m, 2H, arom), 7.42 -7.36 (m, 5H, arom.), 7.39-6.97 (br s, 3H, NH, NH₂ partially superimposed to arom.), 6.92 (br s, 1H, NH), 4.05 (s, 2H, CH₂), 2.91- 2.78 (m, 2H, pip), 2.51-2.49 (m, 2H, pip superimposed to DMSO signal), 2.36 (t, *J* = 7.4 Hz, 2H, pip), 1.80 (p, *J* = 7.6 Hz, 2H, pip). ¹³C NMR (101 MHz, DMSO-*d*₆) δ 157.93, 156.39, 144.17, 133.18, 133.07 (2C), 132.13, 130.57 (2C), 130.32 (2C), 129.27, 128.99 (2C), 123.11, 50.19 (2C), 45.87, 23.21, 21.34.

Ethyl 4-(2,4-diamino-8-benzyl-1,3,5,8-tetraazaspiro[5.5]undeca-2,4-dien-1-yl)-benzoate (3e)

Yield: 22% ¹H NMR (400 MHz, DMSO-*d*₆): δ 8.01 (d, *J* = 8.8 Hz, 2H, arom), 7.40 (d, *J* = 8.8 Hz, 2H, arom.), 7.30-7.26 (m, 4H, arom.), 7.25-7.20 (m, 1H, arom.), 6.63 (br s, 2H, NH₂), 6.45 (s, 1H, NH), 4.33 (q, *J* = 7.1 Hz, 2H, CH₂OEt), 3.65 (s, 2H, CH₂), 2.52-2.49 (m, 2H, pip superimposed to DMSO signal) 2.45 (t, *J* = 7.1 Hz, 2H, pip), 2.36 (t, *J* = 7.6 Hz, 2H, pip), 1.49 (p, *J* = 7.3 Hz,

2H,pip), 1.33 (t, $J = 7.1$ Hz, 3H, CH₃OEt). ¹³C NMR (101 MHz, DMSO-*d*₆) δ 162.28, 160.23, 156.86, 145.12, 134.66, 132.94 (2C), 129.55, 128.48 (2C), 127.82, 127.77 (2C), 112.07 (2C), 95.05, 61.92, 61.24, 54.23, 49.10, 33.75, 25.89, 16.29.

4-(2,4-diamino-8-benzyl-1,3,5,8-tetraazaspiro[5.5]undeca-2,4-dien-1-yl)phenol (3f)

Yield: 86% ¹H NMR (400 MHz, DMSO-*d*₆): δ 10.12 (s, 1H, OH); 9.43 (s, 1H, NH⁺); 8.24-7.76 (brs, 3H, 1NH + NH₂); 7.60-7.50 (m, 2H, H arom.); 7.46-7.35 (m, 3H, H arom.); 7.19 (d, $J=8.6$ Hz, 2H, H arom.); 6.92 (d, $J=8.4$ Hz, 2H, H arom.); 6.89 (brs, 1H, NH); 4.06 (s, 2H, CH₂); 2.83 (pseudo s, 2H, pip.); 2.52-2.50 (m, 2H, pip. Superimposed to DMSO signal); 2.34 (t, $J=7.4$ Hz, 2H pip.); 1.82 (p, $J=7.5$ Hz, 2H, pip.). ¹³C NMR (101 MHz, DMSO-*d*₆) δ 169.04, 158.41, 155.94, 141.95, 132.06, 130.10 (2C), 129.26 (2C), 128.90, 128.65 (2C), 124.11, 116,22 (2C), 79.26, 49.76, 45.50, 23.06, 21.13.

8-benzyl-5-(*p*-tolyl)-1,3,5,8-tetraazaspiro[5.5]undeca-1,3-diene-2,4-diamine (3g)

Yield: 9.5% ¹H NMR (400 MHz, DMSO-*d*₆): δ 7.74-7.25 (br s, 3H, superimposed to H arom, NH + NH₂); 7.37-7.26 (m, 5H, H arom.); 7.24 (d, $J=7.8$ Hz, 2H, H arom.); 7.08 (d, $J=8.2$ Hz, 2H, H arom.); 6.41 (s, 1H, NH); 3.75 (s, 2H, CH₂); 2.53 (t, $J=7.4$ Hz, 2H, pip.); 2.52-2.50 (m, 2H, pip. Superimposed to DMSO signal); 2.34 (s, 3H, CH₃); 2.28 (t, $J=7.4$ Hz, 2H, pip.); 1.56 (p, $J=7.5$ Hz, 2H, pip).

^{13}C NMR (101 MHz, DMSO-*d*₆) δ 145.19, 141.57, 136.62, 129.64 (2C), 128.40 (2C), 127.83, 127.79 (2C), 112.08 (2C), 100.36 (2C), 95.03, 61.94, 54.28, 49.17, 33.75, 25.82, 21.30.

8-benzyl-5-(4-methoxyphenyl)-1,3,5,8-tetraazaspiro[5.5]undeca-1,3-diene-2,4-diamine (3h)

Yield: 17%. ^1H NMR (400 MHz, DMSO-*d*₆): δ 7.39-7.27 (br s, 3H, partially superimposed to H arom. NH + NH₂); 7.34-7.22 (m, 5H, H arom.); 7.11 (d, $J=8.9$ Hz, 2H, H arom.); 6.98 (d, $J=9.0$ Hz, 2H, H arom.); 6.39 (s, 1H, NH); 3.78 (s, 3H, OCH₃); 3.70 (s, 2H, CH₂); 2.52-2.50 (m, 2H, superimposed to DMSO-*d*₆ pip.); 2.48-2.45 (m, 2H, partially superimposed to DMSO-*d*₆ signal, pip.); 2.27 (t, $J=7.4$ Hz, 2H, pip.). ^{13}C NMR (101 MHz, DMSO-*d*₆) δ 160.92, 159.84, 156.85, 145.17, 136.66, 128.43 (2C), 127.87, 127.71 (2C), 124.63 (2C), 114.59 (2C), 95.00, 61.93, 56.07, 54.26, 49.16, 33.74, 25.89.

9-benzyl-5-(4-fluorophenyl)-1,3,5,9-tetraazaspiro[5.5]undeca-1,3-diene-2,4-diamine hydrochloride (4a)

Yield:15% ^1H NMR (400 MHz, DMSO-*d*6): δ 9.12 (s, 1H, NH⁺); 7.80 (m, 2H, NH₂); 7.53 (br s, 1H, NH); 7.48-7.08 (m, 9H, H arom.); 6.45 (br s, 1H, NH); 3.44 (s, 2H, CH₂); 2.65 (m, 2H, CH₂ pip); 2.41 (t, $J=12.2$ Hz, 2H, CH₂ pip.) 1.86-1.78 (m, 2H, CH₂ pip.); 1.58-1.46 (m, 2H, CH₂ pip.). ^{13}C NMR (101 MHz, DMSO-*d*6) δ 162.93, 161.27, 158.43 (d, $^1J_{\text{CF}}=241.4$ Hz), 138.36, 134.94, 132.63 (d, $^3J_{\text{CF}}=9.2$ Hz, 2C), 128.66 (2C), 128.28 (2C), 127.00, 117.27 (d, $^2J_{\text{CF}}=22.6$ Hz, 2C), 79.26, 70.02, 47.66 (2C), 34.31 (2C).

9-benzyl-5-(4-bromophenyl)-1,3,5,9-tetraazaspiro[5.5]undeca-1,3-diene-2,4-diamine (4b)

Yield:8% ^1H NMR (400 MHz, DMSO-*d*6): δ 9.16 (s, 1H, NH⁺); 7.55-7.48 (m, 3H, NH + NH₂); 7.44-7.40 (m, 2H, H arom.); 7.40-7.36 (m, 4H, H arom.); 7.34-7.29 (m, 3H, H arom); 6.41 (s, 1H, NH); 3.47 (s, 2H, CH₂); 2.71-2.68 (m, 2H, CH₂ pip.); 2.47-2.40 (m, 2H, CH₂ pip.); 1.78-1.70 (m, 2H, CH₂ pip.); 1.59-1.46 (m, 2H, CH₂ pip.). ^{13}C NMR (101 MHz, DMSO-*d*6) δ 160.92, 156.84, 145.18, 136.66, 131.74 (2C), 128.43 (2C), 128.82, 127.75 (2C), 127.61 (2C), 122.33, 95.07, 61.94, 51.45 (2C), 36.28 (2C).

9-benzyl-5-(4-methoxyphenyl)-1,3,5,9-tetraazaspiro[5.5]undeca-1,3-diene-2,4-diamine hydrochloride (4c)

Yield: 22,7% ¹H NMR (400 MHz, DMSO-*d*₆): δ 9.18 (s, 1H, NH⁺); 7.78-7.56 (m, 3H, NH + NH₂); 7.30-7.24 (m, 4H, H arom); 7.23-7.17 (m, 3H, H arom.); 7.07 (d, *J*=8.9 Hz, 2H, H arom.); 6.31 (s, 1H, NH); 3.81 (s, 3H, OCH₃); 3.44 (s, 2H, CH₂); 2.66-2.59 (m, 2H, pip.); 2.48-2.39 (m, 2H, pip.); 1.83-1.74 (m, 2H, pip.); 1.58-1.46 (m, 2H, pip.). ¹³C NMR (101 MHz, DMSO-*d*₆) δ 160.39, 158.42, 158.33, 138.93, 131.88 (2C), 129.13 (2C), 128.76 (2C), 127.47, 127.38, 115.90 (2C), 70.48, 61.88, 56.54, 55.96, 48.15, 34.85, 19.10.

SERIE 3

General synthesis for compounds

To a solution of the appropriate aniline (4.36 mmol) in 40mL of acetone and 5mL of MeOH is added conc. HCl (4.36 mmol, 1eq.) and cyanoguanidine (4.58 mmol, 1.05 eq.) and allowed to react r.t. for 24h. At the end, the formation of a white precipitate is observed, which is filtered, washed with acetone and recrystallised from EtOH/Et₂O.

General synthesis for (5)

A solution of the aniline derivative (4.0 mmol) plus 0.33 mL (1.05 equiv.) conc. HCl and a carbonyl derivative (8.0 mmol) dissolved

in 15 mL of absolute EtOH are reacted with 4.1 mmol (1.05 equiv.) of cyanoguanidine. Reaction is heated to reflux for 8 h with stirring e.m. At room temperature, the formation of a crystalline precipitate is observed, which is filtered on a porous septum s.v. and washed with a 2:1 mixture of acetone and Et₂O an.

1-(3-chlorophenyl)-6,6-dimethyl-1,6-dihydro-1,3,5-triazine-2,4-diamine hydrochloride (5a)

Yield: 75%. M.p. 228-231°C. Anal. calcd. for C₁₁H₁₅ClN₅·HCl C, 45.85; H, 5.25; N, 24.07 found C, 45.91; H, 5.24; N, 24.30⁽¹²⁰⁾

6,6-dimethyl-1-(3-(trifluoromethyl)phenyl)-1,6-dihydro-1,3,5-triazine-2,4-diamine hydrochloride (5b)

Yield: 71.4%. M.p. 209-210°C. Anal. calcd. for C₁₂H₁₄F₃N₅·HCl C, 44.80; H, 4.70; N, 21.77 found C, 44.67; H, 4.84; N, 21.91⁽¹²¹⁾.

1-(3,4-dichlorophenyl)-6,6-dimethyl-1,6-dihydro-1,3,5-triazine-2,4-diamine hydrochloride (5c)

Yield: 72%. M.p. 209-210°C. Anal. calcd. for C₁₁H₁₃Cl₂N₅·HCl C, 40.95; H, 4.37; N, 21.71 found C, 41.02; H, 4.25; N, 21.87⁽¹²⁰⁾

5-(3-(trifluoromethyl)phenyl)-1,3,5-triazaspiro[5.5]undeca-1,3-diene-2,4-diamine hydrochloride (5d)

Yield: 34%. M.p. 225-226 °C. Anal. calcd. for C₁₅H₁₈F₃N₅ · HCl
C, 49.80; H, 5.29; N, 19.36 found C, 49.89; H, 5.48; N, 19.52⁽¹²³⁾.

**5-(4-Methoxyphenyl)-1,3,5-triazaspiro[5.5]undeca-1,3-diene-
2,4-diamine hydrochloride (5e)**

Yield:47%. M.p. 293 °C. ¹H NMR (400 MHz, DMSO-*d*₆) δ 9.18 (s, 1H, NH⁺), 7.76-7.43 (m, 3H, NH₂ + NH), 7.30-7.21 (m, 2H, H arom.), 7.10-7.01 (m, 2H, H arom.), 6.20 (s, 1H, NH), 3.80 (s, 3H, OCH₃), 1.85 (d, *J* = 12.5 Hz, 2H, CH₂ cyclohexane), 1.77-1.61 (m, 2H, CH₂ cyclohexane), 1.58-1.47 (m, 3H, 2H CH₂ + 1Hα CH₂ cyclohexane), 1.27 (td, *J* = 13.3, 4.1 Hz, 2H, CH₂ cyclohexane), 0.98-0.82 (m, 1H, 1Hβ CH₂ cyclohexane). ¹³C NMR (101 MHz, DMSO-*d*₆) δ 159.79, 157.93, 157.77, 131.35 (2C), 127.05, 115.30 (2C), 71.38, 55.44, 34.76 (2C), 24.03, 20.73 (2C).

**10-(4-Metoxyphehyl)-6,8,10-triazaspiro[4.5]deca-6,8-diene-
7,9-diamine hydrochloride (5f)**

Yield: 39%. M.p. 216.8-217.9 °C. ¹H NMR (400 MHz, DMSO-*D*₆) δ 9.31 (s, 1H), 7.75-7.30 (m, 3H, NH₂ + NH), 7.27 – 7.22 (m,

2H), 7.04 – 7.00 (m, 2H), 6.26 (s, 1H, NH), 3.76 (s, 3H), 1.78 – 1.57 (m, 6H, cyclopentane), 1.49-1.37 (m, 2H, cyclopentane). ¹³C NMR (101 MHz, DMSO-*d*₆) δ 160.90, 159.85, 156.82, 145.16, 124.65 (2C), 114.57 (2C), 95.06, 56.03, 37.32 (2C), 22.31 (2C).

4-(2,4-diamino-1,3,5-triazaspiro[5.5]undeca-2,4-dien-1-yl)phenol (5g)

Yield:41%. M.p. 241.7-242.7 °C. ¹H NMR (400 MHz, DMSO-*d*₆) δ 10.04 (s, 1H, OH), 9.03 (s, 1H, NH⁺), 7.55 (s, 3H, NH₂ + NH), 7.14 – 7.06 (m, 2H, H arom.), 6.92 – 6.84 (m, 2H, H arom.), 6.17 (s, 1H, NH), 1.82 (d, *J* = 12.5 Hz, 2H, CH₂ cyclohexane), 1.61 (q, *J* = 13.2 Hz, 2H, CH₂ cyclohexane), 1.57-1.47 (m, 3H, 2H CH₂ + 1H_α CH₂ cyclohexane), 1.27 (td, *J* = 13.2, 4.2 Hz, 2H, CH₂ cyclohexane), 0.95 – 0.79 (m, 1H, 1H_β CH₂ cyclohexane). ¹³C NMR (101 MHz, DMSO-*d*₆) δ 158.90, 158.36, 131.64 (2C), 125.83, 117.14 (2C), 71.82, 35.21 (2C), 31.25, 24.53, 21.26 (2C).

4-(7,9-diamino-6,8,10-triazaspiro[4.5]deca-7,9-dien-6-yl)phenol (5h)

Yield: 42%. M.p. 216.8-223.8 °C. ¹H NMR (400 MHz, DMSO-*d*₆) δ 10.02 (s, 1H, OH), 9.17 (s, 1H, NH⁺), 7.65-7.15 (m, 3H, NH₂ + NH), 7.09 (dd, *J* = 8.7, 1.8 Hz, 2H, H arom.), 6.85 (dd, *J* = 8.7, 1.8 Hz, 2H, H arom.), 6.23 (s, 1H, NH), 1.79-1.57 (m, 6H, (CH₂)₃ cyclopentane), 1.50-1.35 (m, 2H, CH₂ cyclopentane). ¹³C

NMR δ 158.91 (2C), 158.57, 131.41 (2C), 126.14, 117.24 (2C), 79.54, 36.75 (2C), 21.21 (2C).

5-(4-Methoxyphenyl)-1,3,5-triazaspiro[5.6]dodeca-1,3-diene-2,4-diamine hydrochloride (5i)

Yield:45%. M.p. 171-174 °C. ^1H NMR (400 MHz, DMSO-*d*₆) δ 9.19 (s, 1H, NH⁺), 7.54 (s, 1H, NH), 7.37 (s, 2H, NH₂), 7.32-7.23 (m, 2H, H arom.), 7.07-6.98 (m, 2H, H arom.), 6.11 (s, 1H, NH), 3.77 (s, 3H, OCH₃), 1.95-1.74 (m, 4H, (CH₂)₂ cycloheptane), 1.50-1.22 (m, 6H, (CH₂)₃ cycloheptane), 1.18-1.05 (m, 2H, CH₂ cycloheptane). ^{13}C NMR (101 MHz, DMSO-*d*₆) δ 160.29, 158.32, 158.10, 132.10 (2C), 127.79, 115.86 (2C), 75.23, 55.95, 39.12 (2C), 28.89 (2C), 21.10 (2C).

5-(4-Methoxyphenyl)-9-oxa-1,3,5-triazaspiro[5.5]undeca-1,3-diene-2,4-diamine hydrochloride (5j)

Yield:48%. M.p. 245.5-250 °C. ^1H NMR (400 MHz, DMSO-*d*₆) δ 9.65 (s, 1H, NH⁺), 7.64 (s, 3H, NH₂ + NH), 7.29-7.21 (m, 2H, H arom.), 7.08-6.99 (m, 2H, H arom.), 6.30 (s, 1H, NH), 3.77 (s, 3H, OCH₃), 3.75-3.64 (m, 4H, O(CH₂)₂ tetrahydropirane), 1.73 (d, J = 12.8 Hz, 2H, CH₂ tetrahydropirane), 1.54 (td, J = 12.8, 5.5 Hz, 2H, CH₂ tetrahydropirane). ^{13}C NMR (101 MHz, DMSO-*d*₆) δ 159.91, 157.94, 157.74 131.36 (2C), 126.78, 115.39 (2C), 69.23, 62.11 (2C), 55.46, 35.11 (2C).

Synthesis of intermediates: PABA-Boc synthesis

To a solution of p-amino benzoic acid (PABA) (11 mmol; 1 eq) in 30 mL of 0.5 N NaOH and 15 mL of dioxane, di-tert-butyl dicarbonate is added (12 mmol; 1.6 eq) at 0°C. The reaction is allowed to proceed at room temperature with stirring e.m. for 24 hours. Acidify the solution to pH 2 with HCl 6 N, until precipitation of a white solid which is filtered through a Büchner filter by washing with water.

General synthesis of compound 8 a-g

PABA-Boc (4.21 mmol; 1 eq) is solubilised in 25 mL of THF an. The flask is placed on an ice bath and EDC (6.32 mmol; 1.5 eq), HOBT (6.32 mmol; 1.5 eq), Et₃N (6.32 mmol; 1.5 eq) and finally the appropriate benzylamine (6.32 mmol; 1.5 eq) are added in order. Allow to react at room temperature under stirring e.m. for 12 hours. At the end the solution is taken up again with 20 mL of 1 N HCl and extracted three times with 30 mL of AcOEt. The organic solution is brought to dryness, the solid is taken up with EtOH abs. and/or DCM and filtered through a Büchner filter. The intermediates for the synthesis of compounds 1 and 2 were purified by DC chromatography (Si₂O₂/DCM+MeOH 9:1).

General synthesis of compounds 7 a-g

The appropriate N-benzylbenzamide derivative Boc-protectant (2.81 mmol; 1 eq) is solubilised in 8 mL of DCM. Trifluoroacetic acid (TFA) is added (19.6 mmol; 7 eq) is added and allowed to react at room T for 12 h under e.m. stirring. At the end of the reaction, oils are obtained which are used as as such in the synthesis of the final compounds.

General synthesis of compound 6 a-g

To a solution in methanol (3mL) of the appropriate N-benzylbenzamide derivative (2.49 mmol; 1 eq) are added in sequence cyanoguanidine (4.23 mmol; 1.7 eq), acetone (10 mL) and conc. HCl (2.49 mmol; 1 eq). It is heated to reflux for 72 hours with magnetic stirring. At the end it is left cool to room temperature and filter the white precipitate. The solid obtained is recrystallised with a suitable solvent.

Tert-butyl (4-(benzylcarbamoyl)phenyl)carbamate (8a)

Yield: 71%. M.p. 201-202 °C (EtOH/Et₂O). ¹H NMR (400 MHz, DMSO-*d*₆): δ 9.63 (s, 1H, NH), 8.88 (t, *J* = 6.0 Hz, 1H, NH), 7.81 (pseudo d, *J* = 8.8 Hz, 2H, H arom.), 7.53 (pseudo d, *J* = 8.8 Hz, 2H, H arom.), 7.35 – 7.27 (m, 4H, H arom.), 7.27 – 7.20 (m, 1H, H arom.), 4.46 (d, *J* = 6.0 Hz, 2H, CH₂), 1.48 (s, 9H, (CH₃)₃ Boc). ¹³C NMR (101 MHz, DMSO-*d*₆): δ 165.73, 152.62, 142.33, 139.90, 128.27 (2C), 128.10 (2C), 127.66, 127.22 (2C), 126.69, 117.14 (2C), 79.49, 42.52, 28.09 (3C).

Tert-butyl (4-((3-chlorobenzyl)carbamoyl)phenyl)carbamate (8b)

Yield: 71%. M.p. 198 -200 °C (EtOH). ¹H NMR (400 MHz, DMSO-*d*₆): δ 9.65 (s, 1H, NH), 8.93 (t, *J* = 6.0 Hz, 1H, NH), 7.81 (pseudo d, *J* = 8.8 Hz, 2H, H arom.), 7.53 (pseudo d, *J* = 8.8 Hz, 2H, H arom.), 7.40 – 7.23 (m, 4H, H arom.), 4.45 (d, *J* = 5.9 Hz, 2H, CH₂), 1.48 (s, 9H, (CH₃)₃ Boc). ¹³C NMR (101 MHz, DMSO-*d*₆): δ 165.83, 152.63, 142.55, 142.46, 132.94, 130.22, 128.14 (2C), 127.40, 127.06, 126.69, 125.95, 117.17 (2C), 79.53, 42.07, 28.09 (3C).

Tert-butyl (4-((4-chlorobenzyl)carbamoyl)phenyl)carbamate (8c)

Yield: 72%. M.p. 203-205 °C (EtOH). ¹H NMR (400 MHz, DMSO-*d*6): δ 9.63 (s, 1H, NH), 8.91 (t, *J* = 6.0 Hz, 1H, NH), 7.80 (pseudo d, *J* = 8.9 Hz, 2H, H arom.), 7.52 (pseudo d, *J* = 8.8 Hz, 2H, H arom.), 7.38 (pseudo d, *J* = 8.5 Hz, 2H, H arom.), 7.32 (pseudo d, *J* = 8.8 Hz, 2H, H arom.), 4.43 (d, *J* = 5.9 Hz, 2H, CH₂), 1.48 (s, 9H, (CH₃)₃ Boc). ¹³C NMR (101 MHz, DMSO-*d*6): δ 165.79, 152.63, 142.41, 138.98, 131.24, 129.12 (2C), 128.23 (2C), 128.12 (2C), 127.49, 117.14 (2C), 79.53, 41.92, 28.09 (3C).

Tert-butyl (4-((3,4-dichlorobenzyl)carbamoyl)phenyl)carbamate (8d)

Yield: 83%. M.p. 214.6-214.9 °C (EtOH/MeOH). ¹H NMR (400 MHz, DMSO-*d*6): δ 9.65 (s, 1H, NH), 8.94 (t, *J* = 6.0 Hz, 1H, NH), 7.80 (pseudo d, *J* = 8.8 Hz, 2H, H arom.), 7.58 (pseudo d, *J* = 8.3 Hz, 1H, H arom.), 7.56 – 7.51 (m, 3H, H arom.), 7.30 (dd, *J* = 8.3, 2.0 Hz, 1H, H arom.), 4.44 (d, *J* = 5.9 Hz, 2H, CH₂), 1.48 (s, 9H,

(CH₃)₃ Boc). ¹³C NMR (101 MHz, DMSO-*d*₆): δ 165.88, 152.62, 142.51, 141.22, 130.83, 130.52, 129.27, 129.23, 128.16 (2C), 127.67, 127.29, 117.17 (2C), 79.54, 41.62, 28.09 (3C).

Tert-butyl (4-((3-methoxybenzyl)carbamoyl)-phenyl)carbamate (8e)

Yield: 60%. M.p. 179-181 °C (EtOH). ¹H NMR (400 MHz, DMSO-*d*₆): δ 9.63 (s, 1H, NH), 8.86 (t, *J* = 6.0 Hz, 1H, NH), 7.80 (pseudo d, *J* = 8.8 Hz, 2H, H arom.), 7.52 (pseudo d, *J* = 8.8 Hz, 2H, H arom.), 7.23 (t, *J* = 8.1 Hz, 1H, H arom.), 6.92 – 6.84 (m, 2H, H arom.), 6.84 – 6.76 (m, 1H, H arom.), 4.42 (d, *J* = 6.0 Hz, 2H, CH₂), 3.72 (s, 3H, OCH₃), 1.48 (s, 9H, (CH₃)₃ Boc). ¹³C NMR (101 MHz, DMSO-*d*₆): δ 165.73, 159.29, 152.63, 142.33, 141.52, 129.35, 128.10 (2C), 127.65, 119.38, 117.14 (2C), 112.95, 111.99, 79.50, 54.97, 42.46, 28.09 (3C).

Tert-butyl (4-((4-methoxybenzyl)carbamoyl)phenyl)carbamate (8f)

Yield: 73%. M.p. 182-184 °C (EtOH). ¹H NMR (400 MHz, DMSO-*d*₆): δ 9.62 (s, 1H, NH), 8.81 (t, *J* = 6.0 Hz, 1H, NH), 7.79 (pseudo d, *J* = 8.8 Hz, 2H, H arom.), 7.51 (pseudo d, *J* = 8.9 Hz, 2H, H arom.), 7.23 (pseudo d, *J* = 8.8 Hz, 2H, H arom.), 6.87 (pseudo d,

$J = 8.8$ Hz, 2H, H arom.), 4.38 (d, $J = 5.9$ Hz, 2H, CH_2), 3.72 (s, 3H, OCH_3), 1.48 (s, 9H, $(CH_3)_3$ Boc). ^{13}C NMR (101 MHz, DMSO- d_6): δ 165.60, 158.16, 152.63, 142.27, 131.87, 128.61 (2C), 128.08 (2C), 127.74, 117.11 (2C), 113.67 (2C), 79.50, 55.06, 41.98, 28.09 (3C).

Tert-butyl (4-((3,4-dimethoxybenzyl)carbamoyl)-phenyl)carbamate (8g)

Yield: 85%. M.p. 227-228 °C (EtOH). 1H NMR (400 MHz, DMSO- d_6): δ 9.62 (s, 1H, NH), 8.80 (t, $J = 6.0$ Hz, 1H, NH), 7.79 (pseudo d, $J = 8.8$ Hz, 2H, H arom.), 7.51 (pseudo d, $J = 8.8$ Hz, 2H, H arom.), 6.93 (d, $J = 2.0$ Hz, 1H, H arom.) 6.88 (d, $J = 8.2$ Hz, 1H, H arom.), 6.82 (dd, $J = 8.2, 1.9$ Hz, 1H, H arom.), 4.38 (d, $J = 5.9$ Hz, 2H, CH_2), 3.72 (s, 3H, OCH_3), 3.71 (s, 3H, OCH_3), 1.48 (s, 9H, $(CH_3)_3$ Boc). ^{13}C NMR (101 MHz, DMSO- d_6): δ 165.69, 152.67, 148.61, 147.74, 142.30, 132.33, 128.12 (2C), 127.80, 119.42, 117.16 (2C), 111.74, 111.46, 79.54, 55.59, 55.44, 42.36, 28.11 (3C).

N-benzyl-4'-(4,6-diamino-2,2-dimethyl-1,3,5-triazin-1(2H)-yl)-[1,1'-biphenyl]-4-carboxamide (6a)

Yield 43%. M.p. 203-206°C (EtOH). ¹H NMR (400 MHz, DMSO-*d*₆) δ 9.35 (t, *J* = 6.0 Hz, 1H, NH amide), 9.21 (s, 1H, NH⁺), 8.09 (d, *J* = 8.6 Hz, 2H, H arom.), 7.71 (s, 1H, NH), 7.49 (d, *J* = 8.5 Hz, 2H, H arom.), 7.42 – 6.94 (br. s, 2H, NH₂ partially superimposed to H arom.) 7.34 – 7.31 (m, 3H, H arom.), 7.28 – 7.19 (m, 1H, H arom.), 6.42 (s, 1H, NH), 4.50 (d, *J* = 6.0 Hz, 2H, CH₂), 1.35 (s, 6H, (CH₃)₂). ¹³C NMR (101 MHz, DMSO-*d*₆) δ 165.07, 157.71, 157.05, 139.65, 137.45, 134.99, 130.10 (2C), 129.16 (2C), 128.28 (2C), 127.29 (2C), 126.80, 69.74, 42.68, 27.27 (2C).

N-(3-chlorobenzyl)-4'-(4,6-diamino-2,2-dimethyl-1,3,5-triazin-1(2H)-yl)-[1-1'-biphenyl]-4-carboxamide (6b)

Yield 41%. M.p. 188-190°C (MeOH). ¹H NMR (400 MHz, DMSO-*d*₆) δ 9.38 (t, *J* = 6.1 Hz, 1H, NH amide), 9.09 (s, 1H, NH⁺), 8.08 (d, *J* = 8.7 Hz, 2H, H arom.), 7.69 (s, 1H, NH), 7.50 (d, *J* = 8.7 Hz, 2H, H arom.), 7.39 – 7.27 (m, 4H, H arom.), 7.35 – 6.99 (br. s, 2H, NH₂ partially superimposed to H arom.), 6.42 (s, 1H, NH), 4.50 (d, *J* = 6.1 Hz, 2H, CH₂), 1.36 (s, 6H, (CH₃)₂). ¹³C NMR (101 MHz, DMSO-*d*₆) 165.17, 157.63, 157.05, 142.24, 137.53, 134.76, 132.93, 130.19, 130.13 (2C), 129.15 (2C), 127.06, 126.75, 126.02, 69.75, 42.19, 27.23 (2C).

N-(4-chlorobenzyl)-4'-(4,6-diamino-2,2-dimethyl-1,3,5-triazin-1(2H)-yl)-[1,1-biphenyl]-4-carboxamide (6c)

Yield 49%. M.p. 207-208°C (EtOH/MeOH). ¹H NMR (400 MHz, DMSO-*d*₆) δ 9.37 (t, *J* = 6.0 Hz, 1H, NH amide), 9.14 (s, 1H NH+), 8.04 (d, *J* = 8.5 Hz, 2H, H arom.), 7.68 (s, 1H, NH), 7.45 (d, *J* = 8.6 Hz, 2H, H arom.), 7.38 – 7.28 (m, 4H, H arom.), 7.10 (br. s, 2H, NH₂), 6.39 (s, 1H, NH), 4.44 (d, *J* = 5.9 Hz, 2H, CH₂), 1.31 (s, 6H, (CH₃)₂). ¹³C NMR (101 MHz, DMSO-*d*₆) δ 165.14, 157.70, 157.06, 138.72, 137.53, 134.84, 131.35, 130.14 (2C), 129.20 (4C), 128.25 (2C), 69.75, 42.08, 27.28 (2C).

4'-(4,6-diamino-2,2-dimethyl-1,3,5-triazin-1(2H)-yl)-N-3,4-dichlorobenzyl)-[1,1'-biphenyl]-4-carboxamide (6d)

Yield 56%. M.p. 230-232°C (MeOH). ¹H NMR (400 MHz, DMSO-*d*₆) δ 9.37 (t, *J* = 6.0 Hz, 1H, NH amide), 8.92 (s, 1H, NH+), 8.07 (d, *J* = 8.5 Hz, 2H, H arom.), 7.70 (s, 1H, NH), 7.61 (d, *J* = 8.2 Hz, 1H, H arom.), 7.57 (d, *J* = 2.0 Hz, 1H, H arom.), 7.50 (d, *J* = 8.5 Hz, 2H, H arom.), 7.32 (dd, *J* = 8.3, 2.0 Hz, 1H, H arom.), 7.22 – 6.88 (br. s, 2H, NH₂ partially superimposed to H arom.) 6.43 (s, 1H, NH), 4.49 (d, *J* = 5.9 Hz, 2H, CH₂), 1.35 (s, 6H, (CH₃)₂). ¹³C NMR (101 MHz, DMSO-*d*₆) δ 165.23, 157.68, 157.05, 140.97, 137.61, 134.65, 130.84, 130.51, 130.17 (2C), 129.31 (2C), 129.21 (2C), 127.76, 69.75, 41.73, 27.26 (2C).

4'-(4,6-diamino-2,2-dimethyl-1,3,5-triazin-1(2H)-yl)-N-(3-methoxybenzyl)-[1-1'-biphenyl]-4-carboxamide (6e)

Yield 32%. M.p. 211-213°C (EtOH/Et₂O). ¹H NMR (400 MHz, DMSO-*d*₆) δ 9.33 (t, *J* = 6.1 Hz, 1H, NH amide), 9.19 (s, 1H, NH+), 8.09 (d, *J* = 8.5 Hz, 2H, H arom.), 7.71 (s, 1H, NH), 7.49 (d, *J* = 8.6 Hz, 2H, H arom.), 7.26 – 7.00 (br. s, 2H, NH₂ partially superimposed to H arom.) 7.24 (t, *J* = 8.1 Hz, 1H, H arom.), 6.92 – 6.86 (m, 2H, H arom.), 7.02 – 6.77 (m, 1H, H arom.), 6.43 (s, 1H, NH), 4.47 (d, *J* = 5.9 Hz, 2H, CH₂), 3.73 (s, 3H, OCH₃), 1.35 (s, 6H, (CH₃)₂). ¹³C NMR (101 MHz, DMSO-*d*₆) δ 165.09, 159.30, 157.71, 157.06, 141.26, 137.46, 134.99, 130.12 (2C), 129.38, 129.17 (2C), 119.45, 113.18, 111.93, 69.75, 55.02, 42.61, 27.28 (2C).

4'-(4,6-diamino-2,2-dimethyl-1,3,5-triazin-1(2H)-yl)-N-(4methoxybenzyl)-[1-1'biphenyl]-4-carboxamide (6f)

Yield 47%. M.p. 198.5-199.6°C (EtOH/Et₂O). ¹H NMR (400 MHz, DMSO-*d*₆) δ 9.23 (t, *J* = 6.0 Hz, 1H, NH amide), 9.16 (s, 1H, NH+), 8.06 (d, *J* = 8.6 Hz, 2H, H arom.), 7.70 (s, 1H, NH), 7.48 (d, *J* = 8.5 Hz, 2H, H arom.), 7.25 (d, *J* = 8.7 Hz, 2H, H arom.), 7.44 – 7.00 (br. s, 2H, NH₂ partially superimposed to H arom.), 6.92 – 6.84 (m, 2H, H arom.), 6.41 (s, 1H, NH), 4.42 (d, *J* = 5.9 Hz, 2H, CH₂), 3.72 (s, 3H, OCH₃), 1.35 (s, 6H, (CH₃)₂). ¹³C NMR (101 MHz, DMSO-*d*₆) δ 164.95, 158.23, 157.66, 157.07, 137.40,

135.09, 131.61, 130.09 (2C), 129.12 (2C), 128.68 (2C), 113.67 (2C), 69.75, 55.09, 42.15, 27.24 (2C).

4'-(4,6-diamino-2,2-dimethyl-1,3,5-triazin-1(2H)-yl)-N-(3,4-dimethoxybenzyl)-[1,1'-biphenyl]-4-carboxamide (6g)

Yield 52%. M.p. 187-188°C (EtOH/MeOH). ¹H NMR (400 MHz, DMSO-*d*₆) δ 9.14 (t, *J* = 6.0 Hz, 1H, NH amide), 9.03 (s, 1H, NH⁺), 8.04 (d, *J* = 8.5 Hz, 2H, H arom.), 7.69 (s, 1H, NH), 7.48 (d, *J* = 8.6 Hz, 2H, H arom.), 7.37 (br. s, 2H, NH₂ partially superimposed to H arom.), 6.96 (d, *J* = 2.0 Hz, 1H, H arom.), 6.93 – 6.80 (m, 2H, H arom.), 6.42 (s, 1H, NH), 4.43 (d, *J* = 5.9 Hz, 2H, CH₂), 3.74 (s, 3H, OCH₃), 3.72 (s, 3H, OCH₃), 1.35 (s, 6H, (CH₃)₂). ¹³C NMR (101 MHz, DMSO-*d*₆) 165.03, 157.55, 157.09, 148.62, 147.84, 137.38, 135.15, 132.03, 130.07 (2C), 129.09 (2C), 119.52, 111.75, 111.66, 69.78, 55.59, 55.49, 42.52, 27.17 (2C).

6. References

- 1) WHO. Working to overcome the global impact of neglected tropical diseases. First WHO report on neglected tropical diseases. World Health Organization, Geneva, 2010.
https://www.who.int/neglected_diseases/resources/9789241564090/en/.
- 2) Neglected tropical diseases. https://www.who.int/neglected_diseases/diseases/en/.
- 3) Miranda-Arboleda, A. F.; González-Barrera, L. G.; Liblik, K.; Farina, J.; Zaidel, E. J.; Saldarriaga, C.; Zhou, Z.; Al-Rawi, R.; López-López, J. P.; Juárez-Lloclla, J. P.; Gupta, S.; Prabhakaran, D.; Krishna Kumar, R.; Sosa-Liprandi, A.; Baranchuk, A. Neglected Tropical Diseases and Sudden Cardiac Death: The NET-Heart Project. *Rev. Cardiovasc. Med.* **2022**, *23*(7), 254.
- 4) Neglected tropical diseases -- GLOBAL.
<https://www.who.int/health-topics/neglected-tropical-diseases>
(Accessed May 1, **2023**)
- 5) Hotez, P.J. “The biblical diseases” and U.S. vaccine diplomacy. *Brown World Aff J.* **2006**. 247-58.
- 6) Lammie, P. J.; Fenwick, A.; Utzinger, J. A blueprint for success: integration of neglected tropical disease control programmes. *Trends Parasitol.* **2006**. 313-21.

- 7) Hotez, P. J.; Ottesen, E.; Fenwick, A.; Molyneux, D. H. The neglected tropical diseases: the ancient afflictions of stigma and poverty and the prospects for their control and elimination. *Adv Exp Biol Med.* **2006.** 22-33.
- 8) Hotez, P. J.; Ferris, M. T. The antipoverty vaccines. *Vaccine.* **2006.** 5787-99.
- 9) Alvar, J.; Yactayo, S.; Bern, C. Leishmaniosis and poverty. *Trends Parasitol.* **2006.** 552-7.
- 10) https://www.who.int/health-topics/neglected-tropical-diseases#tab=tab_2
- 11) Why do neglected tropical diseases suffer low priority?
<https://www.afro.who.int/news/why-do-neglected-tropical-diseases-suffer-low-priority> (Accessed May 1, **2023**).
- 12) Antonovics, J. Transmission Dynamics: Critical Questions and Challenges. *Philos. Trans. R. Soc. Lond. B. Biol. Sci.*, **2017**, 372, 20160087.
- 13) Lindner, A.K.; Priotto, G. The unknown risk of vertical transmission in sleeping sickness-aliterature review. *Plos Negl Trop Dis.* **2010.** 783
- 14) Rocha, G.; Martins, A.; Gama, G.; Brandão, F.; Atouguia, J. Possible cases of sexual and congenital transmission of sleeping sickness. *Lancet.* **2004.** 247.

- 15) Hira, P. R.; Huswin, S. F. Some transfusion-induced parasitic infections in Zambia. *J Hyg Epidemiol Microbiol Immunol.* **1979.** 436-44.
- 16) Kennedy, P. G. Clinical features, diagnosis, and treatment of human African trypanosomiasis (sleeping sickness), *The Lancet Neurology.* 12 (2013) 186–194. [https://doi.org/10.1016/S1474-4422\(12\)70296-X](https://doi.org/10.1016/S1474-4422(12)70296-X).
- 17) Picozzi, K.; Carrington, M.; Welburn, S. C. A multiplex PCR that discriminates between *Trypanosoma brucei brucei* and zoonotic *Tb rhodesiense*. *Exp Parasitol.* **2008.** 41- 46.
- 18) Radwanska, M.; Claes, F.; Magez, S.; Magnus, E.; Perez Morgia, D.; *et all.* Novel primer sequences for polymerase chain reaction-based detection of *Trypanosoma brucei gambiense*. *Am J Trop Med Hyg.* **2002.** 289-295.
- 19) Picozzi, K.; Fe`vre, E. M.; Odiit, M.; Carrington, M.; Eisler, M. *et al.* Sleeping sickness in Uganda: a thin line between two fatal diseases. *BMJ* **2005.** 1238–1241.
- 20) Kuepfer, I.; Hhary, E.P.; Allan, M.; Edielu, A.; Burri, C.; Blum, J. A. Clinical Presentation of T.b. rhodesiense Sleeping Sickness in Second Stage Patients from Tanzania and Uganda, *PLoS Neglected Tropical Diseases.* 5 (2011) e968.
- 21) Ndung’u, K.; Murilla, G. A.; Thuita, J. K.; Ngae, G. N.; Auma, J. E.; Gitonga, P. K.; Thungu, D. K.; Kurgat, R. K.; Chemuliti, J. K.; Mdachi, R. E.; Differential virulence of *Trypanosoma brucei rhodesiense* isolates does not influence the outcome of treatment

- with anti-trypanosomal drugs in the mouse model, *PLOS ONE*. 15 (2020) e0229060.
- 22) Fe`vre1, E. M.; Wissmann, B. V.; Welburn, S. C.; Lutumba, P. The Burden of Human African Trypanosomiasis. *PLoS Neglected Tropical Diseases*. (2008) (12) e333.
- 23) World Health Organization, Control and surveillance of Human African Trypanosomiasis. Report of a Who Expert Committee. Who Technical Report Series 984. Geneva, Switzerland: World Health Organization; 2013.
- 24) Radwanska, M.; Chamekh, M.; Vanhamme, L.; *et all*. The serum resistance-associated gene as a diagnostic tool for the detection of *Trypanosoma brucei rhodesiense*. *Am J Trop Med Hyg*. 2002. 684-690.
- 25) Berberof, M.; Perez-Morga, D.; Pays, E. A receptor-like flagellar pocket glycoprotein specific to *Trypanosoma brucei gambiense*. *Mol Biochem Parasitol*. 2001. 127-138.
- 26) Vickerman, K.; Developmental cycles and biology of pathogenic trypanosomes. *Br Med Bull*. 1985. 41(2):105-114.
- 27) Sharma, R.; Gluenz, E.; Peacock, L.; Gibson, W.; Gull, K.; Carrington, M. The heart of darkness: growth and form of *Trypanosoma brucei* in the tsetse fly. *Trends Parasitol*. 2009. 25(11):517-524.
- 28) Rotureau, B.; Van Den Abbeele, J. Through the dark continent: African trypanosome development in tsetse fly. *Front Cell Infect Microbiol*. 2013. 3:53.1-7.

- 29) Dyer, N.A.; Rose C.; Ejeh, N.O.; Acosta-Serrano, A. Flying trips: survival and maturation of trypanosomes in tsetse flies. *Trends Parasitol.* **2013**. 29(4):188-196.
- 30) Büscher, P.; Cecchi, V.; Jamonneau, V.; Priotto, G. Human African Trypanosomiasis. *Lancet.* **2017**.
- 31) <https://www.cdc.gov/dpdx/trypanosomiasisafrican/index.html>.
- 32) Brun, R.; Blum, J.; Chappuis, F.; Burri, C. Human African Trypanosomiasis. *Lancet.* **2010**. 148-159.
- 33) Peacock, L.; Ferris, V.; Sharma, R *et al.* Identification of the meiotic life cycle stage of *Trypanosoma brucei* in the tsetse fly. *Proc Natl Acad Sci USA.* **2011**. 3671-3676.
- 34) Franco, J.R.; Simarro, P. P. *et al* Epidemiology of Human African Trypanosomiasis. *Clinical Epidemiology.* **2014**. 257-275.
- 35) Welburn, S. C.; Maudlin, I. The nature of teneral state in *Glossina* and its role in the acquisition of trypanosome infection in tsetse. *Ann Trop Med Parasitol.* **1992**. 529-536.
- 36) Kaba, D.; Koffi, M.; Kouakou, L.; E.K. N’Gouan, E. K.; Djohan, V.; Courtin, F.; N’Djetchi, M. K.; Coulibaly, B.; Adingra, G. P.; Berté, D.; Ta, B. T. D.; Koné, M.; Traoré, B. M.; Sutherland, S. A.; Crump, R. E.; Huang, C. I.; Madan, J.; Bessell, P. R.; Barreaux, A.; Solano, P.; Crowley, E. H.; Rock, K. S.; Jamonneau, V. Towards the sustainable elimination of gambiense human African trypanosomiasis in Côte d’Ivoire using an integrated approach, *PLOS Neglected Tropical Diseases.* 17 (2023) e0011514.

- 37) Gehrig, S.; Efferth, T.; Development of drug resistance in *Trypanosoma brucei rhodesiense* and *Trypanosoma brucei gambiense*. Treatment of human African trypanosomiasis with natural products (Review)., *International Journal of Molecular Medicine*. 22 (2008) 411–9.
- 38) Checchi, F.; Filipe, J. A. N.; Barret, M. P.; Chandramohan, D. The progression of *gambiense* sleeping sickness: what is the evidence? *PloS Negl Trop Dis*. 2008. E303.
- 39) Oscherwitz, S. L. East African trypanosomiasis. *J Travel Med*. 2003. 141-143.
- 40) Urech, K.; Neumayr, A.; Blum, J. Sleeping sickness in travelers-do they really sleep? *PloS Negl Trop Dis*. 2011. E1538.
- 41) Simarro, P. P.; Franco, J.; Diarra, A.; Postigo, J. A.; Jannin, J. Update on field use of the available drugs for the chemotherapy of human African trypanosomiasis. *Parasitology*. 2012. 842-846.
- 42) Pohlig, G.; Bernhard, S. C.; Blum, J. et al. Efficacy and safety of pafuramidine versus pentamidine maleate for treatment of first stage sleeping sickness in a randomized, comparator-controlled, international phase 3 clinical trial. *PloS Negl Trop Dis*. 2016. E0004363.
- 43) Jaime Franco, Laura Scarone, Marcelo A. Comini, Chapter Three - Drugs and Drug Resistance in African and American Trypanosomiasis, Editor(s): Maurizio Botta, *Annual Reports in Medicinal Chemistry*, Academic Press, Volume 51, 2018, Pages 97-133.

- 44) Priotto, G.; Kasparian, S.; Mutombo, W. et al. Nifurtimox-eflornithine combination therapy for second-stage African *Trypanosoma brucei gambiense* trypanosomiasis: a multicentre, randomised, phase III, non-inferiority trial. *Lancet*. **2009**. 56-64.
- 45) Alirol, E.; Schimpf, D.; Amici, H.; J. et al. Nifurtimox - eflornithine combination therapy for second-stage gambiense human African trypanosomiasis: Medecins Sans Frontiers experience in the Democratic Republic of the Congo. *Clin Infect Dis*. **2013**. 195-203.
- 46) Kasozi, K. I.; MacLeod, E. T.; Ntulume, I.; & Welburn, S. C. (2022). An Update on African Trypanocide Pharmaceuticals and Resistance. *Frontiers in veterinary science*. (2022) 9, 828111.
- 47) Chappuis, F.; Udayraj, N.; Stietenroth, K.; Meussen, A.; Bovier, P. A. Eflornithine is safer than melarsoprol for the treatment of second-stage *Trypanosoma brucei gambiense* human African trypanosomiasis. *Clin Infect Dis*. **2005**. 748-51.
- 48) World Health Organization (WHO). Factsheet. Available online: <https://www.afro.who.int/health-topics/Leishmaniasis> (accessed on 2 March 2020).
- 49) Zulfiqar, B.; Shelper, T.B.; Avery, V.M. Leishmaniasis drug discovery: recent progress and challenges in assay development. *Drug Discov Today*. (2017); 22(10):1516-1531.
- 50) www. Who.int.
- 51) Georgiadou, S. P.; Makaritsis, K. P.; Dalekos, G. N. Leishmaniasis revisited: Current aspects on epidemiology, diagnosis and

- treatment. *Journal of Translational Internal Medicine*. **2013**. 43-50.
- 52) Mann, S.; Frasca, K.; Scherrer, S.; Henao-Martínez, A. F.; Newman, S.; Ramanan, P.; Suarez, J. A. A Review of Leishmaniasis: Current Knowledge and Future Directions. *Curr Trop Med Rep*. **2021**;8(2):121-132.
- 53) Boelaert, M.; Sundar, S. 47- Leishmaniasis. In: Farrar, J.; Hotez, P. J.; Junghanss, T.; Kang, G.; Lalloo, D.; White, N. J. editors. *Manson's Tropical Infectious Disease*. **2014**. 631-51.
- 54) Organization PAHO. Manual of procedures for leishmaniasis surveillance and control in the Americas **2019**. <https://iris.paho.org/handle/10665.2/51838>.
- 55) CDC. Leishmaniasis: Biology. [Available from: <https://www.cdc.gov/parasites/leishmaniasis/biology.html>].
- 56) Olivo Freites, C.; Gundacker, N. D.; Pascale, J. M.; Saldaña, A.; Diaz Suarez R.; Jimenez, G. et al. First case of diffuse leishmaniasis associated with *Leishmania panamensis*. *Open Forum Infect Dis*. **2018**;5(11):ofy281.
- 57) Herwaldt, B. L.; Leishmaniasis. *Lancet*. **1999**. 354(9185):1191–9.
- 58) Weller, P. F.; Durand, M. L.; Pilch, B. Z.; Case 4-2005. *New England Journal of Medicine*. **2005**. 352(6):609-15.
- 59) Seaman, J.; Mercer, A. J.; Sondorp, H. E.; Herwaldt, B. L. Epidemic visceral leishmaniasis in southern Sudan: treatment of severely debilitated patients under wartime conditions and with limited resources. *Ann Intern Med*. **1996**. 124(7): 664-72.

- 60) Ejazi, S. A.; Ali, N. Developments in diagnosis and treatment of visceral leishmaniasis during the last decade and future prospects. *Expert Rev Anti Infect Ther.* **2013.** 11:79-98.
- 61) Chattopadhyay, A.; Jafurulla, M. A novel mechanism for an old drug: amphotericin B in the treatment of visceral leishmaniasis. *Biochem Biophys Res Commun.* **2011.** 416:7-12.
- 62) Singh, S.; Sivakumar, R. Challenges and new discoveries in the treatment of leishmaniasis. *J Infect Chemother.* **2004.** 10:307-315.
- 63) Thakur, C.; Kumar, A.; Mitra, G. et al. Impact of amphotericin of kala-azar on the incidence of PKDL in Bihar, India. *Indian J Med Res.* **2008.** 128:38.
- 64) Olliaro, P. L.; Guerin, P. J.; Gerstl, S. et al. Treatment options for visceral leishmaniasis: a systematic review of clinical studies done in India, 1980-20054. *Lancet Infect Dis.* **2005.** 5:763-774.
- 65) Sundar, S.; Jha, T.; Thaku, C. et al Oral miltefosine for Indian visceral leishmaniasis. *N Eng J Med.* **2002.** 347:1739-1746.
- 66) Croft, S. L.; Neal, R. A.; Pendergast, W. et al. The activity of alkyl phosphorylcholines and related derivates against *Leishmania donovani*. *Biochem Pharmacol.* **1987.** 36:2633-2636.
- 67) Paris, C.; Loiseau, P. M.; Bories, C. et al. Miltefosine induces apoptosis-like death in *Leishmania donovani* promastigotes. *Antimicrob Agents Chemother.* **2004.** 48:852-859.
- 68) Ong, H. B.; Sienkiewicz, N.; Wyllie, S.; Fairlamb, A. H. Dissecting the metabolic roles of pteridine reductase 1 in *Trypanosoma brucei* and *Leishmania major*. *J Biol Chem.* **2011.** 286:10429-10438.

- 69) Werner-Felmayer, G.; Golderer, G.; Werner, E. R. Tetrahydrobiopterin Biosynthesis, Utilization and pharmacological effects. *Curr Drug Metab.* **2002.** 3:159-173.
- 70) Donnelly, J. G. Folic Acid. *Crit Rev Clin Lab Sci.* **2001.** 38:183-223.
- 71) Oullette, M.; Drummelsmith, J.; El Fadili, A.; Kunding, C.; Richard, D.; Roy, G. Pterin transport and metabolism in *Leishmania* and related trypanosomatid parasites. *Int J Parasitol.* **2022.** 32:385-398.
- 72) Ouameur, A. A.; Girad, I.; L'egar'e, D.; Oullette, M. Functional analysis and complex gene rearrangements of the folate/biopterin transporter (FBT) gene family in the protozoan parasite *Leishmania*. *Mol Biochem Parasitol.* **2008.**162:155-164.
- 73) Dewar, S.; Sienkiewicz, N.; Ong, H. B.; Wall, R. J.; Horn, D.; Fairlamb, A. H. The role of folate Transposrt in antifolate drug Action in *Trypanosoman brucei*, *J Bil Chem.* **2016.** 291:24768-24778.
- 74) Vickers, T. J.; Beverley, S. M. Folate metabolic pathways in *Leishmania*. *Essays Biochem.* **2011.** 51:63-80.
- 75) Sienkiewicz N, Jarosławski S, Wyllie S, Fairlamb AH. Chemical and genetic validation of dihydrofolate reductase-thymidylate synthase as a drug target in African trypanosomes. *Mol Microbiol.* **2008;**69(2):520-533.
- 76) A)Zuccotto, F.; Martin, A. C. R.; Laskowski, R. A.; Thornton, J. M.; Gilbert, I. H. *J. Comput Aid Mol Des.* **1998.** 12: 241-257.

- B) Gilbert, I. H. *Biochim Biophys Acta Mol Basis Dis.* **2002.** 1587:249-257.
- 77) Sharma, V. K.; Abbat, S.; Bharatam, P. V.; *Mol. Inform.* **2017**, 36, 1600156.
- 78) Vanichtanankul, J.; Taweechai, S.; Yuvaniyama, J.; Vilaivan, T.; Chitnumsub, P.; Kamchonwongpaisan, S.; Yuthavong, Y. Trypanosomal Dihydrofolate Reductase Reveals Natural Antifolate Resistance. *ACS Chem Biol* **2011**, 6, 905–911.
- 79) Dawson, A.; Tulloch, L.B.; Barrack, K.L.; Hunter, W.N. High-Resolution Structures of Trypanosoma Brucei Pteridine Reductase Ligand Complexes Inform on the Placement of New Molecular Entities in the Active Site of a Potential Drug Target. *Acta Crystallogr D Biol Crystallogr.* **2010.** 66: 1334
- 80) Nare, B.; Hardy, L.; Beverley, S. M. *J Biol Chem.* **1997.** 272:13883-13891.
- 81) Papadopoulou, B.; Roy, G.; Ouellette, M. *EMBO J.* **1992.** 11:3601-3608.
- 82) Eichwald, T.; da Silva, L.B.; Staats Pires, A.C.; Niero, L.; Schnorrenberger, E.; Filho, C.C.; Espíndola, G.; Huang, W. L.; Guillemin, G. J.; Abdenur, J. E.; Latini, A. Tetrahydrobiopterin: Beyond Its Traditional Role as a Cofactor. *Antioxidants* (Basel). **2023** May 3;12(5):1037.
- 83) Bello, A. R.; Nare, B.; Freedman, D.; Hardy, L.; Beverley, S. M. PTR1: a reductase mediating salvage of oxidized pteridines and

Methotrexate resistance in the protozoan parasite *Leishmania Major*. *Proc Natl Acad Sci USA*. **1994**. 91:11442-11446.

- 84) Nare, B.; Luba, J.; Hardy, L. W.; Beverley, S. New approaches to *Leishmania* chemotherapy: Pteridine Reductase 1 (PTR1) as a target and modulator of antifolate sensitivity. *Parasitology*. **1997**. 114:101-110.
- 85) Robello, C.; Navarro, P.; Castanys, S.; Gamarro, F. A Pteridine Reductase gene PTR1 contiguous to a P-glycoprotein confers resistance to antifolates in *Trypanosoma cruzi*. *Mol Biochem Parasitol*. **1997**. 90:525-535.
- 86) Gourley, D. G.; Schüttelkopf, A. W.; Leonard, G. A.; Luba, J.; Hardy, L. W.; Beverley, S. M.; Hunter, W. N. Pteridine reductase mechanism correlates pterin metabolism with drug resistance in trypanosomatids parasites. *Nat Genet*. **2001**. 8:521-525.
- 87) Hawser, S.; Lociuoro, S.; Islam, K. Dihydrofolate Reductase Inhibitors as Antibacterial Agents. *Biochem Pharmacol*. **2006**. 71:941-948.
- 88) Yuthavong, Y.; Yuvaniyama, J.; Chitnumsub, P.; Vanichtanankul, J.; Chusacultanachai, S.; Tarnchompoo, B.; Vilaivan, T.; Kamchonwongpaisan, S. Malarial (*Plasmodium Falciparum*) Dihydrofolate Reductase-Thymidylate Synthase: Structural Basis for Antifolate Resistance and Development of Effective inhibitors. *Parasitology*. **2005**. 130:249-259.
- 89) Pöhner, I.; Quotadamo, A.; Panecka-Hofman, J.; Luciani, R.; Santucci, M.; Linciano, P.; Landi, G.; Di Pisa, F.; Dello Iacono, L.;

- Pozzi, C.; et al. Multitarget, Selective Compound Design Yields Potent Inhibitors of a Kinetoplastid Pteridine Reductase 1. *J. Med. Chem.* **2022**, *65*, 9011–9033, doi:10.1021/acs.jmedchem.2c00232.
- 90) Landi, G.; Linciano, P.; Tassone, G.; Costi, M.P.; Mangani, S.; Pozzi, C. High-Resolution Crystal Structure of Trypanosoma Brucei Pteridine Reductase 1 in Complex with an Innovative Tricyclic-Based Inhibitor. *Acta Crystallogr D Struct Biol* **2020**, *76*, 558–564, doi:10.1107/S2059798320004891
- 91) Dize, D.; Tata, R.B.; Keumoe, R.; Kouipou Toghueo, R.M.; Tchataat, M.B.; Njanpa, C.N.; Tchuenguia, V.C.; Yamthe, L.T.; Fokou, P.V.T.; Laleu, B.; et al. Preliminary Structure-Activity Relationship Study of the MMV Pathogen Box Compound MMV675968 (2,4-Diaminoquinazoline) Unveils Novel Inhibitors of Trypanosoma Brucei Brucei. *Molecules* **2022**, *27*, 6574, doi:10.3390/molecules27196574.
- 92) Linciano P, Quotadamo A, Luciani R, Santucci M, Zorn KM, Foil DH, Lane TR, Cordeiro da Silva A, Santarem N, B Moraes C, Freitas-Junior L, Wittig U, Mueller W, Tonelli M, Ferrari S, Venturelli A, Gul S, Kuzikov M, Ellinger B, Reinshagen J, Ekins S, Costi MP. High-Throughput Phenotypic Screening and Machine Learning Methods Enabled the Selection of Broad-Spectrum Low-Toxicity Antitrypanosomatidic Agents. *J Med Chem.* (2023) Nov 23;66(22):15230-15255.
- 93) Bhattacharya, A.; Leprohon, P.; Ouellette, M. Combined Gene Deletion of Dihydrofolate Reductase-Thymidylate Synthase and

Pteridine Reductase in *Leishmania Infantum*. *PLoS Negl Trop Dis* **2021**, *15*, e0009377, doi:10.1371/journal.pntd.0009377.

- 94) Landi, G.; Linciano, P.; Borsari, C.; Bertolacini, C. P.; Moraes, C. B.; Cordeiro-da-Silva, A.; Gul, S.; Witt, G.; Kuzikov, M.; Costi, M. P. et al. Structural insights into the development of Cycloguanil derivative as *Trypanosoma brucei* Pteridine-Reductase-1. *ACS Infect Dis.* **2019**. *5*:1105-1114.
- 95) Kamchonwongpaisan, S.; Charoensetakul, N.; Srisuwannaket, C.; Taweechai, S.; Rattanajak, R.; Vanichtanankul, J.; Vitsupakorn, D.; Arwon, U.; Thongpanchang, C.; Tarnchompoo, B.; Vilaivan, T.; Yuthavong, Y. Flexible diaminodihydrotriazine inhibitors of *Plasmodium falciparum* dihydrofolate reductase: Binding strengths, modes of binding and their antimalarial activities. *Eur J Med Chem.* **2020** Jun 1;195:112263.
- 96) Baker, B.R.; Vermeulen, N.M.J. Irreversible Enzyme Inhibitors. CLXXVII. Active-Site-Directed Irreversible Inhibitors of Dihydrofolate Reductase Derived from 4,6-Diamino-1,2-Dihydro-2,2-Dimethyl-1-(Phenylalkylphenyl)-s-Triazines. II. *J. Med. Chem.* **1970**, *13*, 1154–1160.
- 97) Brown, J. I.; Wang, P.; Wong, A. Y. L.; Petrova, B.; Persaud, R.; Soukhtehzari, S.; Lopez McDonald, M.; Hanke, D.; Christensen, J.; Iliev, P.; Wang, W.; Everton, D. K.; Williams, K. C.; Frank, D. A.; Kanarek, N.; Page, B. D. G. Cycloguanil and Analogues Potently Target DHFR in Cancer Cells to Elicit Anti-Cancer Activity. *Metabolites.* **2023**.13(2):151.

- 98) Tassone, G.; Landi, G.; Linciano, P.; Francesconi, V.; Tonelli, M.; Tagliazucchi, L.; Costi, M. P.; Mangani, S.; Pozzi, C. Evidence of Pyrimethamine and Cycloguanil Analogues as Dual Inhibitors of *Trypanosoma brucei* Pteridine Reductase and Dihydrofolate Reductase. *Pharmaceuticals*. **2021**.14(7):636.
- 99) Francesconi, V.; Rizzo, M.; Schenone, S.; Carbone, A.; Tonelli, M. State-of-the-art Review on the Antiparasitic Activity of Benzimidazole-based Derivatives: Facing Malaria, Leishmaniasis, and Trypanosomiasis. *Curr Med Chem*. **2023**.
- 100) Dolzhenko, A.V.; Chui, W.-K. Synthesis of 2-Amino-s-Triazino[1,2-a]Benzimidazoles as Potential Antifolates from 2-Guanidino- and 2-Guanidino-5-Methylbenzimidazoles. *Journal of Heterocyclic Chemistry* **2006**, *43*, 95–100, doi:10.1002/jhet.5570430115.
- 101) King, F.E.; Acheson, R.M.; Spensley, P.C. 275. Benzimidazole Analogues of Paludrine. *J. Chem. Soc.* **1948**, 1366–1371, doi:10.1039/JR9480001366.
- 102) Linciano P, Pozzi C, Iacono LD, di Pisa F, Landi G, Bonucci A, Gul S, Kuzikov M, Ellinger B, Witt G, Santarem N, Baptista C, Franco C, Moraes CB, Müller W, Wittig U, Luciani R, Sesenna A, Quotadamo A, Ferrari S, Pöhner I, Cordeiro-da-Silva A, Mangani S, Costantino L, Costi MP. Enhancement of Benzothiazoles as Pteridine Reductase-1 Inhibitors for the Treatment of Trypanosomatidic Infections. *J Med Chem*. **2019**. 62(8):3989-4012.

- 103) LigPrep, Schrödinger, LLC, New York, NY, 2023.
- 104) Linciano, P.; Dawson, A.; Pohner, I. *et al.* Exploiting the 2-Amino-1,3,4-thiadiazole Scaffold To Inhibit Trypanosoma brucei Pteridine Reductase in Support of Early-Stage Drug Discovery. *ACS Omega* **2017**, *2*, 5666– 5683.
- 105) Sanschagrín, P. C.; Kuhn, L. A. Cluster analysis of consensus water sites in thrombin and trypsin shows conservation between serine proteases and contributions to ligand specificity. *Protein Sci.* **1998**, *7*, 2054–2064.
- 106) Sastry, G. M.; Adzhigirey, M.; Day, T.; Annabhimoju, R.; Sherman, W. Protein and ligand preparation: parameters, protocols, and influence on virtual screening enrichments. *J Comput Aided Mol Des* **2013**, *27*, 221–234.
- 107) Schrodinger, LLC, New York, NY, Prime v4.2. Schrödinger Release 2022-1, **2022**.
- 108) Epik, Schrödinger, LLC, New York, NY, 2023. Schrödinger Release 2022-1, **2022**.
- 109) Schormann, N.; Senkovich, O.; Walker, K.; Wright, D.L.; Anderson, A.C.; Rosowsky, A.; Ananthan, S.; Shinkre, B.; Velu, S.; Chattopadhyay, D. Structure-based approach to pharmacophore identification, in silico screening, and three-dimensional quantitative structure-activity relationship studies for inhibitors of Trypanosoma cruzi dihydrofolate reductase function. *Proteins.* **2008**. *73*: 889-901.

- 110) Cody, V.; Luft, J.R.; Pangborn, W. Understanding the role of Leu22 variants in methotrexate resistance: comparison of wild-type and Leu22Arg variant mouse and human dihydrofolate reductase ternary crystal complexes with methotrexate and NADPH. *Acta Crystallogr D Biol Crystallogr.* **2005.** 61: 147-155.
- 111) Glide, Schrödinger, LLC, New York, NY, 2022.**2022.** Schrödinger Release 2022-1
- 112) Desmond Molecular Dynamics System, D. E. Shaw Research, New York, NY, 2022. Maestro-Desmond Interoperability Tools, Schrödinger, New York, NY, 2022. Schrödinger Release 2022-1.
- 113) Lamb, K.M., G-Dayananandan, N., Wright, D.L., Anderson, A.C. Elucidating features that drive the design of selective antifolates using crystal structures of human dihydrofolate reductase. *Biochemistry.* **2013.** 52: 7318-7326.
- 114) Induced Fit Docking protocol; Glide, Schrödinger, LLC, New York, NY, 2022; Prime, Schrödinger, LLC, New York, NY, **2022.** Schrödinger Release 2022-1.
- 115) The PyMOL Molecular Graphics System, Version 2.0 Schrödinger, LLC.
- 116) QikProp, Schrödinger, LLC, New York, NY, **2022.** Schrödinger Release 2022-1.
- 117) Modest, E. J. Chemical and Biological Studies on 1,2-Dihydro-s-triazines. II. Three-Component Synthesis¹, *J. Org. Chem.* 21 (**1956**), 1–13.

- 118) Fisher, M. W. 1-m-Trifluoromethylphenyl-4,5-diamino-1,2-dihydro-2,2-dimethyl-1,3,5-triazine, Patent DE 1118790, **1961**.
- 119) Panecka-Hofman, J.; Poehner, I.; Wade, R. C. Anti-trypanosomatid structure-based drug design - lessons learned from targeting the folate pathway. *Expert Opin Drug Discov.* **2022**.17(9):1029-1045.
- 120) Linciano, P.; Moraes, C. B.; Alcantara, L. M.; Franco, C. H.; Pascoalino, B.; Freitas-Junior, L.H.; Macedo, S.; Santarem, N.; Cordeiro-da-Silva, A.; Gul, S.; Witt, G.; Kuzikov, M.; Ellinger, B.; Ferrari, S.; Luciani, R.; Quotadamo, A.; Costantino, L.; Costi, M. P. Aryl thiosemicarbazones for the treatment of trypanosomatidic infections. *Eur J Med Chem.* **2018**.146:423-434.
- 121) Tonelli, M.; Naesens, L.; Gazzarrini, S.; Santucci, M.; E. Cichero, E.; Tasso, B.; Moroni, A.; M.P. Costi, M. P.; Loddo, R.; Host dihydrofolate reductase (DHFR)-directed cycloguanil analogues endowed with activity against influenza virus and respiratory syncytial virus, *European Journal of Medicinal Chemistry.* 135 (2017), 467–478.
- 122) King, F. E.; Acheson, R. M.; Spensley, P. C.; 275. Benzimidazoles Analogues of Paludrine. *J. Chem. Soc.* **1948**. 1366-1371.
- 123) Dolzhenko, A. V.; Chui, W. K. Synthesis of 2-Amino-s-Triazino[1,2-a]Benzimidazoles as potential antifolates from 2-Guanidino- and 2-Guanidino-5-Methylbenzimidazoles. *Journal of Heterocyclic Chemistry.* **2006**. 43, 95-100.

